The University Of Sheffield.

Design, growth and fabrication and characterisation of InGaN Micro Light Emitting Diodes using a Direct Epitaxial Approach

Peter Samuel Fletcher

A thesis submitted in partial fulfilment of the requirements for the degree of Doctor of Philosophy

The University of Sheffield

Department of Electronic and Electrical Engineering

March 2022

ABSTRACT

Free standing micro disks have been the focus of a significant amount of research in recent years. This is due to the ease in creating low threshold micro lasers and micro array devices. Unfortunately, there are issues with the fabrication process that limit the overall efficiency and quality of such devices. The top-down approach used with these micro disk leads to severe sidewall damage from the etching process. Therefore, we present a novel approach using a direct epitaxial method to selectively grow micro disks in a patterned SiO_2 template. This thesis presents the design process in which we made these devices and the use of characterisation to optimise the method to create highly efficient micro-LEDs

We also take these devices further and created micro laser cavities using a hybrid epitaxial/ dielectric cavity. Using lattice matched nanoporous GaN/undoped GaN Distributed Bragg Reflectors (DBR) and a dielectric SiO_2/SiN based DBR, we can create optically pumped micro disks arrays with stimulated emission with a wavelength of 510nm.

Finally, we investigate a new limiting factor in the growth of ultra-small micro disks (<3.5µm) in the form the circularity of the micro disks themselves rather than the roughness of the sidewall.

ACKNOWLEDGEMENTS

I would like to thank all the people who helped during my Ph.D., through guidance, teaching or just by being wonderful friends during my time at the University of Sheffield. I would like to first express gratitude towards my supervisor Professor Tao Wang, through his support and help throughout my studies has enabled me to become the researcher I am today. I also want to give thank for the opportunity to work with III-nitride optoelectronics and help with the creation of microstructures. I have learnt a considerable amount and have worked with amazing materials and characterisation setups. I would also like to thank Dr Rick Smith for training me in all aspects of photoluminescence spectroscopy and their set ups. I am also very grateful towards Dr Jie Bai with whom was always available for discussions about our work and has always helped me with good advice.

I would also want to give special thanks towards Dr Nicolas Poyiatzis who has always been an enormous help and has given me guidance throughout my Ph.D., as well as being a great friend and colleague. I would like to thank the other member of our group and fellow students. Mr. Xuanming Zhao, Mr Chenqi Zhu, Mr. Peng Feng, Mr Ye Tian, Mr Jack Haggar, Mr. Volkan Esendag, Mr. Guillem Martinez de Arriba, Dr Yuefei Cai, and Mr Valerio Trinito and former collegues Dr. Yipin Gong and Dr. Suneal Ghataora for their help on all my projects.

For their brilliant work at keeping our building safe and functioning I would also like to give thanks towards the technical staff Mr. Paul Haines, Mr, Jonathan Milner and Mr. Stephen Atkin.

During my time at this university, I have made lifelong friends that have supported me and kept me sane during the long journey. Much thanks, towards Mr Oliver Harris, Mr Josh Wood, Mr Fred Gill, Mr Peter Ramsay, Mr Nick Chapman, and Miss Lucie Winship. Of course, I owe a great deal to my family, my mother and brother Elvira and Philip Fletcher who were always ready to talk even about subjects they have no knowledge of.

Finally, during my time studying I have lost four family members that I hope I did them proud through my research and I will always miss them. Thanks to my grandmother Daisy, and my lola (grandmother) Pina, my uncle Andrew and last but not least my father Francis Fletcher.

LIST OF PUBLICATIONS

JOURNAL CONTRIBUTIONS

1. **Peter Fletcher** *et al* (2022) Optical characterisation of InGaN-based microdisk arrays with nanoporous GaN/GaN DBRs *J. Phys. D: Appl. Phys.* **55** 464001
2. V. Esendag, J. Bai, **P. Fletcher**, P. Feng, C. Zhu, Y. Cai and T. Wang, (2021) *Investigation of electrical properties of InGaN based micro light emitting diode (μLED) arrays achieved by direct epitaxy,* physica status solidi (a)
3. J. R. Pugh, E. G. H. Harbord, A. Sarua, **P. S. Fletcher**, Y. Tian, T. Wang and M. J. Cryan, (2021) A Tamm *Plasmon-Porous GaN Distributed Bragg Reflector Cavity*, Journal of Optics

4. X. Zhao, K. Huang, J. Bruckbauer, S. Shen, C. Zhu, **P. Fletcher**, P. Feng, Y. Cai, J. Bai, C. Trager-Cowan, R. W. Martin and T. Wang**,** (2020) *Influence of an InGaN superlattice pre-layer on the performance of semi-polar (11–22) green LEDs grown on silicon*, Scientific Reports, 10, 12650

5. J. Bai, Y. Cai, P. Feng, **P. Fletcher**, C. Zhu, Y. Tian, and T. Wang, (2020) *Ultrasmall, Ultracompact and Ultrahigh Efficient InGaN Micro Light Emitting Diodes (μLEDs) with Narrow Spectral Line Width*, ACS Nano, 14, 6, 6906–6911

6. S. Jiang, Y. Cai, P. Feng, S. Shen, X. Zhao, P. **Fletcher**, V. Esendag, K. Lee & T. Wang**,** (2020) *Exploring an approach toward the intrinsic limits of GaN electronics*, ACS Appl. Mater. Interfaces

7. J. Bai, Y. Cai, P. Feng, **P. Fletcher**, X. Zhao, C. Zhu, & T. Wang**,** (2020) *A Direct Epitaxial Approach To Achieving Ultrasmall and Ultrabright InGaN Micro Light-Emitting Diodes (µLEDs)*, ACS Photonics, 7, 2, 411-415

8. J. Bai, L. Jiu, N. Poyiatzis, **P. Fletcher**, Y. Gong & T. Wang**,** (2019) *Optical and polarization properties of nonpolar InGaN-based light-emitting diodes grown on micro-rod templates*, Scientific Reports, volume 9, Article number: 9770

CONFERENCE CONTRIBUTIONS

1. L. Jiu, J. Bai, N. Poyiatzis, **P. Fletcher**, and T. Wang, "Nonpolar (11-20) InGaN/GaN light-emitting diodes overgrown on a micro-rod Template", Semiconductor and Integrated Opto-Electronics, Cardiff, UK, April 2019.

2. L. Jiu, J. Bai, N. Poyiatzis, **P. Fletcher**, Y. Gong, and T. Wang, "Nonpolar a-plane (11-20) InGaN-based light-emitting diodes grown on micro-rod templates", UK Nitrides Consortium Winter, Glasgow, UK, January 2019

TABLE OF CONTENTS

LIST OF FIGURES

LIST OF TABLES

DECLARATION

*I, Peter Fletcher, confirm that the Thesis is my own work. I am aware of the University's Guidance on the Use of Unfair Means (**WWW.SHEFFIELD.AC.UK/SSID/UNFAIR-MEANS**). This work has not previously been presented for an award at this, or any other, university*

1 INTRODUCTION

1.1 MINIATURISATION OF OPTICAL DEVICES

Moore's law states as advances in technology are made the number of transistors on a microchip every two years will double [1]. This observation was due to the large drive to miniaturize electrical components to create more intricate devices. Research of optoelectrical technologies was initially focused on the opposite direction, to create larger scale devices due to the difficulties in growing group III-V semiconductors, for instance a light emitting diode (LED) was reported to have 1W light output over a $1mm^2$ area [2]. On the other hand, recent studies have shown an increased interest in micro and nano semiconductor devices since the discovery of vertical nanostructures that are free of extended defects. GaN based technologies are of particular interest with its wide bandgap and potential for higher internal quantum efficiency. This has made them suitable for a large range of miniaturised applications such as high-speed communications due to its thermal stability [2], high power density [3] and compatibility with other material technologies [4].

The main reason for the surge in miniaturisation of GaN devices is from two recent innovations [4]. Firstly, the ability to grow vertical nano structures such as core-shell LEDs make it possible for other forms of extreme miniaturisation [5]. Previous studies have struggled with converting lateral GaN devices because of the limitations to voltage breakdown capabilities, therefore the miniaturisation research for other III-V semiconductors is further advanced as they can overcome such obstacles [6]. The second innovation is the possibility of transferable optoelectronic GaN structures, using laser lift off methods [7] or electrochemical etching [8]. These GaN layers can be transferred from the sapphire substrates needed to grow high quality GaN onto silicon wafers for integrated devices [9] or flexible materials for wearable technologies [10]. Being able to transfer entire

wafer sized areas can introduce a whole new range of optoelectrical devices like the micro displays and nano sensors required for augmented reality technology.

As methods for miniaturisation of GaN based LEDs and InGaN variants devices become widely available, this should lead to successful new paths of research in superior micro displays and nano sensor devices.

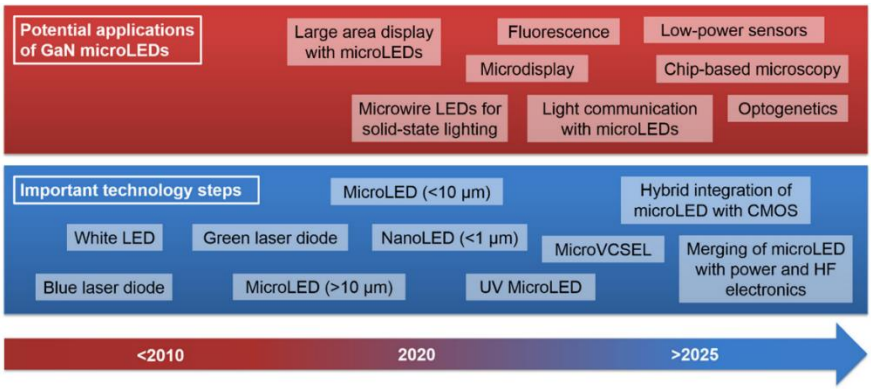

Figure 1.1 - Estimated roadmap for main technological milestones for GaN based micro-LEDs [4]

1.2 History of GaN based optoelectrical devices

Figure 1.1 has the estimated roadmap for GaN based micro-LED technologies for the next decade as well as the major milestones that have happened recently. GaN has been a focus of III-nitride semiconductor research for the past two decades due to its unique optical and electrical properties, such as having a wide energy bandgap (3.49 eV) [11], very high breakdown voltage and current density. Large scale growth of GaN was difficult since a suitable substrate with the required properties was hard to obtain. Si is widely available and can be integrated with other technologies but has the wrong lattice constant and SiC with a low lattice mismatch of 3% is too expensive for a substrate [12]. At the end of the 20th century the works of Akasaki and Nakamura [13] led to the wide use of the Metalorganic Chemical Vapour Deposition (MOCVD) growth method on sapphire substrate. Despite its

large lattice mismatch with GaN, (reported at 16%) [12], it is cheap, available in a single crystal in large sizes, stable at the high temperatures needed to grow high quality GaN, and transparent in the spectral range of GaN [14]. The other purpose of the experiments at the time was the creation of commercial grade blue and white LEDs. The incorporation of indium into GaN quantum wells has led to the ability to engineer the band gap of GaN based devices. In its basic state it has a bandgap corresponding to the ultraviolet (UV) range at 365nm, while doping with indium leads to a red shift of the band gap, leading to the creation of blue and longer wavelength LED emitters [15]. Currently, white LEDs are made by combining blue LEDs with a yellow phosphor coating creating white light. The process of creating white LEDs has several complex challenges in its current state, therefore there is a large drive to create an all GaN based white LED and the greater challenge of creating a white laser [16].

Further developments have been made towards GaN based laser diodes; the first blue continuous wave (CW) laser diode (LD) was reported by Nakamura [17] which used etched facets as mirrors to form the lasing cavity. Recent works have demonstrated the fabrication of green laser diodes above 500nm. For example, a CW 524nm LD was fabricated to operate at room temperature [18] using a higher indium content in c-plane InGaN multi quantum wells (MQWs) but the properties have been shown to be inferior to those of shorter wavelength counterparts. This is due to inbuilt strain induced piezoelectric fields from the lattice mismatch between InGaN and GaN that will be discussed in the next section [19].

Finally, advances in miniaturisation have led to current projects in making micro-LEDs and nano wire QWs. Top-down fabrication methods have attracted lots of attention, as a high degree of control can be achieved during the etching and lithography processes on bulk LED wafers [20]. Top-down fabrication is when a bulk material is etched down to the desired shape and size verses the bottom-up approach where we design a template and allow chemical and physical forces to form the structures from an atomic level. Typically, micro-LEDs are formed using hard material masks patterned via lithography, then finalised with a form of plasma dry etching such as inductively coupled plasma (ICP). Paramanik, et al reported the most common structures created using this method are micro and nano

columns and using these masks has enabled the easy creation of large wafers covered in these structures [22]. Unfortunately, using these dry etching techniques has often led to side wall damage from the ion bombardment [21], which causes an increase in the density of non - radiative recombination centres leading to limit in output efficiencies for structures less than 10um [23].

Creating a laser diode at the micro level has been difficult as it requires a cavity to be formed. While micro columns could be confined laterally from air, vertical confinement remained an obstacle. This was overcome by the use of free-standing micro disks, as undercutting the area under the MQWs exposes the bottom GaN layer, creating an air/GaN boundary that confines the light vertically [24]. This has allowed Whispering Gallery Modes (WGM) to form in the micro disks, a type of wave that forms within a circular structure [25]. With this approach micro disk lasing became viable, as the WGMs led to low lasing thresholds and the ability to support a range of wavelengths for multi peak lasing [26]. Other similar methods of forming micro-LEDs cavities are using a Distributed Bragg Reflector (DBR) under the MQWs to act as mirror surface [27]. While these methods also suffer from side wall damage that limit their effectiveness, they are one step closer creating large area micro-LEDs and towards the nanoscale.

1.3 GREEN/YELLOW GAP

Along with the issues of creating miniature GaN based devices, GaN has another limitation in creating longer wavelength MQWs. The difference in lattice constants between sapphire and GaN has led to further mismatches between GaN and InGaN MQW. This strain induced issues limit the amount of indium that can be incorporated into InGaN MQWs, and above 500nm devices have notably inferior properties to shorter wavelength counterparts leading to the colloquially called ‘Green/Yellow Gap’ [19].

At the moment a lot of research in GaN has gone into novel solutions towards solving this green/yellow gap problem. The main body of research has been towards solving the largest source of the lattice mismatch, which has been revealed to be from growing C-plane GaN. *C-plane* (0001) is the easiest direction to grow GaN on a-plane sapphire, though large strides have been made in mitigating this mismatch through use of buffer layers such as AIN [28] and IN [29], or even using strain releasing structures like superlattices (SL) and nanomembranes (NM). This difference creates a side effect in the active region made of InGaN quantum wells and GaN barriers, where there is reduced overlap between electron and hole wave-functions preventing short radiative recombination times which overall leads to low quantum efficiency. This side effect is called the Quantum Confined Stark Effect (QCSE). These effects are when strong spontaneous polarization occurs creating piezoelectric fields along the growth direction of the material which is along the c- plane direction due to the wurtzite structure of GaN [30]. This piezoelectric field causes the electron and holes wave-function to be forced apart, decreasing the wave-function overlap reducing the radiative recombination rate. Unfortunately, when growing alloys with high indium content these QCSEs become more prominent due to the increase in lattice mismatch, thereby reducing the effectiveness of these materials even more [31].

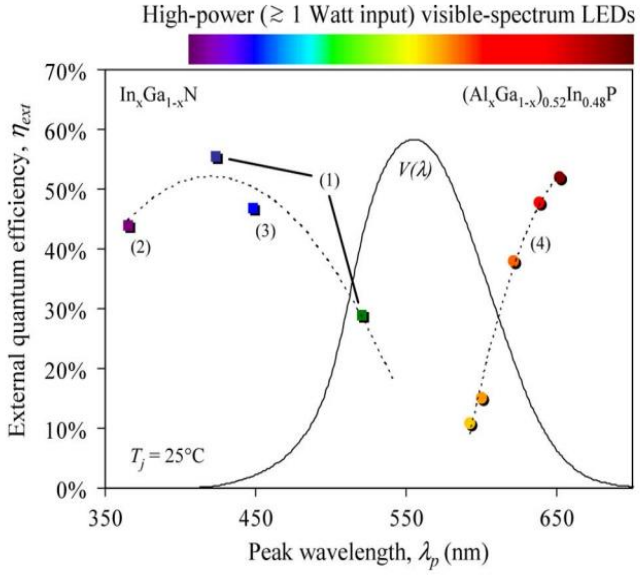

Figure 1.2 - External quantum efficiency for InGaN and AlGaNInP with varying indium and aluminium content respectively [32]

Another issue is that longer wavelength GaN based LEDs are created from the InGaN/GaN (MQW) layers and the amount of indium needed to red shifted the peak wavelength. Due to the growth conditions for higher indium incorporation, only *C-plane* MQWs have been able to create green wavelength LEDs. To create higher indium alloys there needs to be lower temperature and high flux ammonium gas during growth, but this also leads to a reduction in quality of *C-plane* LEDs as there is an increase in non-radiative centres and therefore a reduction of efficiencies [32]. **Figure 1.2** shows data collected of external quantum efficiencies of InGaN MQWs with increasing indium content and the decrease at longer wavelengths due to the higher amount of indium. Data for aluminum gallium indium phosphide (AlGaInP) is also shown as it is an alternative GaN based material by trying to create shorter wavelengths, towards the red side of the spectrum, with varying aluminium content. [33]

Changing the growth direction has been shown to be a promising solution to these problems. It can reduce the QCSE by mitigating how the polarization field effects the wave functions, also semi-polar has been shown to allow higher indium incorporation without reducing the quality of the LEDs. Semiconductors can be grown in other planes a- or m- but to date these have been inferior quality as the main difficulty in growing on these planes is that most techniques are designed for C-plane growth.

1.4 SEMI-POLAR AND NON-POLAR GAN

When grown in a plane perpendicular to c-plane such as (1120) and (1010) the electric fields disappear completely, creating non-polar GaN samples, as the electric field is no longer acting against the wave functions [33]. Semi-polar planes are grown inbetween the two extremes. This has led to difficulties in growing these planes as most techniques are designed for c-plane growth. **Figure 1.3** shows a series of orientations for growth with (a) being c-plane, (b) and (c) are examples of non-polar and (d)–(i) are various possible semi-polar orientations [34]. Semi-polar substrates can incorporate more indium due to the indium

atoms having a lower repulsive interaction allowing them to be grown at higher temperatures [35].

There are a large number of possible semi-polar orientations, but it is agreed that the plane must be inclined 45-60° for the best advantages of semi-polar GaN [36]. Wernicke et al [36] performed a series of experiments comparing the optical properties of MQW's grown on various semi-polar GaN substrates, focusing on (10-11), (10-12), (11-22) and (20-21). Using photoluminescence (PL) they were able to measure the emission energies of substrates grown at the same temperature (750°c). By measuring the redshift of the peak wavelength, they found that (11-22) and (10-11) have the highest emission energy compared to the amount of indium in the alloy.

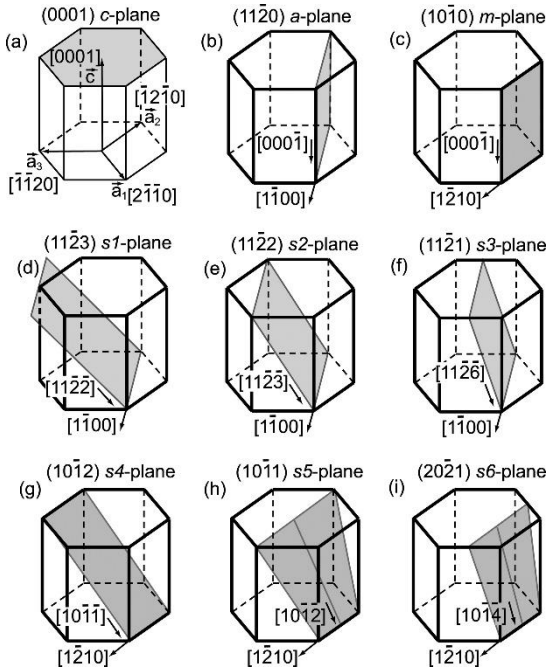

Figure 1.3 - Schematics of crystallographic planes of common semi and non-polar GaN [34]

1.5 BRIEF HISTORY OF SEMI-POLAR GAN

Growths of (11-22) semi-polar GaN onto sapphire substrates generally suffer from a high density of dislocations and basal stacking faults. Therefore, many current techniques use tilted substrates to grow better quality semi-polar samples. For example, to create (11-22) GaN it requires a theoretical angled substrate of 58°. Okada et al [37] reported that by etching a series of stripes onto r-sapphire, the resultant angle from the planar axis will be 57.6°. This means that the growth of semi-polar GaN can be achieved along the patterned sapphire with c-plane growth direction, which helps integration with current techniques.

Another technique is the use of nanorods as a scaffold for growing semi-polar and non-polar samples, as shown by Xing et al [38]. By depositing a layer of SiO2 and Ni as a mask and creating a nano rod layer by etching techniques, semi-polar GaN can be grown directly onto standard m-plane sapphire, without the need for etching sapphire. These nanorods act as a scaffold for any further overgrowth, the overgrown GaN fills in the gaps between nanorods and creates a higher quality semi-polar layer above the SiO2 layer. The SiO2 is used to prevent any further growth on top of the nanorods that can interfere with the semi-polar structure. **Figure 1.4a** is an SEM image of the nanorods before overgrowth and **figure 1.4b** is the overgrown semi-polar layers; the holes are gaps between the nanorods that did not fill in properly.

This is very important work as recently long wavelength emitters have gained attention due to the applications in optogenetics [39]. III-nitride emitters with long wavelengths have been shown to be able to manipulate neurons which can assist in understanding neural circuit behaviours. This is vital in finding a solution to curing Parkinson's disease and mood disorders [40].

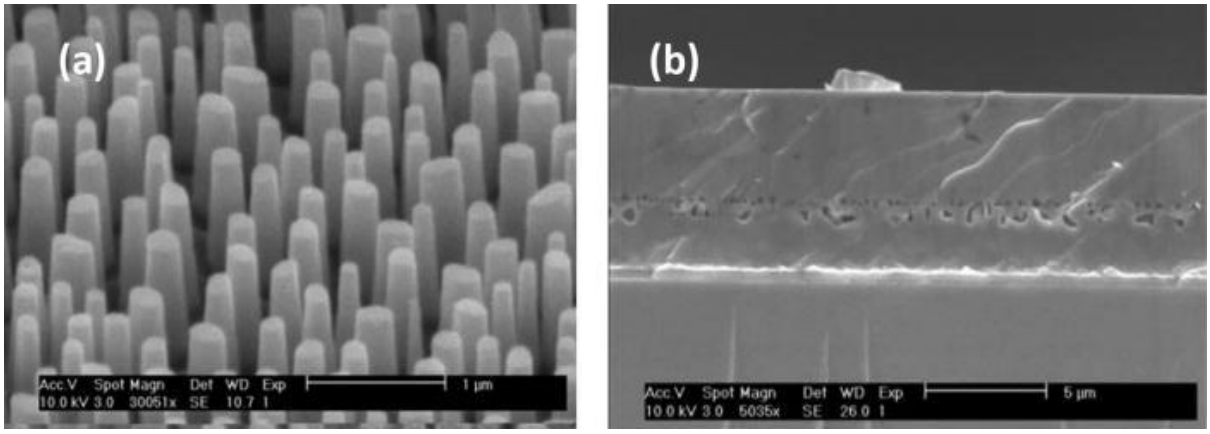

Figure 1.4 – (a) SEM image of nanorods used to grow semi-polar GaN (b) SEM image of other grown semi-polar GaN [37]

1.6 THESIS OUTLINE

The research presented in this PhD thesis is the development of a new overgrowth method for creating GaN based micro disk arrays. This method was created with the hypothesis of reducing the side wall damage that occurs during top-down methods and which limits the efficiency and optical properties of micro disks. Initial wafers were designed and grown from bulk InGaN/GaN LED recipes, and a range of photoluminescence measurements were carried out to refine the recipes. Through such investigations new growth structures such as superlattices and distributed Bragg reflectors were added to improve the quality and optical properties. Chapter 4 details the development of arrays from bulk LEDs to ultra-efficient micro disk arrays and the formation of whispering gallery modes (WGM).

Chapter 5 describes attempts to transform these arrays into lasers by creating a lasing cavity with the addition of a dielectric DBR on top of the MQW. Supplementary photoluminescence and reflection studies were used to confirm the effects of the dielectric DBR as well as refinement of the stop band.

Chapter 6 describes a systematic study into the difficulties of creating smaller micro disks with uniform arrays through a combination of finite difference time domain simulations (FDTD) and photoluminescence mapping. This study will allow us to further advance techniques to grow high quality micro disk arrays and lasers.

I would greatly like to express my acknowledgement to all members of the Centre of GaN and Device at the University of Sheffield who contributed to my PhD projects. All samples were grown by Chenqi Zhu and Peng Feng. Guillem Martinez de Arriba and Nicolas Poyiatzis fabricated devices into electrical arrays. Ye Tian etched and developed our nano porous DBRs. Professor Tao supervised and helped advance the project.

I performed all the optical measurements in chapters 4, 5 and 6 using a variety of photoluminescence techniques and reflectivity. In chapter 6 a large amount of the project was done through FDTD simulations which I performed but was taught and helped by Guillem Martinez de Arriba.

1.7 REFERENCES

[1] Moore, G. E., (1998) *Cramming More Components onto Integrated Circuits.* Proceedings of the IEEE, **86**(1), 82–85. https://doi.org/10.1109/JPROC.1998.658762

[2] Hahn, B., Galler, B., and Engl, K. (2014) *Development of high-efficiency and high-power vertical light emitting diodes*, Jpn. J. Appl. Phys., Part 1 **53**(10), 100208

[3] Wun, J.-M., Lin, C.-W., Chen, W., Sheu, J.-K., Lin, C.-L., Li, Y.-L., Bowers, J.E. Shi, J.-W., Vinogradov, J. Kruglov, R. & Ziemann, O. (2012) *GaN-Based Miniaturized Cyan Light-Emitting Diodes on a Patterned Sapphire Substrate with Improved Fiber Coupling for Very High-Speed Plastic Optical Fiber Communication*. IEEE Photonics Journal, **4**(5), 1520–1529. https://doi.org/10.1109/JPHOT.2012.2210867

[4] Nikoo, S., Jafari, A., & Matioli, E. (2019) *GaN Transistors for Miniaturized Pulsed-Power Sources*. IEEE Transactions on Plasma Science, **47**(7), 3241–3245. https://doi.org/10.1109/TPS.2019.2917657

[5] Wasisto, T., Prades, J. D., Gülink, J., & Waag, A. (2019) *Beyond solid-state lighting: Miniaturization, hybrid integration, and applications of GaN nano- and micro-LEDs*. Applied Physics Reviews, **6**(4), 41315. https://doi.org/10.1063/1.5096322

[6] Li, W., & Waag, A. (2012) *GaN based nanorods for solid state lighting. Journal of Applied Physics*, **111**(7), 071101–071101–23. https://doi.org/10.1063/1.3694674

[7] Mantooth, H. A., Glover, M. D., & Shepherd, P. (2014) *Wide Bandgap Technologies and Their Implications on Miniaturizing Power Electronic Systems*. IEEE Journal of Emerging and Selected Topics in Power Electronics, **2**(3), 374–385. https://doi.org/10.1109/JESTPE.2014.2313511

[8] Kelly, M.K. et al. (1999) *Large Free-Standing GaN Substrates by Hydride Vapor Phase Epitaxy and Laser-Induced Liftoff*, Japanese Journal of Applied Physics, **38**(Part 2, No. 3A), pp. L217–L219. doi:10.1143/JJAP.38. L217.

[9] Kang, J.-H., Jeong, D.K. and Ryu, S.-W. (2017) *Transparent, Flexible Piezoelectric Nanogenerator Based on GaN Membrane Using Electrochemical Lift-Off*, ACS applied materials & interfaces, **9**(12), pp. 10637–10642. doi:10.1021/acsami.6b15587.

[10] Liu, L., Chong, W. C., Wong, K. M., & Lau, K. M. (2015) *GaN-based LED micro-displays for wearable applications*. Microelectronic Engineering, **148**, 98–103. https://doi.org/10.1016/j.mee.2015.09.007

[9] Shervin, S., et al. (2021) *Flexible single-crystalline GaN substrate by direct deposition of III-N thin films on polycrystalline metal tape*, Journal of materials chemistry. C, Materials for optical and electronic devices, **9**(7), pp. 2243–2251. doi:10.1039/d0tc04634e.

[10] Runton, D. W., Trabert, B., Shealy J.B., and Vetury, R. *History of GaN: High-Power RF Gallium Nitride (GaN) from Infancy to Manufacturable Process and Beyond*, in IEEE Microwave Magazine, vol. **14**, no. 3, pp. 82-93, imsspecialissuemay 2013. doi: 10.1109/MMM.2013.2240853

[11] Melton, W., and Pankove, J. (1997) *GaN growth on sapphire*. Journal of Crystal Growth, **178**(1-2), pp.168-173.

[12] Heber, J. (2014) Nobel Prize 2014: Akasaki, Amano & Nakamura. Nature Physics, **10**(11), pp.791-791.

[13] Grandjean, N., Massies, J., Martinez, Y., Vennéguès, P., Leroux, M. and Laügt, M. (1997) *GaN epitaxial growth on sapphire (0 0 0 1): the role of the substrate nitridation*. Journal of Crystal Growth, **178**(3), pp.220-228

[14] Nakamura, S., Mukai, T., and Senoh, M., (1994) *Candela-class high brightness InGaN/AlGaN double-heterostructure blue-light emitting diodes* Appl. Phys. Lett. **64** 1687

[15] Jia, H., Guo, L., Wang, W. and Chen, H. (2009) *Recent Progress in GaN-Based Light-Emitting Diodes*. Adv. Mater., **21**: 4641-4646. https://doi.org/10.1002/adma.200901349

[16] Nakamura, S. (1997) *CW operation of InGaN MQW laser diodes* Digest of the IEEE/LEOS Summer Topical Meeting: Vertical-Cavity Lasers/Technologies for a Global Information Infrastructure/WDM Components Technology/Advanced Semiconductor Lasers and Application, 1997, pp. 19-20, doi: 10.1109/LEOSST.1997.619242.

[17] Avramescu, A., Lermer, T., Müller, J., Eichler, C., Bruederl, G., Sabathil, M., Lutgen, S. and Strauβ, U. (2010*) True green laser diodes at 524 nm with 50 mW continuous wave output power on c-plane GaN* Appl. Phys. Express **3** 061003

[18] Wang, T. (2016) *Topical Review: Development of overgrown semi-polar GaN for high efficiency green/yellow emission.*

[19] Q, Li., et al., (2011) *Optical performance of top-down fabricated InGaN/GaN nanorod light emitting diode arrays*, Opt. Express **19**(25), 25528

[20] Lee, J.-M., Chang, K.-M., Kim, S.-W., Huh, C., Lee, I.-H., and Park, S.-J. (2000) *Dry etch damage in n-type GaN and its recovery by treatment with an N2 plasma* J. Appl. Phys. **87**(11), 7667–7670

[21] Paramanik, A., Motayed, A., Aluri, G. S., Ha, J.-Y., Krylyuk, S., Davydov, A. V., King, M., McLaughlin, S., Gupta, S., & Cramer, H. (2012*) Formation of large-area GaN nanostructures with controlled geometry and morphology using top-down fabrication scheme*. Journal of Vacuum Science & Technology B: Microelectronics and Nanometer Structures, **30**(5), 52202. https://doi.org/10.1116/1.4739424

[22] Tamboli, A.C., Haberer, E. D., Sharma, R., Lee, K.H., Nakamura, S., and Hu, E. L. 2007 *Room-temperature continuous-wave lasing in GaN/InGaN microdisks*, Nat. Photonics **1**, pp. 61–64,

[23] Lee, I.-H., Kim, T.-H., Polyakov, A. Y., Chernykh, A. V., Skorikov, M. L., Yakimov, E. B., Alexanyan, L. A., Shchemerov, I. V., Vasilev, A. A., & Pearton, S. J. (2022). Degradation by sidewall recombination centers in GaN blue micro-LEDs at diameters<30 μm. *Journal of Alloys and Compounds*, ***921***, 166072. https://doi.org/10.1016/j.jallcom.2022.166072

[24] Zhu, G., Li, J., Zhang, N. et al. (2020) *Whispering-Gallery Mode Lasing in a Floating GaN Microdisk with a Vertical Slit*. Sci Rep **10**, 253 https://doi.org/10.1038/s41598-019-57118-y

[25] Athanasiou, M., et al. (2017) *Monolithically multi-color lasing from an InGaN microdisk on a Si substrate*

[26] Ng, H. M., Moustakas, T. D., and Chu, S. N. G., (2000) *High reflectivity and broad bandwidth AlN/GaN distributed Bragg reflectors grown by molecular-beam epitaxy*, Appl. Phys. Lett. 76, pp. 2818–2820.

[27] Amano, H., Sawaki, N., Akasaki, I. and Toyoda, Y. (1986). *Metalorganic vapor phase epitaxial growth of a high quality GaN film using an AlN buffer layer.* Applied Physics Letters, **48**(5), pp.353- 355.

[28] Kachi, T., Tomita, K., Itoh, K. and Tadano, H. (1998). *A new buffer layer for high quality GaN growth by metalorganic vapor phase epitaxy. Applied Physics Letters*, **72**(6), pp.704-706.

[29] Takahashi, K., Yoshikawa, A., Sandhu, A., Ishitani, Y., and Kawakami, Y. (2007) *Wide, bandgap semiconductors: Fundamental properties and modern photonic and 21 electronic devices.* (Springer Berlin Heidelberg, 2007).

[30] Barthel, S., Schuh, K., Marquardt, O., Hickel, T., Neugebauer, J., Jahnke, F., and Czycholl, G., (2013). *Interplay between Coulomb interaction and quantum-confined Stark-effect in polar and nonpolar wurtzite InN/GaN quantum dots*. The European Physical Journal B, 86(11).

[31] Krames, M. et al. (2007) *Status and Future of High-Power Light-Emitting Diodes for Solid-State Lighting', Journal of display technology*, 3(2), pp. 160–175. doi:10.1109/JDT.2007.895339.

[32] Romanov, A. E., Young, E. C., Wu, F., Tyagi, A., Gallinat, C. S., Nakamura, S., DenBaars, S. P., and Speck, J. S., (2011) *Basal plane misfit dislocations and stress relaxation in III-nitride semipolar heteroepitaxy* J. Appl. Phys. 109 103522

[33] Zhuang, Iida, D., & Ohkawa, K., (2021). *InGaN-based red light-emitting diodes: from traditional to micro-LEDs*. *Japanese Journal of Applied Physics*, *61*(SA), SA0809. https://doi.org/10.35848/1347-4065/ac1a00

[34] Feezell, D.F., et al. (2009) *Development of Nonpolar and Semipolar InGaN/GaN Visible Light-Emitting Diodes*, MRS bulletin, 34(5), pp. 318–323. doi:10.1557/mrs2009.93.

[35] Ooi, Y. K. & Zhang, J. *Design analysis of phosphor-free monolithic white lightemitting-diodes with InGaN/ InGaN multiple quantum wells on ternary InGaN substrates*. AIP Adv. 5, 057168 (2015)

[36] Wernicke, T., Schade, L., Netzel, C., Rass, J., Hoffmann, V., Ploch, S., Knauer, A., Weyers, M., Schwarz, U. and Kneissl, M. (2012) *Indium incorporation and emission wavelength of polar, nonpolar and semipolar InGaN quantum wells*. Semiconductor Science and Technology, **27**(2), p.024014

[37] Okada, N., Kurisu, A., Murakami, K., and Tadatomo, K. (2009) *Growth of semi polar (11-22) GaN layer by controlling anisotropic growth rates in r-plane patterned sapphire substrate* Appl. Phys. Express 2091001

[38] Xing, K., Gong, Y., Bai, J. and Wang, T. (2011) *InGaN/GaN quantum well structures with greatly enhanced performance on a-plane GaN grown using self-organized nano-masks*. Applied Physics Letters, **99**(18), p.181907.

[39] Yizhar, O., et al., (2011) *Optogenetics in Neural Systems*, Neuron **71**, 9–34

[40] Lammel, S., Tye, K. M. & Warden, M. R. (2014) *Progress in understanding mood disorders: Optogenetic dissection of neural circuits*, Genes, Brain Behav. **13**, 38–51

2 BACKGROUND

2.1 SEMICONDUCTORS

In terms of electrical conductivity materials are either conductors, insulators, or semiconductors. Semiconductors have an electrical conductivity value between a conductors and insulators, where carriers are can only flow between the valance and conduction bands when the required energy is given to excite the electrons. This energy requirement is the definition of the bandgap in at materials and it is the main factors in determining the electrical and optical properties of semiconductors [1]. Conductive materials, such as metals have the defining property where the carriers in the conduction bands are able to move freely. The large overlap between valence and conduction bands allows this free movement to occur with without any extra input energy needed to overcome band gap differences even at room temperature, therefore it has no meaningful bandgap [2] Insulators have a very large band gap that makes it impossible for the carriers to ever cross leading to very small electrical conductivity values [3]. The variation in band gaps is given in the band gap diagram **Figure 2.1**. The Fermi level is a theoretical energy state that is the highest energy level an electron can exists in at absolute zero. At higher temperatures it is the energy level where probability of finding an electron is 50%. This level is usually found in between the conduction and valance band as at 0K the electrons remain in their lowest energy state [4].

Electrical conductivity is a measure of how easy the electric current can flow through the material and the reciprocal of electrical resistivity. It is defined by **Equation 2.1**

Equation 2.1 $\sigma = ne\mu_n + pe\mu_p$

E is the electronic charge of 1.6 x 10^{19} C, μ_n and μ_p is carrier mobility and n and p is electron and hole concentration respectively [5]. Conductors typically have a very large electrical conductivity value above 10^7 S/m [6] whereas insulators have low conductivity values

reported to 10^-14 S/m [7] but materials can still be considered insulators with values around 10^{-3} S/m [8].

Semiconductors have been shown to have greatest flexibility in thermal conductivity and therefore exhibit the largest variance in optoelectrical properties allowing them to be used for a wide range of applications.

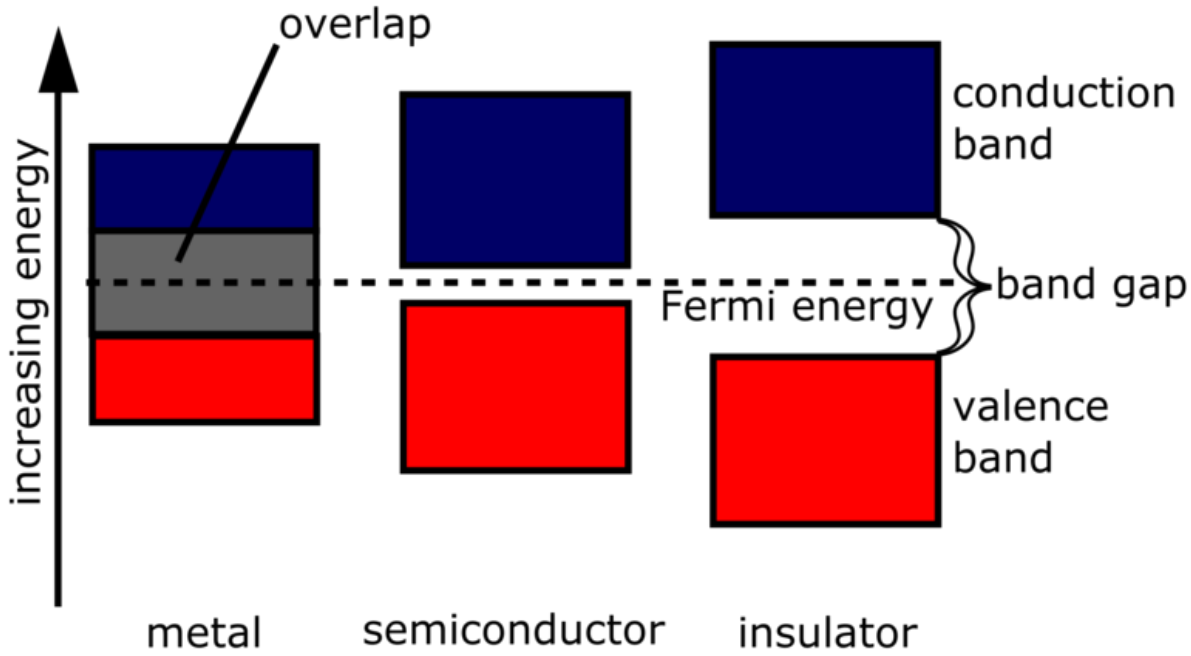

Figure 2.5 - Band diagrams of conductors, semiconductors, and insulators with the definition of the fermi energy [9]

2.2 BAND STRUCTURE

In semiconductors the bandgap comes in two forms either direct or indirect. The minimal energy level in the conduction band and maximum state in the valence band are defined by the k-vector. Direct band gaps have similar k-vectors for both bands at k= 0, while indirect band gaps have different k-vectors [10] **Figure 2.2** shows the band diagrams of direct and indirect semiconductors where eF is the fermi energy. Fermi energy is the energy level in which has a 50% probability of being occupied at 0K [11]. This means that indirect band gaps require an extra particle during its optical transitions during electron-hole recombination to maintain crystal momentum. These extra particles are known as phonons

which are quasiparticles that describe a quantised vibrational wave similar to how photons are a quantised light wave [12].

Radiative recombination is the process in which an excited electron moves towards the conduction band from the valance band, creating an electron-hole pair [13]. This will recombine as the electron decays to a lower energy level, emitting a photon of a similar value to the band gap. In direct semiconductors this is exactly how the process occurs as long as the electron has a k-vector near to the minimum. In indirect semiconductors this is impossible as it requires the absorption and emission of phonons, and the phonons has to have a momentum equal to the difference in the electron-hole momentums [13]. Many indirect semiconductors can also use defect assisted emissions, but due to the slow radiative recombination times, materials such as silicon are unlikely to be used for structures like light emitting diodes.

Examples of direct bandgap semiconductor include the majority of III-nitride semiconductors like GaN, AlN and InN.

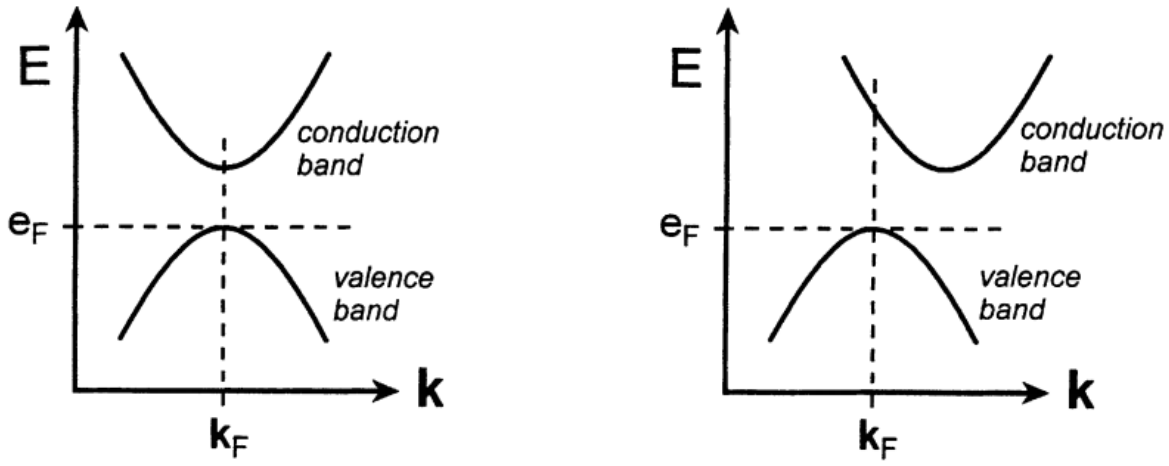

Figure 2.6 - band diagrams of direct and indirect semiconductors [13]

2.3 III – NITRIDE SEMICONDUCTORS

Crystal structure of Group III – Nitrides generally come in three different types of wurtzite, zincblende and rock salt. [14] Bulk GaN, InN and AlN typically have wurtzite structure with a hexagonal unit cell with two lattice constants *c* and *a*. [15] ZnS typically has a cubic zincblende structure with a similar unit cell to that of diamond. The difference of the two types of structures is shown in **Figure 2.3**. [16] Rocksalt structures can only form under high pressures and cannot be grown through normal epitaxial growth, which is undesirable for many applications [17]. Lattice parameters *a* and *c* are used to define the unit cell for GaN which typically is grown in the (0001) *C – plane*, here a parameter is defined in the basal plane direction and the *c* parameter is perpendicular. These were experimentally observed to have *a* and *c* parameter of 3.199Å and 5.186 Å. [18]

Gallium Nitride (GaN) is a wide direct bandgap semiconductor, with an observed band gap at 3.4eV. The material has a high heat capacity and large refractive index of 2.429.[19] This is then suitable for a wide range of applications in optoelectronics. GaN has superior electrical properties compared to other group III-nitrides such as high breakdown field, 5MV/cm, [20] and thermal conductivity, 2.1 $Wcm^{-1}K^{-1}$, [21] Most GaN can be epitaxial grown via metalorganic chemical vapor deposition (MOCVD) on sapphire even with the large lattice mismatch with large dislocations density above 10^8 cm^{-2}. The growth can be modified with dopants either silicon (Si) [33] to produce n-type and magnesium (Mg) [34] for p-type.

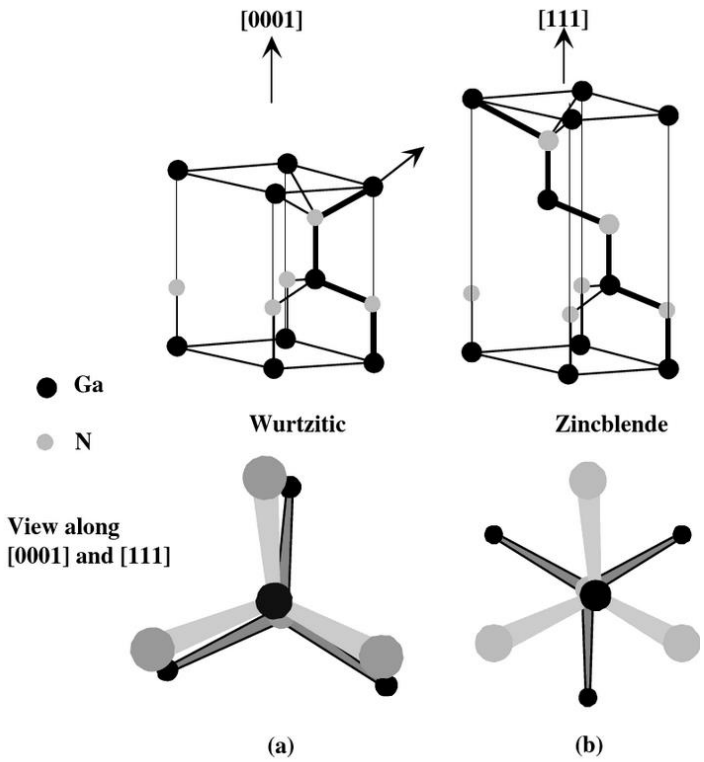

Figure 2.7- ball and stick models of wurtzite and zincblende. The main directions describe the growth directs show these crystal types (a) [0001] and (b) [111] respectively [14]

2.4 LIGHT EMITTING DIODES

Light emitting diodes (LEDs) are simple p-n junction devices that converts electrical power to visible light, through spontaneous emission [22]. The wavelength of the emitting photons is determined by the bandgap of the active region. It has a wide range of applications in all parts of life and can be made from Group III-nitride semiconductors. [paper] Modern LEDs consists of a double heterojunction with an active region being the only layer that absorbs electrons and generates photons in random directions. A typical GaN based LED has an active region with InGaN multiple quantum wells (MQWs) with GaN barriers sandwiched between p- GaN and n-GaN [23]. A current spreading layer is used to ensure current is spread through the device rather than bottlenecking down the path with the smallest resistivity [25]. **Figure 2.4** provides a schematic of a standard InGaN LED structure.

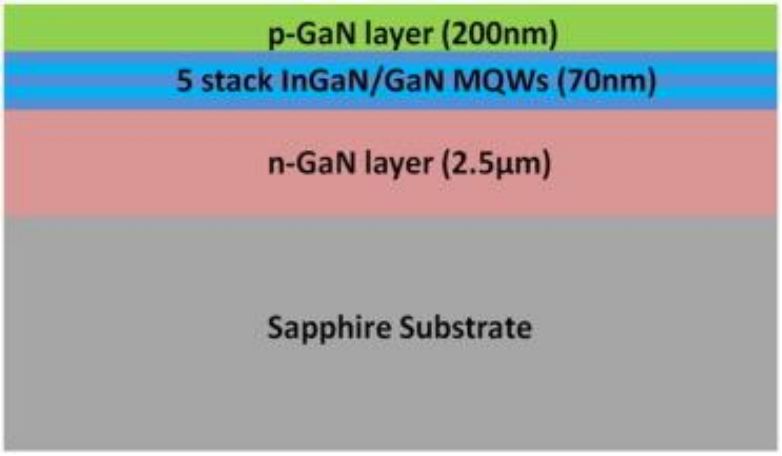

Figure 2.8 - Cross sectional diagram of a standard InGaN LED [24]

2.5 MULTI QUANTUM WELLS

Multi quantum wells (MQWs) are a type of 2D quantum confined structure that is confined in the vertical direction [27]. Usually, these structures consist of a small bandgap layer surrounded by large band gap layers acting as barriers to create a confined structure. In the case of InGaN/GaN MQW the InGaN is the emitting layer with the GaN layers acting as barriers, multiple of these pairs can be used to increase the intensity of light emitted by the LED [26]. Other low dimensional structures exhibit quantum confinement defined on the number of dimensions at which the confinement happens. For instance, a quantum wire is confined in the Z and Y axis and a quantum dot is limited in all three axes, as shown in **Figure 2.5** [28].

There are three main approaches towards growing MQWs; lattice matched, strain-balanced and strained systems [28]. In lattice matched systems [29] the quantum wells and barriers have matching lattice constants along with the substrate, this is the ideal growth conditions for creating high efficiency structures. Strain – balanced systems maintain a balance between the lattice constants between the MQW structures and the growth substrate, this allows the most flexibility in design [30]. Though this has an increased complexity due to the balancing of the various thicknesses of each layer. Finally strained

systems have completely different lattice constants in the structure resulting in limitations in growth efficiencies [31].

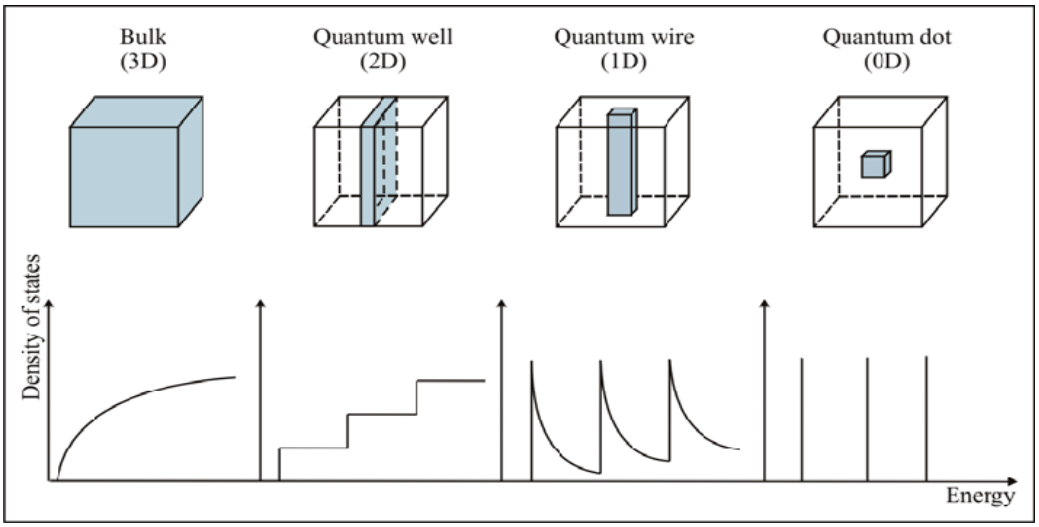

Figure 2.9 - Schematic of low - dimensional structures along with graphs showing the density of energy states vs Energy, showing how energy states are shaped at lower dimensional structures [28]

2.6 LASER THEORY

Lasers of Light Amplification of Simulated Emission of Radiation are characterised are monochromatic, high directional and coherent. This means any light source that emits a narrow emission spectrum, with emitted photons moving the same direct and in the same phase [35]. All lasers require a light source, optical cavity and an optical couple or waveguide. The light source leads to the main different types of lasers, laser diodes, gas, and dye. Gas lasers have gas filled tubes inside the laser cavity, the light comes from an electrical current which excites the gas to produce coherent light. Dye lasers have an organic dye in a liquid solution ac the active medium. Finally, laser diodes use semiconductors using MQWs with in the optical cavity to amplify the emitted light.

The optical cavity reflects the emitted light back at itself creating a standing wave as the light interferes only certain energies and frequencies will resonate. These energies are called resonant modes and at these modes the light will amplify through stimulated emission. Stimulated emission occurs through a series of step that is shown in **Figure 2.6**. First, an incident photon excites an electron to an excited level. Then, during radiative recombination emission, a passing photon acts as an electric field increasing the likelihood that the excited photon undergoes radiative recombination. The newly emitted photons are emitted with the same wavelength, direction, and phase as the passing photon. This creates a feedback loop that will form as the chances for stimulated emission increase, this continues until the number of carriers in a mode exceed that in the lower energy states forming population inversion. At this point light can escape through an optical coupler forming a laser beam [35].

Embedding MQWs within different optical cavities can form a variety of laser modes such as whispering gallery for circular cavities of Fabre Perot for linear one.

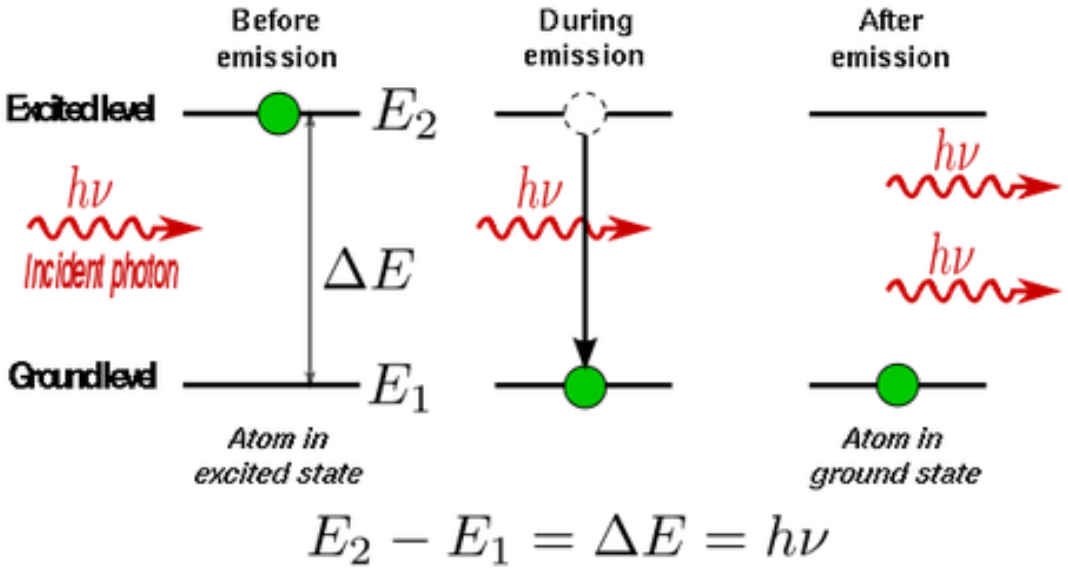

Figure 2.10 - Diagram shows the process of stimulated emission. First an incident photon (with an energy (hν)) excites an electron from ground level (E_1) to an excited level (E_2) with an energy difference (ΔE) equal to the incoming photon. Then during radiative emission another photon interacts with the recombining exciton. This forces the new emitted photons to have similar properties as the incoming photon [35]

2.7 VERTICAL CAVITY SURFACE EMITTING LASERS

Vertical cavity surface emitting lasers (VCSELs) are a type of laser diode with emission perpendicular towards the top surface [36]. This is different for other standard edge emission diodes which emits in plane by cleaving the LEDs to reveal the active region. The VCSEL structure was first proposed by Professor Kenichi Iga [37] in 1977. It used an active region between two distributed Bragg reflectors (DBR) parallel to the wafer surface, creating an optical cavity between the mirror like surfaces. DBRs are to integrate it with electrical devices the bottom and top DBRs can be n and p doped respectively to create a p-n junction or these layers can be embedded around the active region.

Recently GaAs was the main material used in VCSEL; chosen for the creation of VCSELs due to the large refractive index difference and little lattice mismatch [38]. But due to the developments of MOCVD growth for GaN and InGaN has allow the creation of entirely epitaxial grown DBR structures [39]. There are three approaches toward DBR growth for VCSELs entirely epitaxial, hybrid epitaxial/dielectric and double dielectric DBRs. Schematic examples of the three approaches are shown in **Figure 2.7** showing the average number of layers for the different types of DBRs.

Fully epitaxial grown DBRs has the theoretical superior efficiency due to the entire structure being composed of GaN based layers, but as previously stated the large lattice mismatch between InGaN and GaN leads to limitations in growth conditions and band gap

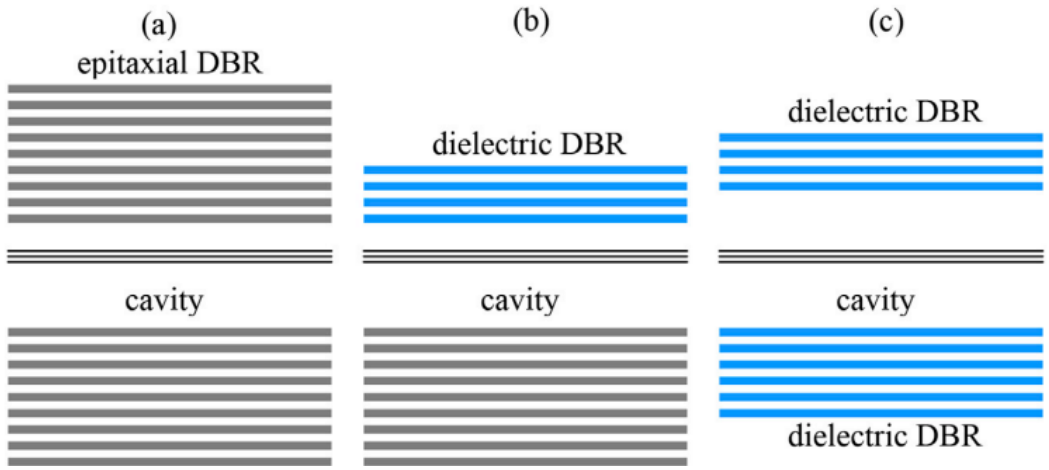

Figure 2.11 - (a) epitaxial/epitaxial DBR cavity (b) hybrid epitaxial/dieletric DBR cavity (c) dieletric/ dielectric DBR cavity [36]

engineering. Further additional growth on top of the MQW can lead to indium phase separation in the active region disrupting the lasing modes [40]. Double dielectric DBRs can lead to relaxed structure as the active region needs to be transferred via laser lift off techniques onto different substrates. This is a complex fabrication process due to the multiple steps needed for the laser lift off entire wafers followed by wafer bonding with the new substrate [41]. Hybrid DBRs offer a compromise between the two other techniques and is the most flexible toward a large range of applications.

Current studies of GaN based VCSELs have reported several obstacles in developing commercial grade devices. The obvious is the growth issues of integrating highly reflective DBRs while maintaining the highly efficient MQW needed for lasers with low thresholds and high Q- factors. Commonly used DBRs include dielectric TiO_2 / SiO_2 which while allow > 95 reflectance does not allow current to pass through it [42]. This leads to the other issue integrating these devices with current technologies to create electrically pumped VCSELs, while the first GaN based electrically pumped VSCEL with a hybrid epitaxial/dielectric DBR pair has been demonstrated it has reported the need for several buffer layers to reduce the internal optical loss from growth issues [43].

2.8 FREE STANDING GAN MICRO DISK LASERS

While the use of dual DBR layer have been the most common use of creating VSCELs, an alternative method has been addressed that will allow a simpler way to create the highly confined optical cavities. Micro disks have of great focus due to the ease of creating high quality WGM and low power consumption [44]. Optical pumped micro disk lasers were reported by under cutting the micro disk to increase the vertical confinement due to the large refractive index difference between GaN (2.41) [45] and air (1) [46], SEM images of such structure is shown in **Figure 2.8**.

Recent studies have reported successes on growing low threshold lasers in both blue [47] and green [48] wavelength. Unfortunately, many of these studies report limitations to the

micro disk properties due to the severe sidewall damage from the top-down fabrication method usually done by using inductively coupled plasma (ICP) etching [49].

Other issues are the difficulty to electrically inject the micro disks, due to the limited ways to make contact with the active regions. Laterally the under-cut shape prevents an easy circuit toward the p and n layers like in normal LEDs and the substrate to MQW path through the supporting pedestal makes current injection very difficult [50]. Also, the AlN buffering layers needed to reduce the cracks during growth have high resistivity reducing electrical conductivity and blocking any vertical electrical injection from happening [52]. There are limited examples of electrically induced GaN micro disk with reduced properties compared to optical counterparts.

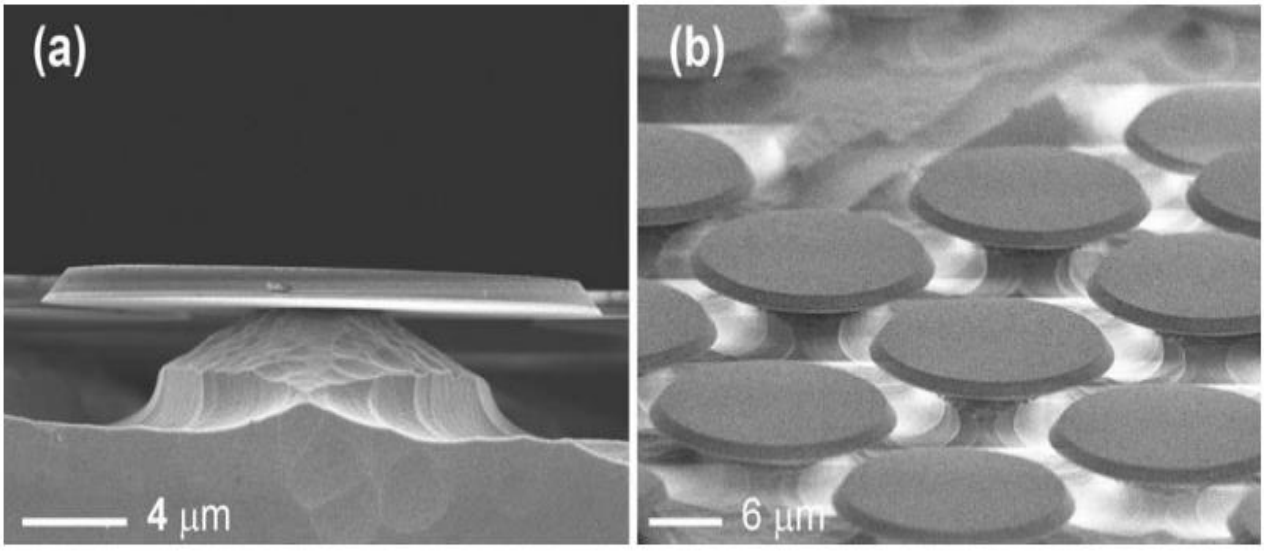

Figure 2. 12 - (a) Cross sectional SEM images of free-standing micro disks (b) Top view of micro disk array [52]

2.9 REFERENCES

[1] HyperPhysics September 26, (2015) *Band Theory of Solids* [Online]. Available: http://hyperphysics.phy-astr.gsu.edu/hbase/solids/band.html

[2] Shockley, William (1950) *Electrons and holes in semiconductors: with applications to transistor electronics*. R. E. Krieger Pub. Co. *ISBN 978-0-88275-382-9*.

[3] Yu, P. (2010) *Fundamentals of Semiconductors* Berlin: Springer-Verlag *ISBN 978-3-642-00709-5.*

[4] Callister, W. D., & Rethwisch, D. G. (2010) *Materials Science and Engineering: An Introduction. Eighth Edition* John Wiley & Sons, Inc.

[5] Kittel, C. (2005) *Introduction to solid state physics* (Eighth edition.). Wiley

[6] Lu, L., Shen, Y., Chen, X., Qian, L., & Lu, K. (2004) *Ultrahigh Strength and High Electrical Conductivity in Copper*. Science American Association for the Advancement of Science, **304**(5669), 422–426. https://doi.org/10.1126/science.1092905

[7] Transmission Lines data. Transmission-line.net. [Accessed 2022-03-20]

[8] Rajagopal, C., & Satyam, M. (1978) *Studies on electrical conductivity of insulator-conductor composites,* Journal of Applied Physics, **49**(11), 5536–5542. https://doi.org/10.1063/1.324474

[9] Abedin, M. (2015) *A SELF-ADJUSTING LIN-LOG ACTIVE PIXEL FOR WIDE DYNAMIC RANGE CMOS IMAGE SENSOR*. 10.13140/RG.2.1.3871.8965.

[10] Cassabois, G., Valvin, P., & Gil, B. (2016) *Hexagonal boron nitride is an indirect bandgap semiconductor* Nature Photonics, **10**(4), 262–266. https://doi.org/10.1038/nphoton.2015.277

[11] Nave, R*. Fermi Energies, Fermi Temperatures, and Fermi Velocities HyperPhysics.* [Accessed 2020-03-21*]*

[12] Martín, P., Raúl, Martínez-Duart, José (2017) *Survey of Solid-State Physics and Quantum Mechanics* 10.1016/B978-0-323-46176-4.00002-X.

[13] Dumke, W.P. (1957) *Spontaneous radiative recombination in semiconductors* Physical Review, **105**(1), 139–144. https://doi.org/10.1103/PhysRev.105.139

[14] Morkoç, H., and Hadis M. (2013) *Nitride Semiconductor Devices, Nitride Semiconductor Devices: Fundamentals and Applications*, John Wiley & Sons, Incorporated. *ProQuest Ebook Central*, http://ebookcentral.proquest.com/lib/sheffield/detail.action?docID=1174136.

[15] Smith, A. R., and Feenstra, R. M., *Determination of wurtzite GaN lattice polarity based on surface reconstruction* Appl. Phys. Lett. **72**, 2114 (1998); https://doi.org/10.1063/1.121293

[16] Winiarski, & Kowalska, D. A. (2020). *Crystal structure of rare earth and group III nitride alloys by ab initio calculations*. Scientific Reports, **10**(1), 16414–16414. https://doi.org/10.1038/s41598-020-73405-5

[17] Xia, H., Xia, Q. & Ruoff, A. L., (1993) *High-pressure structure of gallium nitride: Wurtzite-to-rocksalt phase transition*. Phys. Rev. B **47**, 12925–12928

[18] Bougrov V., Levinshtein M.E., Rumyantsev S.L., Zubrilov A., (2001) in *Properties of Advanced Semiconductor Materials GaN, AlN, InN, BN, SiC, SiGe*. Eds. Levinshtein M.E., Rumyantsev S.L., Shur M.S., John Wiley & Sons, Inc., New York , 1–30

[19] Takahashi, K., Yoshikawa, A., Sandhu, A., Ishitani, Y. & Kawakami, Y., (2007) *Wide bandgap semiconductors: Fundamental properties and modern photonic and electronic devices.* (Springer Berlin Heidelberg, 2007)

[20] Dmitriev, A., & Oruzheinikov, A. (1999) *The rate of radiative recombination in the nitride semiconductors and alloys* Journal of Applied Physics, **86**(6), 3241–3246. https://doi.org/10.1063/1.371196

[21] Edwards, Kimberly, D. (2019) Light Emitting Diodes (PDF). University of California at Irvine. p. 2. Archived from the original (PDF) on February 14. [Accessed 2022-03-20]

[22] Morkoç, H., and Hadis, M. (2013) Light-Emitting Diodes and Lighting*, Nitride Semiconductor Devices: Fundamentals and Applications*, John Wiley & Sons, Incorporated,

ProQuest Ebook Central,
http://ebookcentral.proquest.com/lib/sheffield/detail.action?docID=1174136.

[23] Liu, Z., Chong, W. C., Wong, K. M., & Lau, K. M. (2015) *GaN-based LED micro-displays for wearable applications. Microelectronic Engineering* **148,** 98–103. https://doi.org/10.1016/j.mee.2015.09.007

[24] Zhang, Z.-H., Tan, S. T., Liu, W., Ju, Z., Zheng, K., Kyaw, Z., Ji, Y., Hasanov, N., Sun, X. W., & Demir, H. V. (2013) I*mproved InGaN/GaN light-emitting diodes with a p-GaN/n-GaN/p-GaN/n-GaN/p- GaN current-spreading layer* Optics Express, **21**(4), 4958–4969. https://doi.org/10.1364/OE.21.004958

[25] Kroemer, H. (1963) *A proposed class of hetero-junction injection lasers*. Proceedings of the IEEE. Institute of Electrical and Electronics Engineers (IEEE). ***51*** *(12): 1782–1783. doi*:*10.1109/proc.1963.2706*. *ISSN 0018-9219*.

[26] Kawakami, Wang, S., Simpson, J., Hauksson, I., Adams, S. J., Stewart, H., Cavenett, B., & Prior, K. (1993) *II–VI quantum-confined Stark effect modulators*. Physica. B, Condensed Matter, **185**(1), 496–499. https://doi.org/10.1016/0921-4526(93)90285-E

[27] Selcuk, E., (2009) *Guided and deterministic self-organization of quantum dots*. Nano Letters - NANO LETT.

[28] Sayed, Islam; Bedair, S. M. (2019) *Quantum Well Solar Cells: Principles, Recent Progress, and Potential* IEEE Journal of Photovoltaics. **9** (2): 402–423. *doi*:*10.1109/JPHOTOV.2019.2892079*. *ISSN 2156-3381*. *S2CID 67874610*.

[29] Butté, R., et al (2007) *Current status of AlInN layers lattice matched to GaN for photonics and electronics* Journal of Physics. D, Applied Physics, **40**(20), 6328–6344. https://doi.org/10.1088/0022-3727/40/20/S16

[30] Lazzarini, L., Nasi, L., Ferrari, C., Mazzer, M., Passaseo, A., Barnham, K.W.J. (2001) S*tructural properties of InGaAs-based strain balanced MQW for photovoltaic applications*, Microscopy of Semiconducting Materials , ISBN 9781351074629

[31] Gershoni, G., & Temkin, H. (1989) *Optical properties of III–V strained-layer quantum wells* Journal of Luminescence, **44**(4), 381–398. https://doi.org/10.1016/0022-2313(89)90068-9

[32] Akasaki, I.; Amano, H. (1997) *Crystal Growth and Conductivity Control of Group III Nitride Semiconductors and Their Application to Short Wavelength Light Emitters* Japanese Journal of Applied Physics. **36** (9A): 5393. *Bibcode*:*1997JaJAP.36.5393A*. *doi*:*10.1143/JJAP.36.5393*.

[33] Yang, L., Lin, T., Huang, M., & Chen, Y. (1999) *Optical properties of Si-doped GaN films* Journal of Applied Physics, **86**(11), 6124–6127. https://doi.org/10.1063/1.371662

[34] Akasaki, M., Amano, H., Kito, M., & Hiramatsu, K. (1991) *PHOTOLUMINESCENCE OF MG-DOPED P-TYPE GAN AND ELECTROLUMINESCENCE OF GAN P-N-JUNCTION LED* Journal of Luminescence, **48**-*9*, 666–670.

[35] Siegman, A., Anthony E. (1986). *Lasers*. University Science Books. p. *4*. *ISBN 978-0-935702-11-8*.

[36] Yu, Y., Zheng, Z., Mei, Y., Xu, R., Liu, J., Yang, H., Zhang, B., Lu, T., & Kuo, H. (2018) *Progress and prospects of GaN-based VCSEL from near UV to green emission*. Progress in Quantum Electronics, **57**, 1–19. https://doi.org/10.1016/j.pquantelec.2018.02.001

[37] Iga, K. (2000) *Surface-emitting laser-its birth and generation of new optoelectronics field*. IEEE Journal of Selected Topics in Quantum Electronics, **6**(6), 1201–1215. https://doi.org/10.1109/2944.902168

[38] Dayal, I., Imamura, A., Sakaguchi, T., Matsutani, A., & Koyama, F. (2009) *Multiple-wavelength GaInAs/GaAs VCSELs with grading a spacer layer for short reach WDM applications*. 2009 IEEE International Conference on Indium Phosphide & Related Materials, 182–184. https://doi.org/10.1109/ICIPRM.2009.5012473

[39] Jung-Tang, C., Chu, Liang, W., Kao, C., Huang, H., Lu, T., Kuo, H., & Wang, S. (2005) *Optically pumped GaN-based vertical cavity surface emitting laser at room temperature.* 2005 Pacific Rim Conference on Lasers & Electro-Optics, 293–294. https://doi.org/10.1109/CLEOPR.2005.1569423

[40] Someya, Tachibana, K., Lee, J., Kamiya, T., & Arakawa, Y. (1998) *Lasing emission from an In0.1Ga0.9N vertical cavity surface emitting laser.* Japanese Journal of Applied Physics, Part 2: Letters, **37**(12), L1424–L1426. https://doi.org/10.1143/jjap.37.l1424

[41] Song, D., Diagne, M., Zhou, H., Nurmikko, A., Carter-Coman, C., Kern, R., Kish, F., & Krames, M. (1999) *A vertical injection blue light emitting diode in substrate separated InGaN heterostructures*. Applied Physics Letters, **74**(24), 3720–3722. https://doi.org/10.1063/1.123232

[42] Chu, L., Lu, T.-C., You, M., Su, B.-J., Kao, C.-C., Kuo, H.-C., & Wang, S.-C. (2006) *Emission characteristics of optically pumped GaN-based vertical-cavity surface-emitting lasers*. Applied Physics Letters, **89**(12), 121112–121112–3. https://doi.org/10.1063/1.2355476

[43] Lu, L., Chen, S.-W., Wu, T.-T., Tu, P.-M., Chen, C.-K., Chen, C.-H., Li, Z.-Y., Kuo, H.-C., & Wang, S.-C. (2010) *Continuous wave operation of current injected GaN vertical cavity surface emitting lasers at room temperature*. Applied Physics Letters, **97**(7), 071114–071114–3. https://doi.org/10.1063/1.3483133

[44] He, H., Özdemir, Şahin K., & Yang, L. (2013) *Whispering gallery microcavity lasers.* Laser & Photonics Reviews, **7**(1), 60–82. https://doi.org/10.1002/lpor.201100032

[45] Barker Jr., S., and Ilegems, M. (1973) *Infrared lattice vibrations and free-electron dispersion in GaN*. Phys. Rev. B **7**, 743-750

[46] Zajac, A., Hecht, E. (2003). Optics, Fourth Edit. Pearson Higher Education. *ISBN 978-0-321-18878-6*.

[47] Aharonovich, A., Woolf, A., Russell, K. J., Zhu, T., Niu, N., Kappers, M. J., Oliver, R. A., and Hu, E. L. (2013) *Low threshold, room-temperature microdisk lasers in the blue spectral range*, Appl. Phys. Lett. **103**(2), 021112

[48] Athanasiou, M., Smith, R., Liu, R., and Wang, T. (2015) *Room temperature continuous–wave green lasing from an InGaN microdisk on silicon*, Sci. Rep. **4**(1), 7250

[49] Yang, Y., & Cao, X. A. (2009) *Removing plasma-induced sidewall damage in GaN-based light-emitting diodes by annealing and wet chemical treatments*. Journal of Vacuum Science

& Technology. B, Microelectronics and Nanometer Structures Processing, Measurement and Phenomena, **27**(6), 2337–2341. https://doi.org/10.1116/1.3244590

[50] Mei, M., Xie, M., Xu, H., Long, H., Ying, L., & Zhang, B. (2021) *Electrically injected GaN-based microdisk towards an efficient whispering gallery mode laser*. Optics Express, **29**(4), 5598–5606. https://doi.org/10.1364/OE.416873

[51] Visalli, D., Van Hove, M., Leys, M., Derluyn, J., Simoen, E.,Srivastava, P., Geens, K., Degroote, S., Germain, M., and Nguyen, A. P. D. (2011) *Investigation of light-induced deep-level defect activation at the AlN/Si interface*, Appl. Phys. Express **4**(9), 094101

[52] Feng, M., He, J., Sun, Q., Gao, H., Li, Z., Zhou, Y., Liu, J., Zhang, A., Li, D., Zhang, L., Sun, X., Li, D., Wang, H., Ikeda, M., Wang, R., and Yang, H. (2018) *Room-temperature electrically pumped InGaN-based microdisk laser grown on Si*, Opt. Express **26**(4), 5043–5051

3 METHODOLOGY

3.1 METAL ORGANIC CHEMICAL VAPOUR – PHASE DEPOSITION

Metal organic chemical vapour (MOCVD) is the main growth method of group III -V based optoelectrical samples. Using chemical vapour deposition is able to grow thin layers of complex semiconductor structures, such as quantum wells, superlattices and Distributed Brgg Reflectors (DBRs) [1]. Through the control of time duration and the flow rate of vapour sources the thickness of different layers can be controlled and along with doping concentrations. The careful balancing of other parameters like reactor temperature, atmospheric pressure and surface morphology of the wafer allows for the essential growth of high-quality crystal samples and reproducible layers [2].

MOCVD uses ultra-pure gas sources that are injected into a reactor's core with a non-reactive carrier gas over a semiconductor wafer, which in this case is sapphire. In the case of GaN semiconductors, a group III metalorganic (Trimethylgallium (TMG)) is combined with a group V hydride (ammonia (NH3)) using hydrogen (H2) as a carrier gas [3]. For the purposes of multi quantum wells and n-type or p-type GaN, pure gas dopants are needed such as indium (In), silicon (Si) and aluminium (Al) respectively. As the gasses enter the reactor they interact with the wafer via pyrolysis and absorb onto the wafer, and the reaction causes a new epitaxial layer of semiconductor crystal lattice [4]. Certain doping interactions require specific temperatures to form the chemical bonds such as the incorporation of indium in InGaN needing low temperatures, usually below 500C, but can vary depending on the amount of indium [5].

To confirm doping concentrations and thickness of epitaxial layers, X-ray diffraction (XRD) measurements were used [6]. The X-rays are scattered by the atomic lattice to create a unique diffraction pattern that can act as a fingerprint for the crystal structure. By

comparing the GaN reference data to the XRD spectra, an approximate doping level of the indium can be calculated along with the approximate thickness of the various layers [7].

3.2 PHOTOLUMINESCENCE

Photoluminescence (PL) spectroscopy is a characterisation method used to determine the optical properties of semi-conductors.

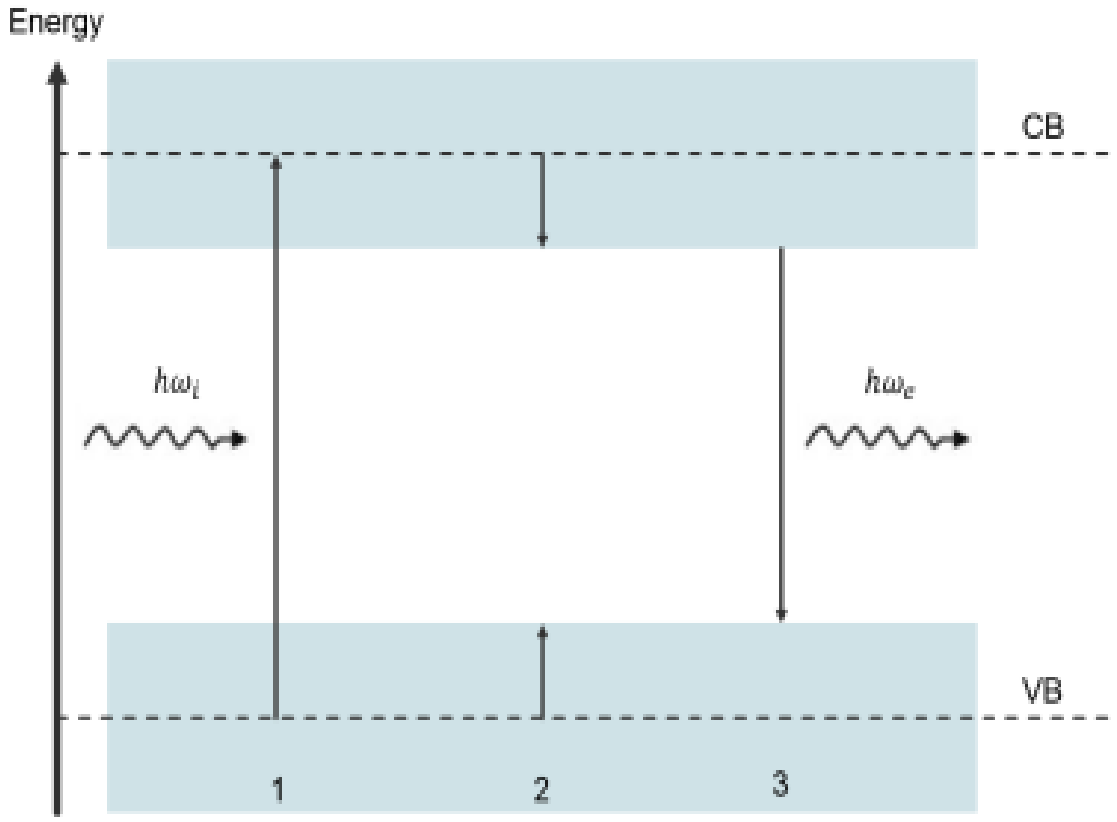

Figure 3.13- Band diagram showing the three steps of photoluminescence. 1) Excitation of an electron from the valance band (VB) to the conduction band (CB), by an incident photon: $h\omega_i$. 2) Relaxation of the electron and hole to the lowest energy level. 3) Recombination of the electron-hole pair, emitting a photon of energy $h\omega_e$, where $h\omega_e < h\omega_i$.

Photoluminescence has three steps to its mechanics: excitation, relaxation, and recombination [8]. First, an electron in the valence band absorbs a photon with energy higher compared to the bandgap of the semiconductor. The electron transitions into the

covalence band creating an electron–hole pair. The electron–hole pair undergo relaxation, moving to their lowest excited energy state. Finally, electron–hole pairs recombine, returning to their ground states and emitting a photon with energy equal to the recombination transition. This process is displayed in **Figure 3.1**.

When the lowest energy states are similar to the bandgap, PL is a method to directly measure the bandgap wavelength normally described as band edge emission. However, in many semiconductors there are many energy states other than just the bandgap. Relaxation can tend to favour these other states due to shorter relaxation times, usually around 10^-12s compared to the 10^-9s of the band gap for radiative recombination [9]. Thus, PL spectra are characterised by broad emission showing a range of wavelengths with the peak wavelength usually corresponding to the bandgap. These types of recombination are usually described as donor-acceptor recombination.

Therefore, photoluminescence is a measure of radiative recombination where an electron – hole pair recombing results in a photon emission. PL can also be modified by other techniques to investigate other optical properties, such as varying power and temperature or even narrowing to smaller resolutions.

The PL system used is made of a continuous wave 375nm Vortran laser which passes through a series of mirrors and then focuses on the sample with an objective lens. The light is then collected and focused through monochromator gratings which separate the light into different wavelengths. This is collected and analysed by a charged coupled detector (CCD) which converts photons into electrical signals. The data is processed and displayed by Origins software where further analysis can be done to find specific properties.

3.3 TEMPERATURE DEPENDENT PHOTOLUMINESCENCE

Temperature dependent PL is a variant technique used to measure emission spectra under different temperatures. At room temperature, the many other relaxation transitions that the exciton can undergo usually result in non-radiative recombination, with the most common being Shockley Reed Hall recombination (SRH). This is caused by energy states caused by defects trapping the exciton, meaning a photon is not the emitted particle. Instead, there are other quasi-particles such as phonons [10] As such by reducing the temperature reduces overall vibrations which reduce the extra energy states cause by such vibrations [11]. This leads to an assumption that at low temperatures there is no non-radiative recombination. However, this assumption is under critique as there will always be non – radiative recombination even at 0K, therefore the radiative recombination measurement must be extrapolated from sub 20K measurements [12] and there are other types of non-radiative recombination that will not be mitigated.

The main other non-radiative recombination is auger recombination, which is when the energy released excites another exciton to a higher energy level instead of producing a photon [13]. For the purposes of the recombination theory, auger recombination is considered negligible since in InGaN and GaN systems the rate is around 10^{-31} cm^6 s^{-1} [14]. This is shown to have little effect in overall recombination, but it can have an effect if carrier concentration becomes too high in a system, due to the increased chance of Auger recombination [15].

Since it is assumed that at low temperatures radiative recombination dominates the system, temperature dependent measurements can be used to calculate the internal quantum efficiency (IQE), which is determined as the ratio of the number of emitted photons versus the number of injected electrons and holes. This is commonly calculated by the ratio of integrated intensities at high and low temperature, as shown in **Equation 3.1**.

IQE is a better measure of the overall efficiency of the active region, compared to only using the intensity and wavelength uniformity of emission [17].

Equation 3.1 - $\eta_{IQE} = I_{RT}/I_{LT}$

I_{RT}/I_{LT} – Integrated intensity of spectra at room and low temperature respectively

Other phenomena caused by temperature dependence, such as the blue shift in the peak wavelength with decreasing temperature [18], can be described by Varshni's law, which is an empirical relationship given by **Equation 3.2**.

Equation 3.2 – $E_g(T) = E_g(0) - \frac{\alpha T^2}{\beta + T}$

$E_{g(0)}$ - bandgap of the crystal at 0K, α - material constant and β - constant physically associated with the Debye temperature of the crystal [19].

This states that when the temperature is lowered, the band gap will shift. When the temperature decreases, the amplitude of atomic vibrations within a material will also decrease due to the reduction in thermal energy. This will cause the lattice atomic spacing to become smaller, and as such the potential felt by electrons will increase, which will therefore shift the band gap towards longer wavelengths. The band gap is thus affected by the thermal dilation of the lattice and temperature-dependent electron-phonon interactions. At high temperatures Varshni's law gives a linear dependence of the bandgap, however at low temperatures this relationship becomes quadratic.

Furthermore, exciton behaviour can also be visible at low temperatures. Excitons are quasi-particles composed of an electron and hole bound together during excitation [20]. Due to this they are commonly modelled using the hydrogen atom model, except with the difference that the hole has less mass than a proton. Excitons decay through radiative recombination, and as such usually emit a photon at a wavelength close to the peak wavelength of the sample. At room temperature these peaks can be obscured because of the peak broadening and an exciton can become unstable due to collisions with phonons [21].

3.4 POWER DEPENDENT PHOTOLUMINESCENCE

Power dependent PL is used to investigate carrier mechanics with regards to varying excitation laser power. As InGaN/GaN MQWs are subject to quantum confined stark effects (QCSE), caused by strong polarization effects from the lattice mismatch between sapphire and InGaN grown in the c-axis, many studies have been done to define such effects using power dependence [22]. As excitation power increases, an electric field is generated by the increase in photo-generated carriers. This forms a partial screening effect that reduces the piezoelectric field generated by QCSEs, leading to a blue shift in PL peak [23].

Another use of power dependent PL is to study the lasing properties of micro/nanostructures. Lasing theory states that photons in a resonant cavity can go through several steps to form a laser. Firstly, there is stimulated emission. Stimulated emission occurs when a photon with a specific wavelength and frequency interacts with an excited atom, this increases the chance of electron decaying which will produce a photon with matching characteristics to the passing photon. As the passing photon is not absorbed this induces a net gain in coherent light intensity. This exclusively occurs when the excitation power goes above a threshold, such that the number of carriers in an excited state exceeds that of those in ground state. Amplified spontaneous emission is step two, which is shown by a dramatic and non-linear increase in light intensity, as well as band gap narrowing due to the resonant cavity. The photons generated by stimulated emission are trapped in the cavity, leading to a higher probability of further stimulated emission [24]. That along with the population inversion creates an amplified number of photons with the same wavelength and coherence, a laser. This can be seen by comparing integrated intensity against power density which should show a typical “s” shape when plotted in log-log axis [26].

This can be seen by comparing the integrated intensity against power density, plotted on log-log axes, measured by power dependent PL, which will exhibit an “s” shape typical to lasing materials [26], as shown in **Figure 3.2**.

Power dependent PL can be used to investigate and quantify the lasing threshold and measure various lasing properties such as quality factors (Q-factors) from the line width. It

can also be used to the measure different types of modes, such as Whispering Gallery (WG) and Fabry–Pérot (F-P). The mode separation for WGM can be calculated by **Equation 3.3**.

Equation 3.3 - $\Delta\lambda = \frac{\lambda}{2\,n\,\pi R}\Delta\lambda$ - mode spacing, λ - peak wavelength, n - refractive index, and R-radius of micro-LED [25].

Spontaneous emission coupling β-factors are another indication of the quality of the lasing threshold. The β-factor can be calculated from integrated intensity during power dependent PL, and it describes the emission efficiency of a single optical mode [27]. **Figure 3.2** shows how this β-factor affects the typical "s" shape in a power dependent study. If the β-factor is below 0.01 the laser can no longer be classified by standard emission characteristics and is considered a thresholdless laser. The β-factor is also a measure of how large the lasing threshold is, with larger β-factors having a smaller threshold as they approach the limit.

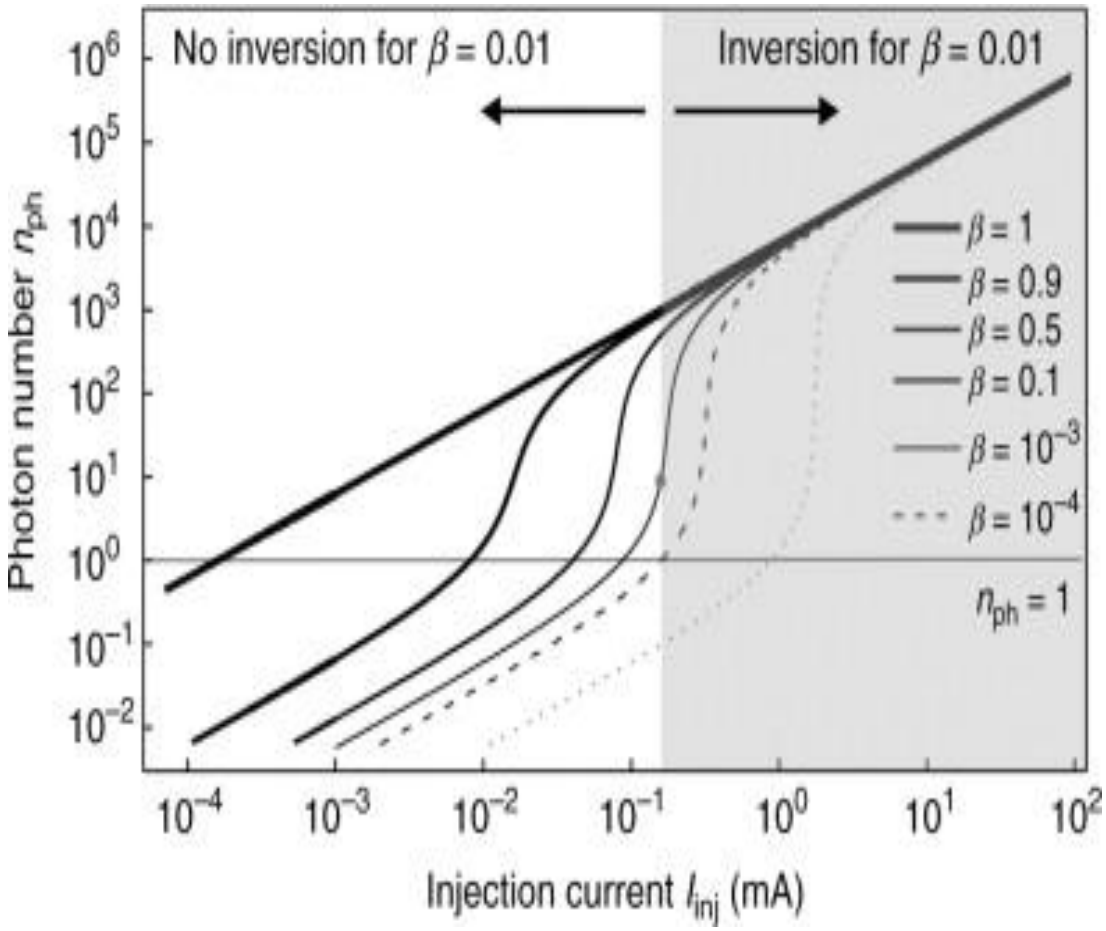

Figure 3.2 - Input–output curves of a micro laser for different β-factors plotted in log–log scale (ξ = 103 β). For β = 0.01 the regions with and without inversion of the gain medium are indicated. The straight horizontal line represents the laser threshold defined by $n_{ph} = 1$. [26]

3.5 Time resolved Photoluminescence

Time-resolved photoluminescence measures the time for the electron to recombine with a hole during excitation. As stated in the previous section, there are two types of recombination, which have different time decay rates, while a total recombination rate can be calculated via **Equation 3.4** [26].

Equation 3.4 - $\tau^{-1} = {\tau_r}^{-1} + {\tau_{nr}}^{-1}$

Where τ_r – radiative lifetime, τ_{nr} – non- radiative, technically for a complete picture there would be a third term accounting Auger recombination but for this model this is considered negligible.

At low temperature, radiative recombination usually has the shortest rate and so it becomes the main contributor to the total time decay, and vice-versa at room temperature for non-radiative recombination. Therefore, a full temperature dependent study of a sample can give great insight to the structure of the QW. Furthermore, since these time decays describe the probability of recombination, it can also be used to calculate the Internal Quantum Efficiency (IQE) of the sample using **equation 3.5**, where IQE is described as the ratio of emitted carriers to the number of carriers undergoing recombination [26].

Equation 3.5 - $\eta_{int} = \frac{{\tau_r}^{-1}}{{\tau_r}^{-1}+{\tau_{nr}}^{-1}}$

This setup uses Time Correlated Single Photon Counter (TCSPC) to measure the time decay. This electronic method uses a pulsed laser with a short emission delay. Before excitation of the sample, a part of the laser beam is directed into a fast photodiode and converted into an electrical signal that is used as the start of the measurement [27]. After excitation, the emitted beam is then directed into a photomultiplier, and then converted to an electrical signal which is used to signal the end of the measurement. The time between the start and stop signals allows the time decay of the sample to be measured. This technique has the disadvantage of only being able to detect at a certain wavelength, usually the peak wavelength of the spectra, and so more complicated spectra will require multiple measurements of different photomultipliers.

This signal can then be fitted, usually using a bi-exponential equation as described in **Equation 3.6**.

Equation 3.6 - $y = A_1 e^{-t_1 b} + A_2 e^{-t_2 b}$ A_1 and A_2 – decay constants, t_1 and t_2 – radiative and non-radiative recombination times depending on the temperature of the experiment [28]

In order to further investigate the lasing properties of these micro-disk lasers, time-resolved micro-PL (μ-TRPL) studies have been conducted as a function of excitation power density from 0.75 - 37 kW/cm2, which spans a wide range from spontaneous emission

through the lasing threshold towards resonant equilibrium. A 375nm pulsed diode laser with a pulse width of 50ps was used as an optical excitation source.

3.6 CONFOCAL MAPPING PL

Conventional optical microscopy suffers from high interference from secondary excitation emissions or scattering, which can obscure certain details in emission spectra. This is because in conventional PL the laser beam illuminates a large area of the sample and collects most of the light, including scattered light from out of focus features [30]. Confocal microscopy focuses light in a smaller area, and only collects photons emitted from the focal area, as shown in the set-up diagram in **Figure 3.3**.

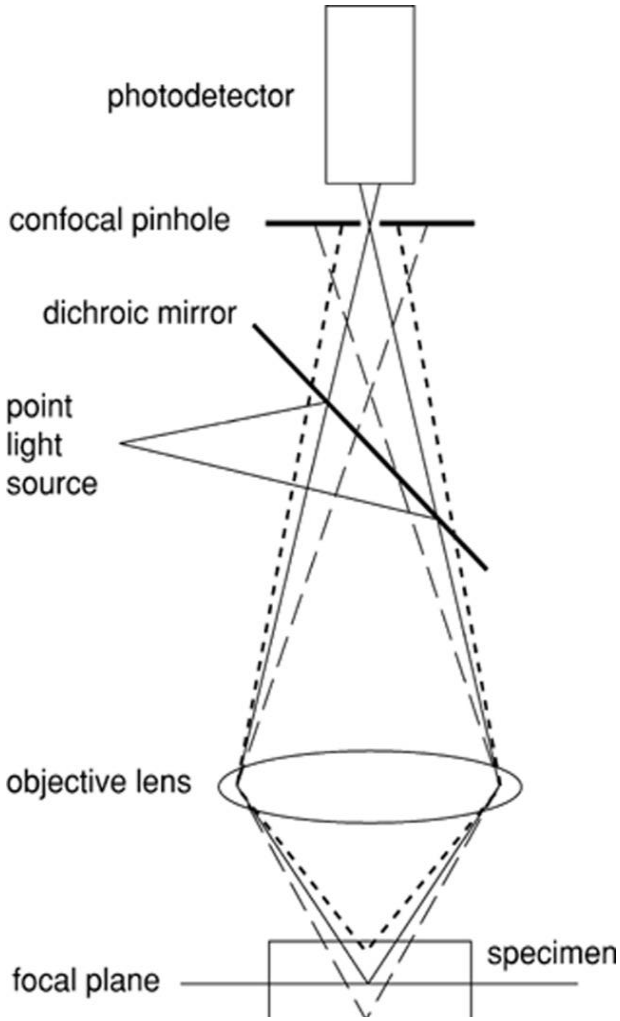

Figure 14.3 - Diagram of a standard confocal microscopy set up [29]

A coherent light source is sent through a pinhole aperture then reflected by a dichromatic filter, afterward it is focused by an objective towards the sample. After excitation the emitted light then passes back along the light path through the dichroic filter and through another pinhole towards the charged coupled device (CCD). The use of pinholes and both emission and excitation light passing along the same light path reduces the amount of scattered or out of focus light from hitting CCD, allowing a higher resolution in spatial measurement [31].

As much of the current work is with micro and nano structures, PL mapping techniques are used to gain a better understanding of how light interacts in such structures. A series of PL measurements are performed in a grid over the structure and by recording the overall properties of each spectrum a data map of such structures. For instance, by creating an intensity map, the way the spectra intensities change throughout the structure becomes visible. This setup uses a WiTech spectral microscope with a piezoelectric remote-controlled x, y, and z axis stage, with a 50x and 100x magnification objective lens that allows measurement of features down to a size of 200nm. The excitation source used is a 375nm Vortran continuous wave laser with a Newton Andor CCD and monochromator. The software WitTech Power can create a map with 150 x 150 PL measurements over a 25µm x 25 µm square area. This has been used to measure the potential whispering gallery modes of a micro disk structure by mapping individual micro disks.

These measurements use a commercial WiTech confocal microscope with a 375nm continuous wave (CW) laser that acts as an excitation source. The emission light is collected and processed through a Princeton instruments monochromator (SP2300i), and a Newton CCD that is air cooled. An objective lens of 100x is used to focus the laser beam, which allows a beam diameter of 220nm to measure micro and nano features. A high-resolution x,y, and z piezoelectric stage enables the creation of PL maps at a micro level.

A similar setup is used to measure micro features as a whole, rather than specific parts of the feature. It uses a confocal set up with a less extreme magnification. To perform micro-PL, a 375nm CW Vortan laser is used to excite the samples. The system is in a confocal arrangement and with a 50x magnification camera it is capable of measuring micro features around 1 µm. The light is collected into a Horiba iHR-550 monochromator and analysed by a

Horiba (CCD). The time-resolved PL (TRPL) system further uses a 375nm pulsed diode laser with a pulse width of 50ps which is collected in a picoquant single photon counter.

3.7 REFLECTION SPECTROSCOPY

Reflection spectroscopy is a non-invasive technique that is used to measure the reflectance of a sample. This is done by measuring the scattered light from the sample surface compared to the incident light from the source directly. This method can be difficult depending on the setup, so usually the comparison is with a standard high reflective mirror with known reflectance. Reflectance is then therefore calculated from **Equation 3.7** [35].

Equation 3.7 - $R = \frac{I_{Scattered}}{I_{standard}} r_{standard}$ $I_{scattered}$ - Integrated Intensity of reflectivity spectra from sample, $I_{standard}$ – Integrated Intensity of reflectivity of standard mirror

When photons hit a material boundary there are several processes that can happen. The electromagnetic wave can experience reflectance, absorption, and/or transmission, as shown in **Figure 3.4** and expressed in **Equation 3.8** [34].

Equation 3.8 - $\alpha + \tau + \rho = 1$ α-Absorptivity, τ-Transmissivity, and ρ-Reflectivity

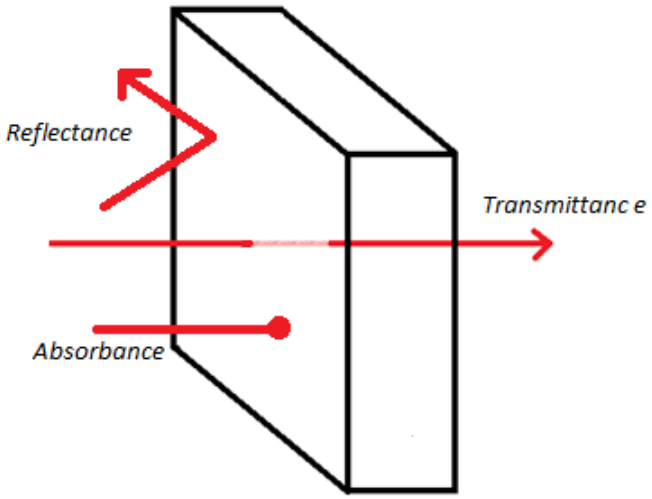

Figure 3.15 - Diagram showing the various light path boundary interactions. Absorbance, Transmittance and Reflection. [34]

Reflectance happens at boundaries where the energy of the incoming wave is transferred to a different medium, creating a new wave with a different propagation [34]. Materials with high reflectance have been used to enhance the emission of semiconductors, typically using AlGaN mirrors. Usually, high reflectance happens at boundaries with materials with very different refractive indexes - for instance the silver/glass boundaries in silver mirrors [35]. Most conventional mirrors suffer from an energy loss that comes from absorption, where energy from the incoming wave is absorbed as heat into the surface electrons.

To mitigate the energy loss and create better reflectors, dielectric mirrors have become widely used. Dielectric mirrors are a series of pairs of differently layered materials with alternating refractive indices. The individual pairs reflect very little light, but a dozen pairs can have a combined reflectivity much greater than a conventional mirror, usually approaching 99.999% [36], making them perfect to use for lasers as the large amount of energy produced is unlikely to damage the mirror. The heat absorbed is also mitigated due to the thinness of each layer, as only a small amount of energy can be absorbed at each boundary compared to a bulk sample.

Distributed Bragg Reflectors (DBR) are an enhanced form of dielectric mirrors that consist of alternating layers. Instead of layers with just different refractive indexes, DBRs use a pair of material layers one with high refractive index and the other with a low refractive

index with a thickness comparable to the central wavelength of reflection [37]. These reflectors can be designed to have ultra-high reflectance at specific wavelengths as described by a stop band; any wavelength outside the stop band is usually transmitted through the reflector. Recently a new method has been developed using selectively etched DBRs; these mirror-like materials can be made entirely out of GaN. By etching highly n-doped GaN, nanoporous GaN layers are formed which have a much lower refractive index creating the large index difference needed for DBRs [38]. These materials are superior for GaN based technologies as they suffer from very few of the growth difficulties that would appear if other materials were used, as they are lattice matched.

3.8 ELECTRO - CHEMICAL ETCHING

Electro-chemical etching (EC) is an etching process that is a combination of oxidation and dissolution mechanics. With the etchant in an acidic solution under an electrical bias, that leads to dissolving of layers. While under a positive bias, the injection of holes causes GaN to oxidise which is then dissolved in the acidic electrolyte. This means that only highly n-doped GaN can be electro- chemically etched due to the high conductivity. However, if either the bias or the doping concentration is too high the whole layer is etched away, which is not needed since the main purpose of these samples is the creation of nanoporous

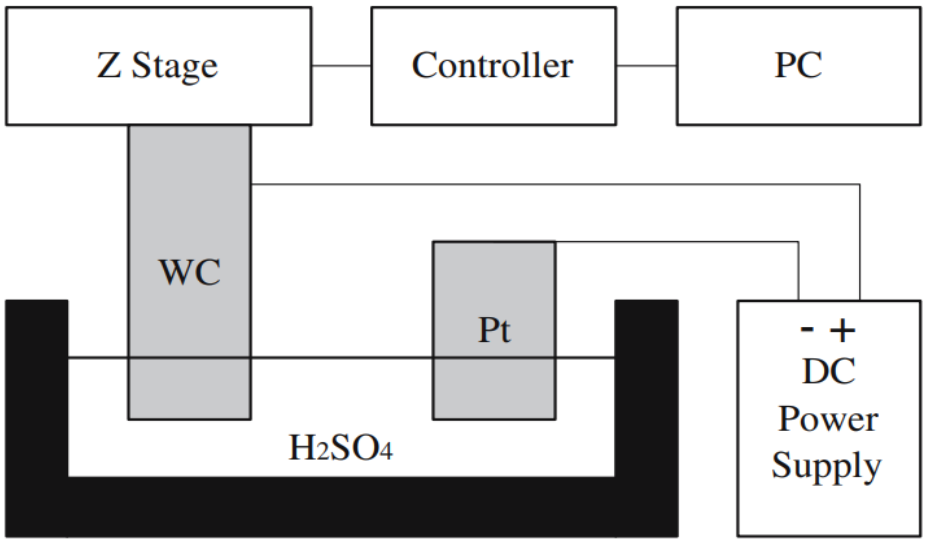

Figure 3.16 - Electro chemical etching set up for Tungsten carbide in a sulphuric acid solution [41]

layers [39]. **Figure 3.5** shows a schematic for etching Tungsten Carbide in sulphuric acid solution [41].

The selected layer is connected to the power supply using an indium contact, which then acts as an anode. The whole sample is suspended in 0.5 mol of nitric acid acting as the cathode and with a platinum plate as the anode, while an electrical bias of 8V was used. When a current is passed through the sample, atoms on the metal surface become positively charged and therefore can disassociate from the bulk material by being attracted to the electrolyte. The positively charged metal atoms pass through the electrolyte and deposit on the cathode.

The etching process is selective since it targets the layer in the sample that is the most electronegative first. This is of great use in creating nanoporous DBRs due to the fact that specific layers can be doped, along with control over the doping concentration during growth. These DBRs were designed to have 11 pairs of alternating highly n doped and undoped GaN layers, which after etching become nanoporous GaN/ GaN pairs these have a large enough difference in refractive index to form a lattice matching DBR structure.

A successful etching requires the sample to be uniformly etched. The process begins from the edge of the sample causing irregular patterns as the etching rates at the edges are higher than those in the middle. Many studies report using the naturally occurring surface defects to allow a uniform etching pattern. Another way is to use a slower etching rate by reducing the voltage bias or decreasing the acid concentration. Though many papers found a way to get around this issue through the use of patterned holes across the sample, allowing the acid to etch uniformly in specific patterns [40]. The etching rate is increased around the holes creating circular patterns, which can lead to islands of unetched areas that are disconnected from the electrical current, slowing down etching rates.

3.9 SCANNING ELECTRON MICROSCOPY

Scanning electron microscopy (SEM) is a method for scanning the surface topology at a micro and nano level. Using an electron beam to scan across a small surface area, an SEM detector is able to collect secondary electrons leaving the sample and transform the collected signal into an intensity value. Any features on the surface modulate the intensity, building up a map of the objects. Some detectors have been able to resolve objects up to 1 nanometre [41].

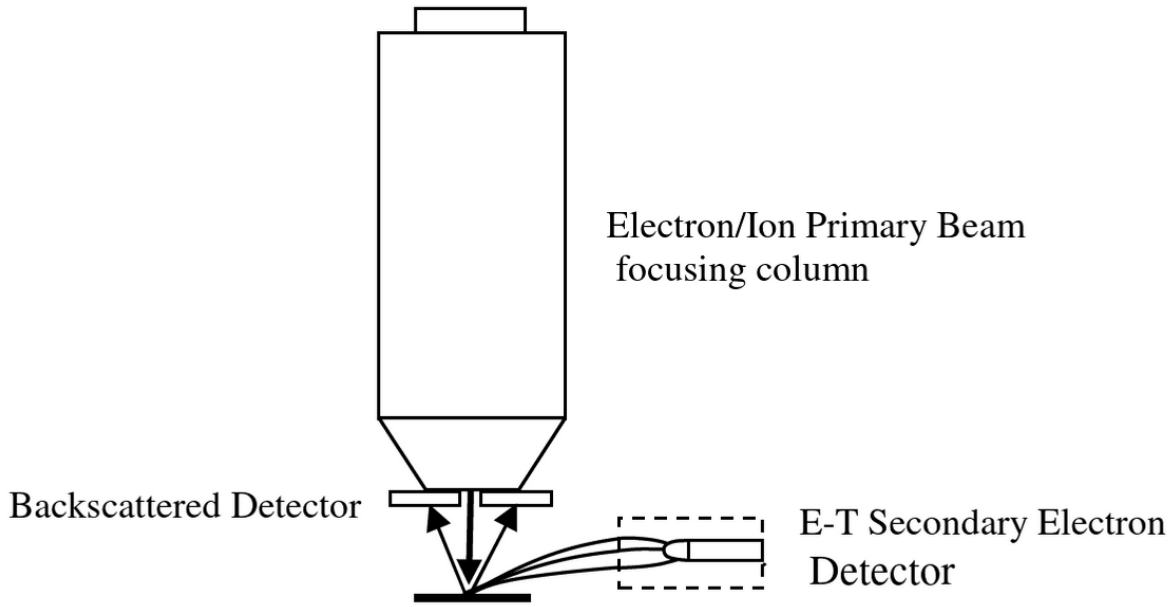

Figure 3.17 - Diagram of a standard set up of Scanning Electron Microscopy with detectors [44]

All SEM systems are built from an electron gun, focusing lens, objective lens, back scattering electron detector and a secondary electron detector, usually called an Everhart-Thornley (E-T) detector, along with a set of deflectors in a vacuum [43] as shown in **Figure 3.6[44]**. The electron gun accelerates a beam towards the sample's surface focused by an objective lens, which excites the atoms in the near surface level, generating a series of signal electrons. There are two types of signal electrons generated by this method: backscattered electrons (BSE) from deep levels in the surface, and secondary electrons created from surface atoms. Other signals generated are from Auger electrons from inner atomic shells,

which are detectable but are usually of higher energies than the secondary electrons, making them easy to differentiate [44].

These electrons are reflected by a series of deflectors into a series of detectors, and the energies of the electrons determine which detectors they are sent to. Lower energy secondary electrons, roughly less than 50eV, pass towards the E-T detectors which build up the high-resolution image of the surface. BSE usually have high energies and are collected directly above the sample, to prevent any scattered light passing through to the E-T detectors, as the amount of such electrons being detected can degrade the image.

The SEM system has been used to scan both top–view surface images of micro disks to measure surface quality and micro disk shape and cross–sectional images to check nano porosity of DBR structures and v-pit defects.

3.10 FDTD SIMULATIONS

Lumerical finite difference time domains (FDTD) are computational analysis method used for calculating electrodynamics. In this case, it can be used to calculate the electric and magnetic fields in semiconductor structure. The electric field was injected by a plane wave source, with emission wavelengths from 400nm-700nm placed above the top DBR. The geometrical data of these devices are from the in-situ growth characterisation. Monitors placed inside the cavity allow the detection of the source signal to calculate the decay in the electric field; this is used to determine the wavelength of the resonant modes. In order to reduce the simulation requirements, boundary conditions were set as periodic on X, Y and perfectly matched layer (PML) in the Z dimension [45].

Standard simulation boundaries are defined by a series of mesh, monitors and FDTD edges. The mesh used has a minimum of ten mesh cells per wavelength and the simulation was run for 1000fs. Frequency domain monitors were used to record the emissions over the simulated region with end apodization, as the simulation is monitoring how photons are trapped within the structure. The spectra are collected by a grid of 5x5 time monitors placed

both inside and in the immediate outside of the structure, to accurately calculate the time domain field signal.

3.11 REFERENCES

[1] How MOCVD. Works Deposition Technology for Beginners Available at: <https://docplayer.net/20894914-How-mocvd-works-deposition-technology-for-beginners.html> [Accessed 2022-03-20].

[2] Davies, J. I., Fan, G., and Williams, J. O. (1985) *Metal-organic chemical vapour deposition (MOCVD) of compound semiconductors. Part 1.—Optimisation of reactor design for the preparation of ZnSe ,*J. CHEM. SOC., FARADAY TRANS. 1, , **81**, 2711-2722 DOI: 10.1039/F19858102711

[3] Liu, B. L., Lachab, M., Jia, A., Yoshikawaa, A., Takahashi K. (2002) *MOCVD growth of device-quality GaN on sapphire using a three-step approach,* Journal of Crystal Growth, Volume 234, **Issue 4**, Pages 637-645, ISSN 0022-0248, https://doi.org/10.1016/S0022-0248(01)01755-9.

[4] Stringfellow, G. B. *(1999*)ORGANOMETALLIC VAPOR-PHASE EPITAXY: THEORY AND PRACTICE. Elsevier Science. pp. **3**–., ISBN 978-0-323-13917-5. https://doi.org/10.1016/B978-0-12-673842-1.X5000-5

[5] Sang, L., Liao, M., Sumiya, M., Yang, X., Shen, B. (2021) *High-pressure MOCVD growth of InGaN thick films toward the photovoltaic applications*, Fundamental Research, ISSN 2667-3258, https://doi.org/10.1016/j.fmre.2021.11.024.

[6] Chen, Y. S., Liao, C. H., Kuo, C. T. *et al.* (2014) *Indium droplet formation in InGaN thin films with single and double heterojunctions prepared by MOCVD*. *Nanoscale Res Lett* **9,** 334 HTTPS://DOI.ORG/10.1186/1556-276X-9-334

[7] Saleh, T., A. (2021) *Chapter 8 - Surface and morphological characterization of hybrid materials, In Plastics Design Library, Polymer Hybrid Materials and Nanocomposites*, William Andrew Publishing, Pages **241-283**, ISBN 9780128132944, https://doi.org/10.1016/B978-0-12-813294-4.00003-0.

[8] Yu, P., and Cardona, M. (2010) *Fundamentals of Semiconductors: Physics and Materials Properties*, Graduate Texts in Physics. Springer

[9] Patanè, A., and Balkan, N. (2014) *Semiconductor research: experimental techniques*, Springer Series in Materials Science. Springer, ISBN 9783642233500

[10] Shockley, W., Read, W. T. (1952) *Statistics of the Recombinations of Holes and Electrons. Physical Review.* ***87*** *(5): 835–842,*

[11] Narukawa, Y., et al. (1999) *Dimensionality of excitons in laser-diode structures composed of InxGa1-xN multiple quantum wells*, Physical review. B, Condensed matter and materials physics, **59**(15), pp. 10283–10288, doi:10.1103/PhysRevB.59.10283.

[12] Lu, T., Ma, Z., Du, C. *et al.* (2014) *Temperature-dependent photoluminescence in light-emitting diodes*. Sci Rep **4,** 6131 https://doi.org/10.1038/srep06131

[13] Römer, F., & Witzigmann, B. (2014) *Effect of Auger recombination and leakage on the droop in InGaN/GaN quantum well LEDs*. Opt. Express **22**, A1440

[14] Brendel, M., Kruse, A., Jönen, H., Hoffmann, L., Bremers, H., Rossow, U., and Hangleiter, A. (2011) *Auger recombination in GaInN/GaN quantum well laser structures*, Appl. Phys. Lett. **99**, 031106 https://doi.org/10.1063/1.3614557

[15] Fu, H., Zhao, Y. Efficiency droop in GaInN/GaN LEDs *in* Nitride Semiconductor Light-Emitting Diodes (LEDs) (Second Edition), 2018, ISBN 978-0-08-101942-9

[16] Guichard, A. R., *et al.* (2008) *Temperature-dependent Auger recombination dynamics in luminescent silicon nanowires*, Physical review. B, Condensed matter and materials physics, **78**(23), doi:10.1103/PhysRevB.78.235422.

[17] Armstrong, A. M., Crawford, M. H., & Koleske, D. D. (2014) *Contribution of deep-level defects to decreasing radiative efficiency of InGaN/GaN quantum wells with increasing emission wavelength*. Appl. Phys. Exp. **7**, 032101

[18] Tamargo, M. C. (2002) *II-VI semiconductor materials and their applications*, volume **12**. CRC Press, Set up

[19] Kumar, V., Sinha, A., M and Farooque, U. (2015) *Concentration and temperature dependence of the energy gap in some binary and alloy semiconductors*. Infrared Physics & Technology, **69**:222–227,

[20] Kittel,*C.(*2004)*Introduction to Solid State Physics*. Wiley.

[21] Pelant. J., and Valenta. J (2012) *Luminescence spectroscopy of semiconductors*. Oxford University Press,

[22] Wu, Y. R., Huang, C. Y., Zhao, Y., Speck, J. S. *(*2014) *8 - Nonpolar and semipolar LEDs, Nitride Semiconductor Light-Emitting Diodes (LEDs),* Woodhead Publishing , Pages 250-275, ISBN 9780857095077

[23] Ryou, J. *et al*. (2009) *Control of Quantum-Confined Stark Effect in InGaN-Based Quantum Wells*, *IEEE Journal of Selected Topics in Quantum Electronics*, vol. **15**, no. 4, pp. 1080-1091, July-aug., doi: 10.1109/JSTQE.2009.2014170.

[24] Laser Theory. (Accessed 2020-03-20). https://chem.libretexts.org/@go/page/67372

[25] Chin, M., Chu, D. and Ho, S. (1994). *Estimation of the spontaneous emission factor for microdisk lasers via the approximation of whispering gallery modes*. Journal of Applied Physics, **75**(7), pp.3302-3307.

[26] *Quantum optics with semiconductor nanostructures*. (2012). Woodhead.

[27] M, Athanasiou, Smith, R. M., Pugh, J., Gong, Y., Cryan, M. J., & Wang, T. (2017). *Monolithically multi-color lasing from an InGaN microdisk on a Si substrate.*

[28] Fy.chalmers.se. (2018). [online] Available at: http://fy.chalmers.se/mbe/WWW/data/presentation.pdf [Accessed 2020-03-20].

[29] Web.vu.lt. (2018). [online] Available at: http://web.vu.lt/ff/m.vengris/images/TR_spectroscopy02.pdf [Accessed 2020-03-20].

[30] Athanasiou, M., Smith, R. M., Pugh, J., Gong, Y., Cryan, M. J., & Wang, T. (2017). *Monolithically multi-color lasing from an InGaN microdisk on a Si substrate*.

[31] Monti, M. (2012) *Basic confocal microscopy*, *European journal of histochemistry*, **56**(1), p. 3–ejh.2012.br3., doi: 10.4081/ejh.2012.br3.

[32] Pawley, J. B. and Masters, B.R. (2008) *Handbook of Biological Confocal Microscopy, Third Edition, Journal of biomedical optics*, **13**(2), p. 29902, doi:10.1117/1.2911629.

[33] Introduction to confocal microscopy. Confocal Microscopy - Introduction | Olympus LS Available at: https://www.olympus-lifescience.com/en/microscope resource/primer/techniques/confocal/confocalintro/. [Accessed 2020-03-20]

[34] EPSILON ENGINEER. 2022. *Radiation, Absorbance, Emissivity and Reflectivity*. [online] Available at: <https://www.epsilonengineer.com/radiation.html> [Accessed 2020-03-20]

[35] Hapke, B. (2012) *Theory of Reflectance and Emittance Spectroscopy* (2nd ed.), Cambridge: Cambridge University Press, doi:10.1017/CBO9781139025683

[36] Hummel, R. E. *Reflectivity of silver- and aluminium-based alloys for solar reflectors*, Solar Energy, Volume **27**, Issue 6,1981, Pages 449-455, ISSN 0038-092X,

[37] Perry, D. L. (1965) *Low-Loss Multilayer Dielectric Mirrors*, Appl. Opt. **4**, 987-991

[38] Ng, H. N., and Moustakas T. D. (2000) *High reflectivity and broad bandwidth AlN/GaN distributed Bragg reflectors grown by molecular-beam epitaxy*, Appl. Phys. Lett. **76**, 2818-2820 https://doi.org/10.1063/1.126483

[39] Park, J., Kang, J. H., and Ryu, S. W. (2013) *High Diffuse Reflectivity of Nanoporous GaN Distributed Bragg Reflector Formed by Electrochemical Etching*, Applied Physics Express, vol. **6**, no. 7, doi:10.7567/APEX.6.072201.

[40] Chang, T., Xiong, K., Park, S., Yuan, G., Ma, Z. and Han, J. (2017). *Strain Balanced AlGaN/GaN/AlGaN nanomembrane HEMTs*. Scientific Reports, **7**(1).

[41] Park, S., Yuan, G., Chen, D., Xiong, K., Song, J., Leung, B. and Han, J. (2014). *Wide Bandgap III-Nitride Nanomembranes for Optoelectronic Applications*. Nano Letters, **14**(8), pp.4293-4298.

[42] Choi, S., Ryu, S., Choi, D.K., Chu, C. (2007) *Fabrication of WC micro-shaft by using electrochemical etching*, The International Journal of Advanced Manufacturing Technology, **31**, 682-687, 10.1007/s00170-005-0241-4.

[43] Smith, K.C.A. and Oatley, C.W. (1955) The scanning electron microscope and its fields of application, British journal of applied physics, **6**(11), pp. 391–399. doi:10.1088/0508-3443/6/11/304.

[44] Khursheed, A. (November 2010) *Scanning Electron Microscope Optics and Spectrometers,* Default Book Series.

[45] Stokes, D. and Royal Microscopical Society (2008) *Principles and practice of variable pressure/environmental scanning electron microscopy (VP-ESEM) [electronic resource]*. Chichester, U.K.: Wiley.

4 OPTICAL INVESTIGATION OF MICRO LED ARRAY AS A FUNCTION OF DIMENSION

4.1 ABSTRACT

Applications such as augmented reality require micro- light emitting diodes (LEDs) with small dimension (<10 µm) and high internal quantum efficiencies (IQE). Current methods have limitations due to the severe side wall damage from the dry etching techniques. In this review we show the process of designing a new overgrowth method to create micro arrays LEDs with high IQE. Using a selective overgrowth approach with patterned SiO_2, InGaN/GaN superlattice and nanoporous GaN/undoped GaN embedded difference Bragg reflectors (DBR) we can create an array of micro disks with 3.5 µm diameter and 34% IQE for long wavelength multi quantum wells.

4.2 INTRODUCTION

III-V semiconductor micro-cavities have attracted large interest for their application in high-performance optoelectronic devices. [1-2] In particular, GaN-based microdisk lasers have gained increasing attention due to its large tuneable potential band gap range covering from Ultraviolet to visible light [2], high quantum efficiency [3], and ultra-low threshold of lasers [4]. Many recent works have focused on making micro-disk lasers by forming a GaN-air cavity with free-standing structures [5-6]. The micro-cavity structures are usually fabricated by means of dry-etching processes, which produces surface damage on the side walls. The lasers will suffer from enhanced non-radiative recombination and degraded optical properties, performing with low *Q*-factors [7]. The issue becomes more severe with decreasing the dimension of micro-disks due to the large volume to surface ratio [8]. Subsequent research has been done to improve surface quality through passivation using dielectric materials such as SiO_2 and have been proved to help reduce plasma-induced damage to some degree [13] However, the issue remains severe, especially for high performance electrically driven devices due to unavoidable current leakage and degraded electrical injection [9,12]. On the other hand, converting these micro cavities into electronical devices is inherently difficult due the delicate nature of attaching contacts to the array. While such electrically driven lasers arrays haven't been realized, reports are able to show single micro disks being excited at a time [9-12].

Recently, a different approach to the creation of InGaN-based micro light-emitting diodes (μLEDs) has been developed [4,14]. By employing a selectively overgrown method, the μLEDs can be formed inside a GaN micro-hole array with a SiO_2 mask on sapphire. Compared to conventional etching methods, it can avoid plasma-induced damage to side walls. Furthermore, the SiO_2 mask provides an easy way to achieve micro-devices based on the overgrown micro-disk arrays.

4.3 SAMPLE PREPARATION

A key component in reducing the side wall damage of micro disk mesas is to remove the dry etching process that is used in conventional fabrication approaches. Our method uses direct epitaxial growth on a pre-patterned template, which allows selective overgrowth inside patterned micro holes in a SiO_2 mask [14].This prevents the etching damage from affecting the micro disks directly and the SiO_2 mask acts as natural side wall passivation without needing any other passivation techniques, reducing the complexity of this fabrication process [15].As well as replacement confinement instead of air while allowing further growth or modifications to be done for future fabrication.

Figure 4.1 a, **b** and **c** shows the step-by-step process of the overgrowth method. First, a silicon doped n-GaN layer is grown on *c-plane* sapphire (α-Al2O3) employing a classic two-step Metalorganic chemical vapor deposition technique, known as "as-grown n-GaN template". Next, a dielectric film of SiO2 is deposited on top of the n-GaN layer using plasma enhanced chemical vapor deposition (PECVD), creating the structure in **Figure 4.1a**. Subsequently, by using photolithography to create a photoresist mask on top of the SiO2, an etching process using standard inductively coupled plasma is carried out to selectively etch microholes down to the n-GaN layer, creating a SiO_2 mask. This procedure gives a high degree of control on the shape, size and interpitch of the micro disk arrays, such as the mask depicted in **Figure 4.1b**, which has micro hole diameters of 3.6 μm and an interpitch distance of 2 μm. Finally, a standard InGaN/GaN LED structure is grown in the patterned SiO_2 mask by MOVPE again. A standard LED structure consists of a silicon doped n-GaN layer followed by a $In_{0.05}GaN_{0.95}$ prelayer. The active region is grown next, with 5 periods of InGaN multi quantum wells (MQW) with GaN barriers, then topped with p-type $Al_{0.2}Ga_{0.8}N$ as a blocking layer to allow the growth of the final p-doped GaN layer. This standard LED recipe is converted into a micro-LEDs recipe as the overgrowth only happens where the exposed n-GaN layer is, in the micro holes shown in **Figure 4.1c**.

An example of one of the final arrays is shown by the top and cross section SEM images in **Figures 4.2 d** and **e** respectively. The image of the wafer demonstrates the high degree of uniformity that can be achieved with this method, which is important for high resolution sensors and micro display technologies [16]. Cross sectional view also shows the high selectivity of the overgrowth, and the matching heights of the micro-LEDs with the SiO_2 mask, these make any further fabrication easier as all future structures will be made at the same layer, reducing any chances of defects. Finally, this method has allowed all micro disks to have a shared n-contact and open p-contacts, which make them perfect for integration with electrical devices

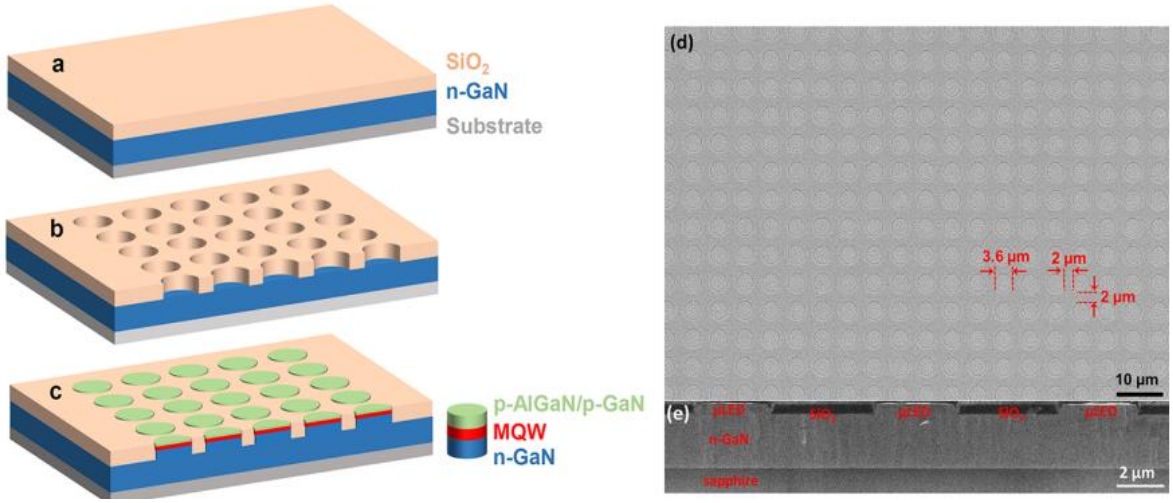

Figure 4.18 – (a) SiO_2 layer deposition (b) SiO_2 mask etching (c) micro-LED selective overgrowth (d) top view SEM of micro disk array (e) cross section of micro disks in patterned SiO_2 holes. [15]

4.4 INITIAL OPTICAL PROPERTIES OF MICRO DISK ARRAYS

The first micro disk arrays grown had a mask with variable micro-LED sizes ranging from 100 µm to 20 µm, and each LED had five MQWs with 5% indium content to create a peak wavelength at around 510 nm. Three samples of micro arrays were grown with similar structures but different growth conditions. Samples A, B and C each have different growth times, with sample A having the longest. To test the quality of the micro-LEDs, power dependent photoluminescent (PL) was used along with calculated internal quantum

efficiency (IQE) using the ratio of integrated intensities at low and high temperatures, **Equation 4.1.**

Equation 4.1 - $\eta_{IQE} = I_{RT}/I_{LT}$ [17]

The lasing measurements were performed with a commercial confocal microscopy system, equipped with a high-resolution x-y-z piezo-stage which allows the excitation and emission collection from a single micro disk device. The devices are non-resonantly excited using a 375nm continuous wave laser, and the emission is then collected into a monochromator and detected with a Charged Coupled Device (CCD). The laser spot diameter allows for spatial resolution for up to 200 nm. **Figures 4.2 a** and **b** display the power dependent PL spectra of 20 µm samples A and C, showing that by increasing the excitation power allows Whispering Gallery Modes (WGMs) to be seen clearer, which proves the high confinement in these micro disks. Sample A exhibits a multi peak spectra where the peak at 510nm becomes dominant after 20mW. It is possible to compare the

separation of experimentally measured peaks with the theoretical calculation of mode separation with **Equation 4.2**.

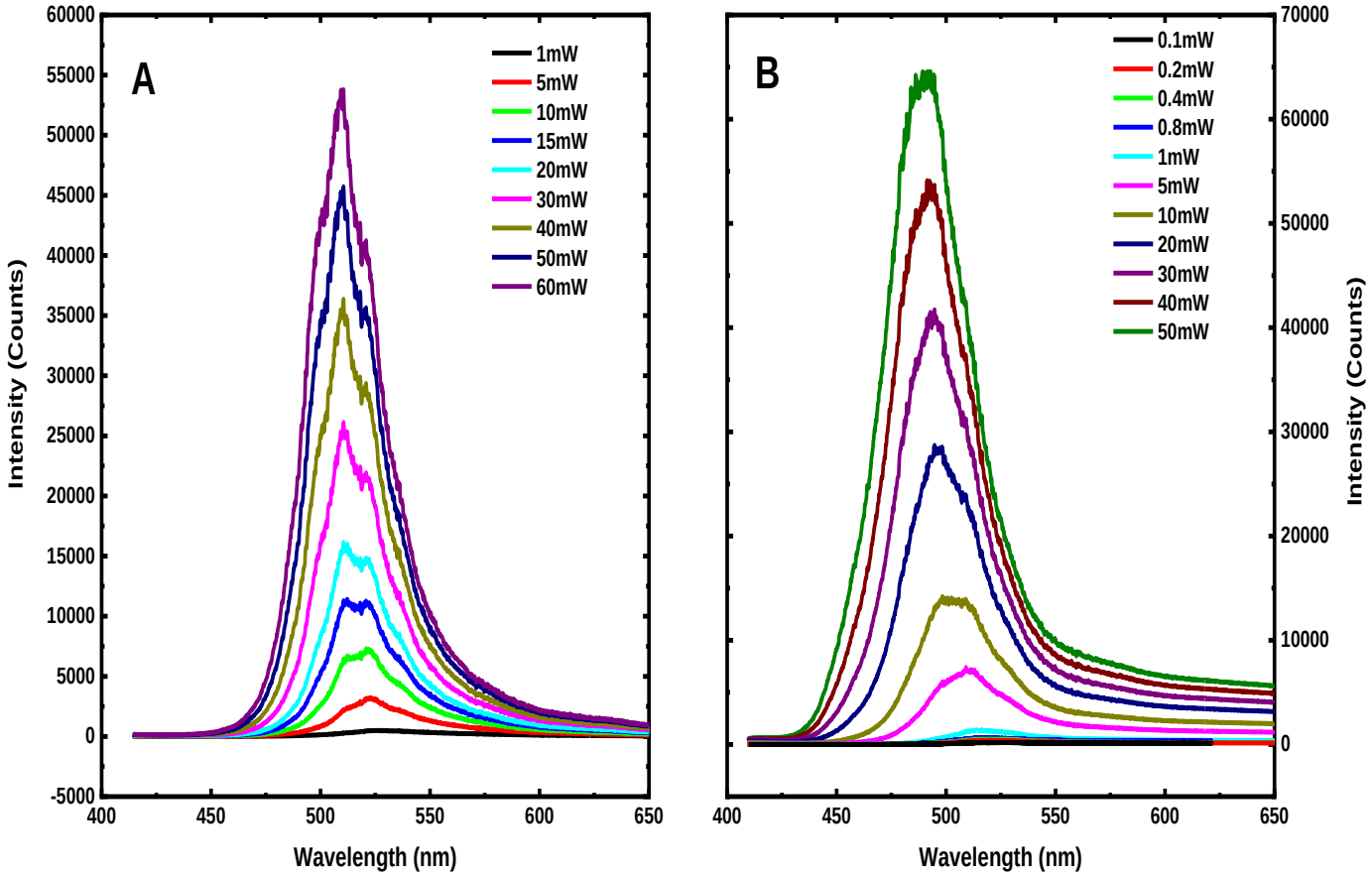

Figure 4.19 - Power dependent photoluminescent spectra of micro disk (A) Sample A and (B) Sample B

Equation 4.2 - $\Delta\lambda = \frac{\lambda^2}{n\pi 2R}$ Where λ is peak wavelength, n is refractive index, R is the radius of the micro disk [18].

The calculated separation for WGMs of 20 µm micro disk at 510nm is 0.85nm, while in **Figure 4.2a** the average separation between the peaks is 10 nm. This means that the separation is probably due to the fluctuation of indium content between the several MQWs [19]. Sample C has a similar peak wavelength and intensity, as it was measured at similar conditions to sample A, with only a small amount of peak fluctuation seen in **Figure 4.2b** in the peak broadening. A shorter growth time may allow a reduced chance of indium separation from occurring.

The other method of comparing quality is by calculating the IQE of the different samples across various sizes. Ideally, the IQE should increase with a reduced size of micro disk, as the optical confinement should increase reducing the overall strain [20]. However, for micro disks it has been reported that there is a reduction in IQE with decreasing micro disk size, as the sidewall area to volume ratio becomes dominant. This means any sidewall defects severely compromises the efficiency of the micro disks, [21] but since the sidewall should be smooth with this new method the inverse should be true [22,23].

Figure 4.3 shows the size dependence of IQE for the different samples. Sample C displays a decreasing trend in IQE, which could mean the sample is affected by side wall damage, as the reduced growth time could limit the micro hole benefits. Sample B has the smallest variation, with a range of 10%, compared to Sample C which has a variation of 19%. This indicates the balance between the side wall damage and the strain relaxation improvements. Finally, Sample A has the desired trend with it increasing to a maximum of 31% at the smallest diameter, with the increase starting with sizes below 80 µm.

To confirm the findings found from the IQE measurements, SEM cross sectional images of 20 µm disks are used to check the quality of growth. **Figure 4.4a** has the view from Sample A, where the smooth edge is connected to the SiO2 mask, but the edge has increased height above the rest of the micro disk. The raised edge will make further growth difficult for later layers but there seems to be a minimal effect on micro disk quality. Sample C shown in **Figure 4.4b** has its surface below the SiO2 mask and has prominent V dips along its surface, this is probably the main reason for its decrease in IQE [24].

The irregular micro disk growths and general low IQE across these samples means more optimisation is needed to help micro disk quality. This can be either through trial and error or the introduction of a new structure which should help growth quality.

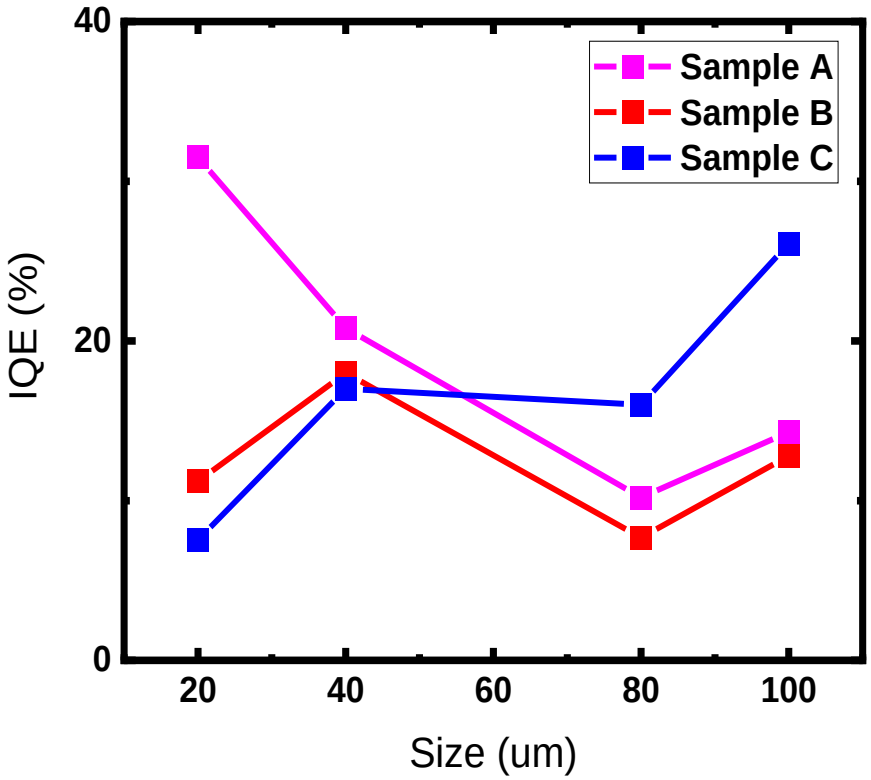

Figure 4.3 - Internal quantum efficiency against size of micro disks across various micro disk array samples

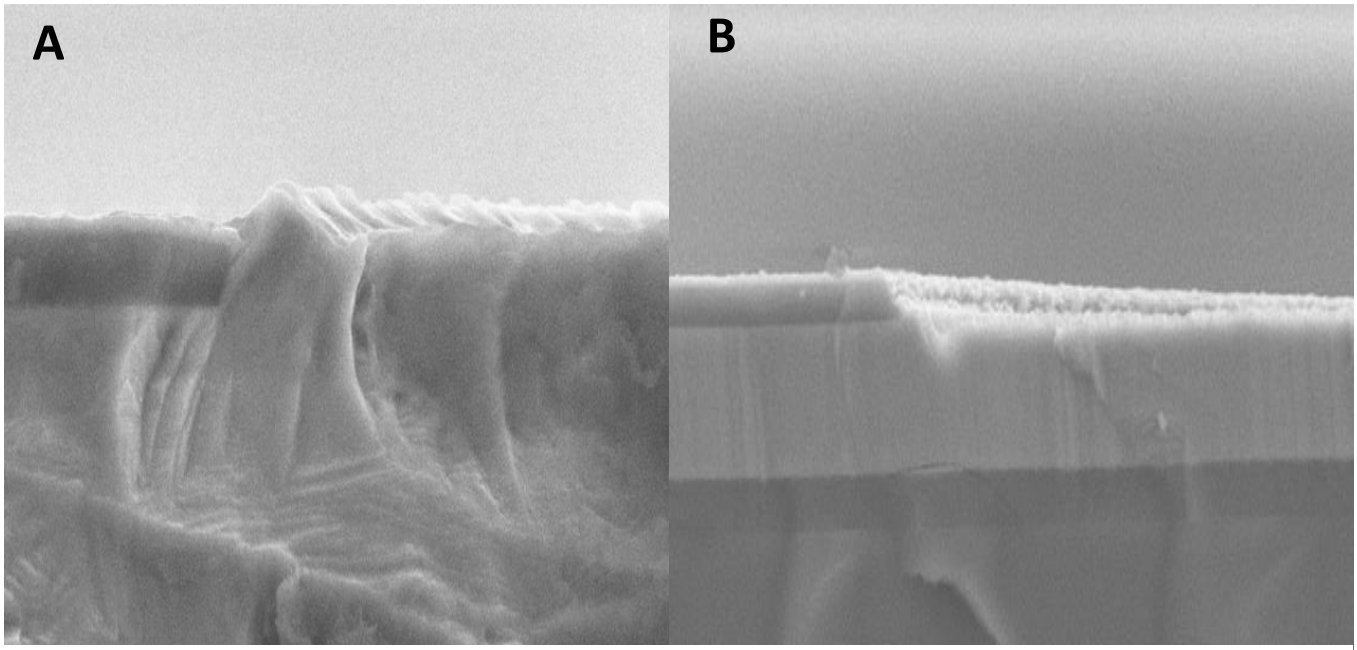

Figure 4.4 - Cross sectional SEM images of micro disk (A) Sample A and (B) Sample C

4.5 SUPERLATTICE

A superlattice is composed of alternating layers of two different semiconductors, where the mismatch between lattices should not induce any new strain related defects [25]. In this case, pairs of InGaN/GaN, with each layer being only a few nanometres thick and consisting of a large number of pairs. Superlattice buffer structures have been used to help relieve the induced strain in MQWs from the lattice constant mismatch between sapphire and GaN, reported to be 16% [26]. Relaxing this strain helps increase the radiative recombination rate, increasing the overall IQE in micro disk arrays [27].

The superlattice structure that was used in the MOCVD recipe includes 20 pairs of InGaN/GaN with 5% indium content grown after the n-GaN and before the SiO2 mask. This allows any future GaN based growths or overgrowths to have a reduced strain which will increase overall micro-LED quality [28]. Samples D, E and F were grown with the new superlattice structures with similar recipes again to attempt to optimise micro disks. From sample D – F and increasing number of superlattice layers were used from 5 – 11 pairs of InGaN/GaN layers. It was found that below 80 µm the micro disk effects take over, and so the new samples have a range of micro disks from 60 µm to 20 µm. **Figure 4.5a** shows the standard PL spectra of Sample E at 10K across all its sizes - the spectra show three peaks at 410nm, 460nm and 510m. The peak at 410nm will be a constant in all spectra since it is the peak from the InGaN in the superlattice. Excitonic behaviour is enhanced at low temperatures and is usually blue shifted compared to the main band gap peak, which explains the peak at 460nm [29], meaning the 510nm is the band gap of these micro disks. The other spectra showed a blue shift in wavelength with the 20 µm micro disk, probably due to an error during growth as the recipes were designed to make 40 µm at 510nm.

Figure 4.5b shows the comparison of IQE between the different samples. The first main change from the previous measurement is that most of the samples across all sizes have an IQE above 20%, proving that the superlattice helps improve the efficiency. Sample D has the optimal trend of increasing IQE with decreasing size, while the other two samples remain

constant. This is a further improvement as it shows that any side wall damage is not severe enough to affect the micro disks.

This current batch of micro disk arrays show marked improvement with the addition of the superlattice structure, but to further enhance the properties the optical confinement needed to be increased. The easiest way to do so was by reducing the size of the micro disks below 20 µm.

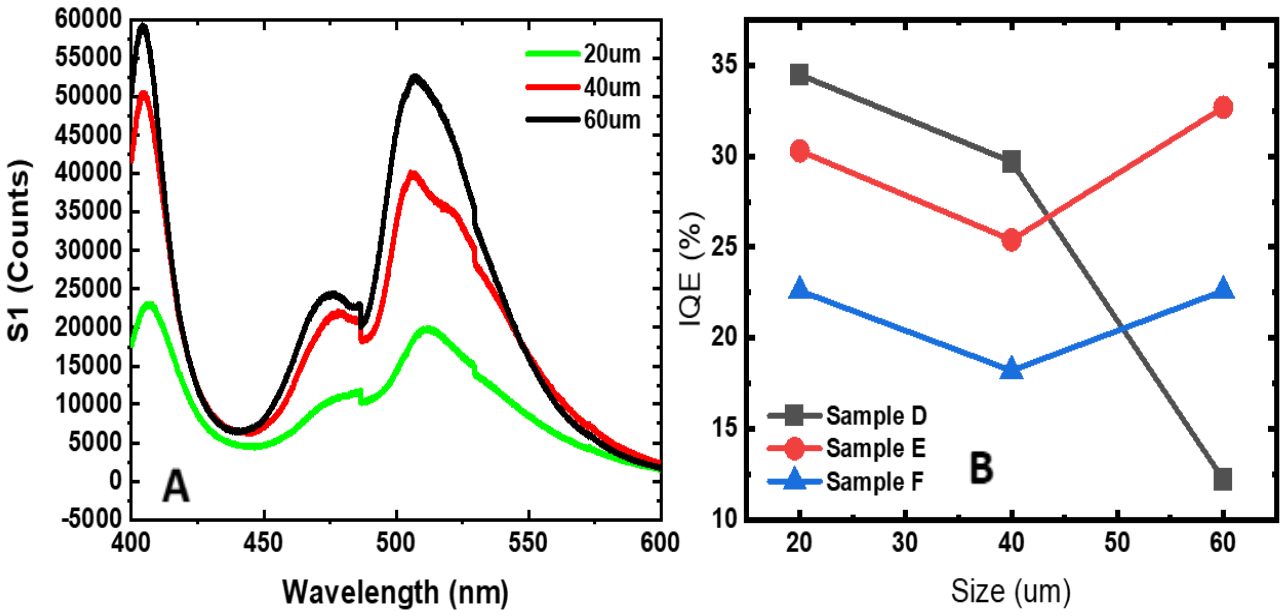

Figure 4.20 - (A) Low temperature photoluminescent spectra of Sample E (B) the IQE comparison across different samples with varying micro disk sizes.

4.6 INVESTIGATION INTO THE EFFECTS OF SURFACE QUALITY ON EFFICIENCY

A new mask was created with only 5 µm micro holes with a 2 µm interpitch. Initial measurements of sample G show a high IQE for the longest wavelength created so far at 539nm, **Table 4.1**. Unfortunately, the top view SEM images show that the surface of the disk is very rough, with many hexagonal V-pits that, while common to LED structures, generally occur in smaller densities. The p-type layer is also above the SiO_2 layer, with a slight concave shape [30]. This surface roughness directly affects the efficiency of the electrical contacts that would be required for future device fabrications. Optimisation of the p-GaN layer was needed, so a study was done to change the growth for the top layer and the effect it has on the micro disk quality. By growing p-type GaN with decreased temperature, the number of dislocations on surface morphology are reduced [31]. Other methods for increasing the surface quality are to reduce the Mg doping concentration, but for the purposes of electrical contacts there is a limit to how low the concentration is allowed to be. **Figure 4.6** shows four samples with varying temperatures, and with each new recipe the density of surface dislocations was reduced and flattened so it is in line with the SiO2 layer. Sample J has virtually no obvious defects and great circularity [32].

Checking the IQE of sample J revealed it had a lower efficiency than the first sample even with a shorter wavelength, and so a study was performed on all these samples as shown in **Table 4.1**. A direct correlation between the surface quality and the measured IQE was detected and comparing this with Sample D shows there is no effect from the wavelength, as it seems to change with every sample. It seems that changing the growth of the top layer affects the InGaN MQW in the active layer, InGaN can suffer from phase separation at lower temperatures so while maintaining a uniform growth there is [33] a decrease in the IQE even at the same wavelength. So, the future growth of samples will require a balance between the surface quality and maintain high efficiency.

With current methods it became increasingly difficult to decrease the size of micro-LEDs, with 3 µm – 3.5 µm micro disks being the limit. As a result, new methods were needed to increase the efficiency and properties of the disks. This could be achieved with optimisation of the growth recipe or new structures like superlattices. The method that was used to enhance the optical cavity with a mirror-like structure known as a distributed Bragg reflector (DBR) which enhanced spectra intensities, vertical confinement, and direct light towards the surface [34].

Table 4.1 - Calculated internal quantum efficiency of samples with various surface quality and wavelength

Sample	IQE (%)	Wavelength (nm)
Sample G	27.66	539.6
Sample H	21.36	511.5
Sample I	15.06	520.3
Sample J	13.48	520.5
Sample D (20 µm)	34.9	515

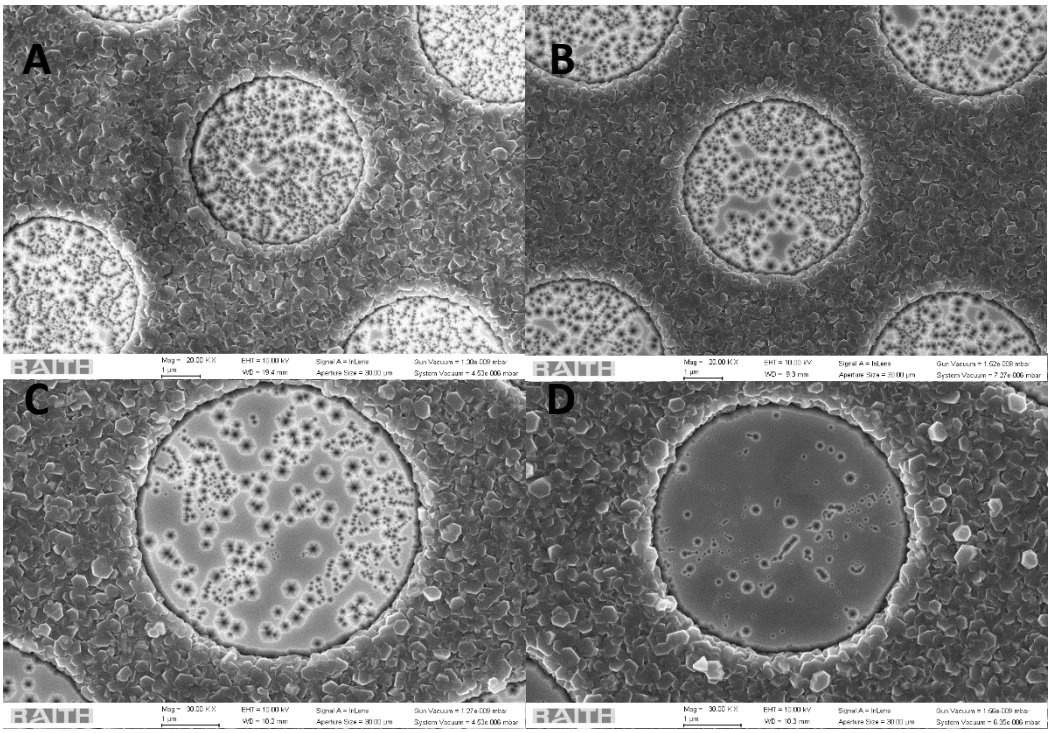

Figure 4.21 - Top view SEM images of (A) Sample G (B) Sample H (C) Sample I and (D) Sample J

4.7 EFFECT OF DBR IN MICRO-DISK LEDS

Lattice matched DBRs are a series of alternating pairs of materials with different refractive indexes and have similar lattice constants to the active region. DBRs have certain requirements to be of use in optoelectronic devices. The reflectivity needs to approach 99% with a large stop band of the reflectivity spectra centred on the peak wavelength of the active region, as InGaN MQW have been shown to suffer from indium content fluctuations. Previously many studies reported the use of AlGaN/GaN DBRs [35,36] but since a large variation in refractive index is needed for high reflectivity this meant that the Al content needed to exceed 10%, which resulted in cracks appearing due to the increase in lattice mismatch [37]. AlInN, with its near matching lattice constants and high contrast index compared to GaN was offered as an alternative, with many reported successes, but it is a difficult material to work with as it is subject to phase separation. To maintain the high degree of lattice matching, a nanoporous GaN/GaN DBR was integrated with these samples. As it is an entirely GaN structure it maintains a consistent lattice constant and offers some

relaxation mechanics similar to a superlattice for the MQWs [38]. Nanoporous DBR is reported to have a large enough index difference that allows for >99% reflectivity, and it has a large stopband of 100 nm at full width half maximum (FWHM) [39].

Each DBR structure was designed with eleven pairs of highly n doped-GaN/undoped GaN, and then etched with electrochemical etching to form a nanoporous layer. The stop band was tuned by changing the thicknesses of the highly n doped/ undoped pair [40]. The electrochemical etching process was tested to allow etched coulombs to form while preventing the whole layer from being etched. It was conducted in 0.5M nitric acid at 8V bias, using the micro-LED as an anode and a Pt plate as a cathode. Reflectivity measurements were carried out at room temperature to investigate reflectivity spectra in the microcavities. The microcavities were illuminated with a broadband unpolarised high-density plasma light source and a calibrated reflectance as a reference. The reflected light is collected into an Andor 500i monochromator and analysed with a Newton couple charged device (CCD).

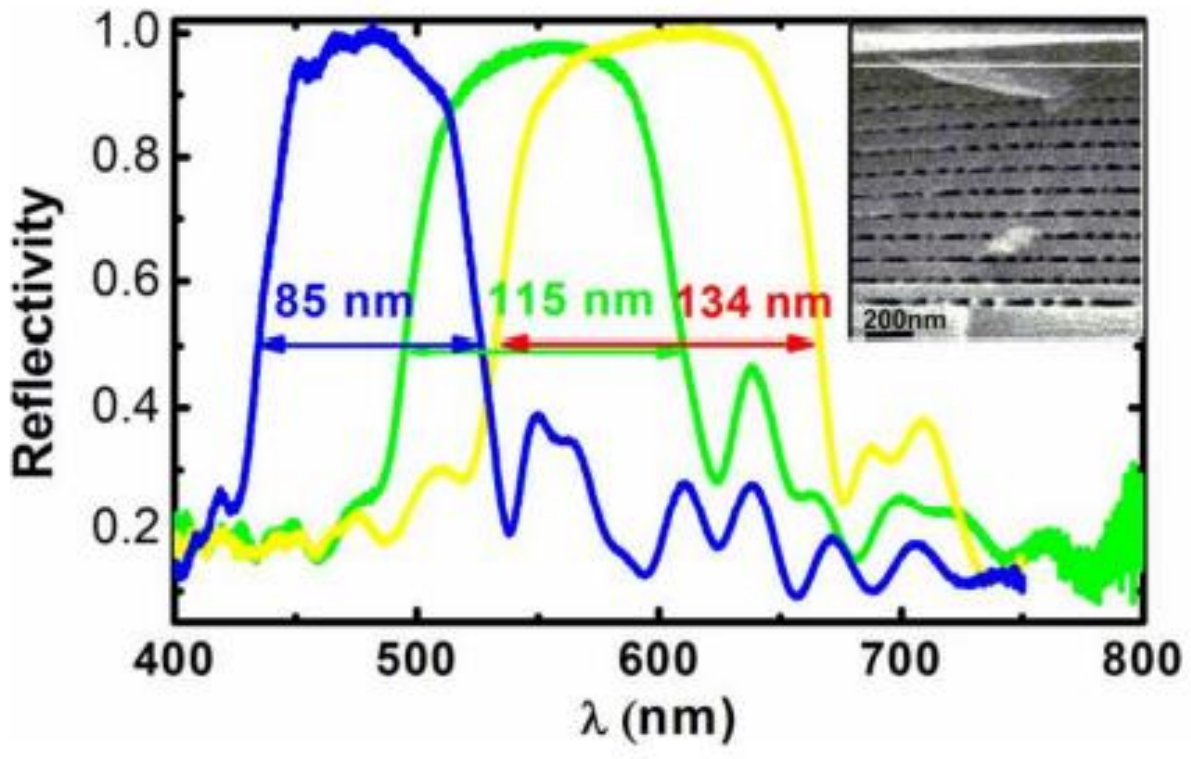

Figure 4.22 - Reflectance spectra for three type of lattice match DBRs with different centra wavelengths. With an insert of SEM image of blue DBR with clear nanoporous layers.[15]

Figure 4.7 shows the range of DBRs that were created in an attempt to match the peak wavelength of the micro disks. Previous micro disks were designed to have a peak wavelength between 510nm and 520nm, but WGM could also form within 50 nm of this peak. It seems that the larger the thickness of the DBR, the longer the wavelength and larger the stop band. All samples regardless of wavelength had a measured reflectance >95%. **Figure 4.7** also shows a cross sectional SEM image of the DBR structure with the etched nanoporous layers clearly visible [15]. These DBR were embedded underneath the superlattice and above the silicon doped n-GaN layer to affect all the micro disks and prevent a large change in the overgrowth recipe.

Sample K is a 3.5 µm micro disk array that has both DBR and super lattice structures to enhance the overall confinement and intensities. The micro disk showed evidence of WGMs as the calculated mode separation is 10.2nm for 520nm compared to the measured average separation of 11.4nm. To confirm this is not just phase separation from the MQWs, power dependent PL was used to induce stimulated emission or even trigger lasing effects, the results will be discussed later. **Figure 4.8** shows the temperature dependent PL spectra of this sample going down to 20K. The superlattice peak has a particularly low IQE since V-pit defects and dislocations are most common in the superlattice, so at low temperature any non-radiative effect from these defects is completely reduced [41]. Therefore, the IQE of the

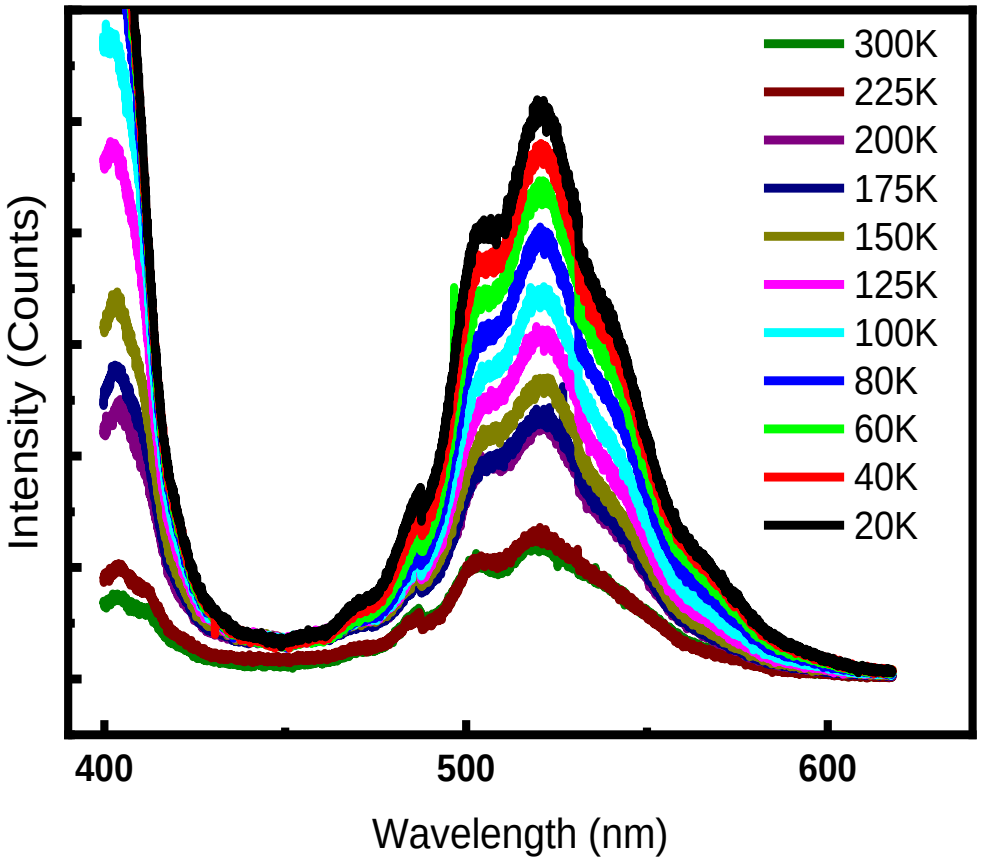

Figure 4.23 - Low temperature PL spectra of sample K from room temperature to 20 K

superlattice and micro-LED must be separated, changing the IQE from 12% to 34.4% at 520nm. There are major WGMs at 509nm, 520nm and 530nm that become more apparent at low temperatures. To conclude the latest sample is a green micro disk array which has enhanced intensities with a large IQE even at room temperatures.

4.8 POWER DEPENDENT PHOTOLUMINESCENCE STUDY

Power dependent PL can be used to investigate lasing properties of sample K. By comparing the integrated intensity against power density with a log-log axis, a typical "s" shape behaviour is formed, which is clear evidence of stimulated emission and demonstrates the lasing threshold needed to activate inversion. These measurements use a commercial WITech confocal microscope with a 375nm continuous wave (CW) laser as an excitation source. The emission light is collected and processed through a Princeton

instruments monochromator (SP2300i), and a Newton CCD camera that is air cooled. An objective lens of 100x is used to focus the laser beam, which allows a beam diameter of 220nm to measure micro and nano features.

Figure 4.9b demonstrates the nonlinear relation between excitation power and integrated intensity of sample K. The sample has an apparent threshold of 0.329mW, but no stabilising intensity at high powers or top of the "s". This seems to indicate that the micro disks can go through some of the steps of the lasing process [42], This is further apparent as the spectra show none of the peak narrowing that is characteristic of lasing spectra [43]. While sample K is unlikely to be a proper laser it has enough confinement to calculate the β- factor. Materials with a β-factor around or below 10^{-2} have a lasing threshold that is still apparent from emission spectra [44]. Sample K has a β- factor of 0.04023 which is on the boundary for being able to measure the lasing threshold. **Figure 4.9a** shows the results from a power dependent PL study that compares the β- factor between the different micro disk sizes. This apparent effect proves that reducing the micro disk size helps reduce the lasing threshold but only below 20um. This limit could be the point where micro disk effects start.

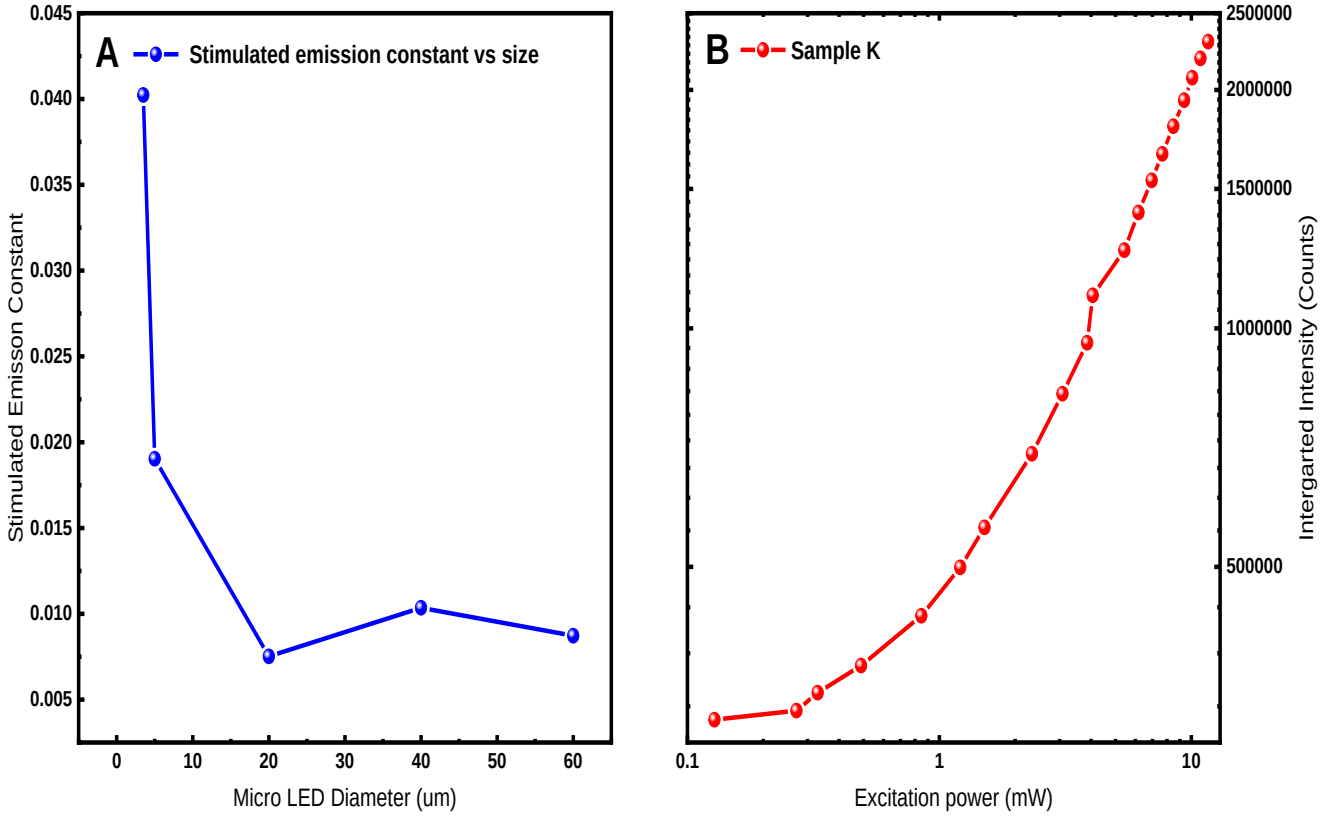

Figure 4.24 – (A) Comparison of stimulated emission constant across various micro disk sizes (B) power dependent study in a log-log graph

While these measurements prove that these micro disks are capable of lasing, further optimisation of the confinement is required. If current fabrication methods improve, smaller micro-LEDs can be created below 3.5 µm, or even nano LEDs. The nanoporous DBR could be improved toward >99% reflectivity at peak wavelength. Another method would be to completely confine the LED with another DBR on top, in an attempt to create a vertically cavity surface emitting laser (VCSEL). However, this comes with its own set of challenges [45].

4.9 CONCLUSION

This chapter goes through the process of designing and improving micro disk arrays and performing investigations into reducing the size of such disks. The overgrowth method was shown to be able to produce uniform micro disk with controllable size and interpatch. Starting with larger micro disks (>10um), IQE was used to check the quality of the disks. Samples were designed with large IQE (34%) at long wavelength (520nm), before experimenting with smaller micro disk sizes (<5um). To maintain the previous high IQE, improvements were introduced through the addition of lattice matched superlattice structures to improve relaxation of lattices in further grown layers. Further, the addition of nanoporous distributed Bragg reflectors, lattice matched to the MQW, allows for the improvement of the optical confinement in the LED structure. Reflectivity measurements showed these DBRs to have a reflectance > 95% with a stop band of 100nm. Power dependent measurements were performed which show the lasing capabilities of these micro disks. Calculated β- factors show that the smaller micro disks were capable of low lasing threshold. Future works will require optimisation of the micro cavity to further enhance these lasing properties, to finally create an integrated micro laser array device.

4.10 REFERENCE

[1] Mei, Y., Xie, M.C., Xu, H., Long, H., Ying L.Y., and Zhang, B.P. 2021 *Electrically injected GaN-based microdisk towards an efficient whispering gallery mode laser* Opt. Express **29** 5598-5606

[2] Wasisto, H.S., et al, 2019 *Beyond solid-state lighting: Miniaturization, hybrid integration, and applications of GaN nano- and micro-LEDs Applied Physics Reviews* **6**(4) p.41315. doi:10.1063/1.5096322

[3] Zhao, C., Tang, C.W., Wang, J. & Lau, K.M. 2020 *Ultra-low threshold green InGaN quantum dot microdisk lasers grown on silicon* Appl. Phys Lett **117** 031104

[4] Bai, J., et al. 2020 *Ultrasmall, Ultracompact and Ultrahigh Efficient InGaN Micro Light Emitting Diodes (μLEDs) with Narrow Spectral Line Width* ACS Nano **14** (6) 6906-6911

[5] Haberer, E., et al. 2004 *Free-standing, optically pumped, GaN/InGaN microdisk lasers fabricated by photoelectrochemical etching* Applied physics letters **85**(22) pp. 5179–5181. doi:10.1063/1.1829167

[6] Choi, H.W., et al. 2006 *Lasing in GaN microdisks pivoted on Si* Applied physics letters **89**(21) pp. 211101–211101–3. doi:10.1063/1.2392673

[7] Wang, D., Zhu, T., Oliver, R.A., & Hu, E. L. 2018 *Ultra-low-threshold InGaN/GaN quantum dot micro-ring lasers* Opt. Lett **43** 799-802

[8] Mishkat-Ul-Masabih, S., et al. 2018 *Nanoporous distributed Bragg reflectors on free-standing nonpolar m-plane GaN* Applied Physics Letters **112** 041109

[9] Rousseau, I., et al. 2018 *Optical absorption and oxygen passivation of surface states in III-nitride photonic devices* Journal of Applied Physics **123**, 113103

[10] Zhao, C., et al. 2015 *An enhanced surface passivation effect in InGaN/GaN disk-in-nanowire light emitting diodes for mitigating Shockley–Read–Hall recombination Nanoscale* **7** 16658 —16665

[11] Wang, J., et al. 2020 *Continuous-wave electrically injected GaN-on-Si micro disk laser diodes* Opt. Express **28** 12201-12208

[12] Lu, S., et al. 2021 *Designs of InGaN Micro-LED Structure for Improving Quantum Efficiency at Low Current Density* Nanoscale Res Lett **16** 99

[13] Seong, T.Y., & Amano, H. 2020 *Surface passivation of light emitting diodes: from nano-size to conventional mesa-etched devices* Surfaces and Interfaces **21** 100765 (1–15)

[14] Esendag, V., et al. 2021 *Investigation of Electrical Properties of InGaN-Based Micro-Light-Emitting Diode Arrays Achieved by Direct Epitaxy Physica status solidi* A Applications and materials science **218**(24) p. 2100474–n/a doi:10.1002/pssa.202100474.

[15] Bai, Cai, Y., Feng, P., Fletcher, P., Zhu, C., Tian, Y., & Wang, T. (2020). *Ultrasmall, ultracompact and ultrahigh efficient InGaN micro light emitting diodes (μLEDs) with narrow spectral line width*.

[16] Fan, Z. Y., Lin, J. Y., Jiang, H. X. (2008) *III-Nitride Micro-Emitter Arrays: Development and Applications*. J. Phys. D: Appl. Phys., **41**, No. 094001.

[17] Watanabe, Y., Yamada, N., Nagashima, M., Ueki, Y., Sasaki, C., Yamada, Y., Taguchi, T., Tadatomo, K., Okagawa, H., & Kudo, H. (2003) *Internal quantum efficiency of highly efficient InxGa1-xN-based near-ultraviolet light-emitting diodes*. Applied Physics Letters, **83**(24), 4906–4908. https://doi.org/10.1063/1.1633672

[18] Zhu, Li, J., Zhang, N., Li, X., Dai, J., Cui, Q., Song, Q., Xu, C., & Wang, Y. (2020) *Whispering-Gallery Mode Lasing in a Floating GaN Microdisk with a Vertical Slit*. Scientific Reports, **10**(1), 253–253. https://doi.org/10.1038/s41598-019-57118-y

[19] Lin, Ma, K.-J., Hsu, C., Feng, S.-W., Cheng, Y.-C., Liao, C.-C., Yang, C., Chou, C.-C., Lee, C.-M., & Chyi, J.-I. (2000) *Dependence of composition fluctuation on indium content in InGaN/GaN multiple quantum wells*. Applied Physics Letters, **77**(19), 2988–2990. https://doi.org/10.1063/1.1323542

[20] Vahala. (2003) *Optical microcavities*. Nature (London), **424**(6950), 839–846. https://doi.org/10.1038/nature01939

[21] Kawakami, Kaneta, A., Su, L., Zhu, Y., Okamoto, K., Funato, M., Kikuchi, A., & Kishino, K. (2010) *Optical properties of InGaN/GaN nanopillars fabricated by postgrowth chemically assisted ion beam etching*. Journal of Applied Physics, **107**(2), 023522–023522–7. https://doi.org/10.1063/1.3280032

[22] Kim, T., Liu, B., Smith, R., Athanasiou, M., Gong, Y., & Wang, T. (2014) *Coherent nanocavity structures for enhancement in internal quantum efficiency of III-nitride multiple quantum wells*. Applied Physics Letters, **104**(16), 161108. https://doi.org/10.1063/1.4873161

[23] Liu, Smith, R., Bai, J., Gong, Y., & Wang, T. (2013) *Great emission enhancement and excitonic recombination dynamics of InGaN/GaN nanorod structures*. Applied Physics Letters, **103**(10), 101108. https://doi.org/10.1063/1.4820794

[24] Oh, Lee, S.-Y., Moon, Y.-T., Ji, H. M., Park, S., Ki, Y. H., Ki, Y. S., Oh, C.-H., Shim, J.-I., Jeong, H.-H., Song, J.-O., Amano, H., & Seong, T.-Y. (2018) *Light output performance of red AlGaInP-based light emitting diodes with different chip geometries and structures*. Optics Express, **26**(9), 11194–11200. https://doi.org/10.1364/OE.26.011194

[25] Yang, Y., & Zeng, Y. (2014) *Enhanced performance of InGaN light-emitting diodes with InGaN/GaN superlattice and graded-composition InGaN/GaN superlattice interlayers*. Physica Status Solidi. A, Applications and Materials Science, **211**(7), 1640–1644. https://doi.org/10.1002/pssa.201431088

[26] Ni, Y., He, Z., Yang, F., Zhou, D., Yao, Y., Zhou, G., Shen, Z., Zhong, J., Zhen, Y., Wu, Z., Zhang, B., & Liu, Y. (2014). *Effect of AlN/GaN superlattice buffer on the strain state in GaN-on-Si (111) system*. Japanese Journal of Applied Physics, **54**(1), 15505. https://doi.org/10.7567/JJAP.54.015505

[27] Min,T., Sabki, S. N., & Othman, N. (2020) *The impact of strained layer superlattice (SLS) to the emission and internal quantum efficiency (IQE) of a GaN LED*. AIP Conference Proceedings, **2203**(1). https://doi.org/10.1063/1.5142111

[28] Huang, G. S., Lu, T. C., Yao, H. H., Kuo, H. C., Wang, S. C., Lin, C.-W., Chang, L. *Crack-Free GaN/AlN Distributed Bragg Reflectors Incorporated with GaN/AlN Superlattices Grown by Metalorganic Chemical Vapor Deposition*. Appl. Phys. Lett. 2006, **88**, No. 061904

[29] Monemar, B., Buyanova, I., Bergman, J., Amano, H., & Akasaki, I. (1997) *Electronic structure and temperature dependence of excitons in GaN*. Materials Science & Engineering. B, Solid-State Materials for Advanced Technology, **43**(1), 172–175. https://doi.org/10.1016/S0921-5107(96)01857-0

[30] Hu, S., Liu, S., Zhang, Z., Yan, H., Gan, Z., & Fang, H. (2015) *A novel MOCVD reactor for growth of high-quality GaN-related LED layers*. Journal of Crystal Growth, **415**, 72–77. https://doi.org/10.1016/j.jcrysgro.2014.12.038

[31] Usami, S., Miyagoshi, R., Tanaka, A., Nagamatsu, K., Kushimoto, M., Deki, M., Nitta, S., Honda, Y., & Amano, H. (2017) *Effect of dislocations on the growth of p-type GaN and on the characteristics of p–n diodes*. Physica Status Solidi. A, Applications and Materials Science, **214**(8). https://doi.org/10.1002/pssa.201600837

[32] Surender, S., Prabakaran, K., Loganathan, R., Pradeep, S., Singh, S., & Baskar, K. (2017) *Effect of growth temperature on InGaN/GaN heterostructures grown by MOCVD*. Journal of Crystal Growth, **468**, 249–251. https://doi.org/10.1016/j.jcrysgro.2016.11.061

[33] Sugahara, T., Hao, M., Wang, T., Nakagawa, D., Naoi, Y., Nishino, K., & Sakai, S. (1998) *Role of dislocation in InGaN phase Separation*. Japanese Journal of Applied Physics, Part 2: Letters, **37**(10), L1195–L1198. https://doi.org/10.1143/jjap.37.l1195

[34] Carlin, & Ilegems, M. (2003) *High-quality AlInN for high index contrast Bragg mirrors lattice matched to GaN*. Applied Physics Letters, **83**(4), 668–670. https://doi.org/10.1063/1.1596733

[35] Ng, H. M., Moustakas, T., & Chu, S. N. (2000) *High reflectivity and broad bandwidth AlN/GaN distributed Bragg reflectors grown by molecular-beam epitaxy*. Applied Physics Letters, **76**(20), 2818–2820. https://doi.org/10.1063/1.126483

[36] Asano, T., Yanashima, K., Asatsuma, T., Hino, T., Yamaguchi, T., Tomiya, S., Funato, K., Kobayashi, T., & Ikeda, M. (1999) *CW Operation of AlGaInN-GaN Laser Diodes*. Physica Status Solidi. A, Applied Research, **176**(1), 23–30. https://doi.org/10.1002/(SICI)1521-396X(199911)176:1<23::AID-PSSA23>3.0.CO;2-G

[37] Carlin, J. F., & Ilegems, M. (2003) *High-quality AlInN for high index contrast Bragg mirrors lattice matched to GaN*. Applied Physics Letters, **83**(4), 668–670. https://doi.org/10.1063/1.1596733

[38] Mishkat-Ul-Masabih, S., Aragon, A. A., Monavarian, M., Luk, T. S., & Feezell, D. F. (2019) *Electrically injected nonpolar GaN-based VCSELs with lattice-matched nanoporous distributed Bragg reflector mirrors*. Applied Physics Express, **12**(3), 36504. https://doi.org/10.7567/1882-0786/ab0576

[39] Park, J., Kang, J.-H., & Ryu, S.-W. (2013) *High Diffuse Reflectivity of Nanoporous GaN Distributed Bragg Reflector Formed by Electrochemical Etching*. Applied Physics Express, **6**(7), 072201–072201–4. https://doi.org/10.7567/APEX.6.072201

[40] Smith, J. M., Ley, R., Wong, M. S., Baek, Y. H., Kang, J. H., Kim, C. H., Gordon, M. J., Nakamura, S., Speck, J. S., DenBaars, S. P. *Comparison of Size-Dependent Characteristics of Blue and Green InGaN MicroLEDs Down.* Applied Physics Letters, **116**(7), 71102. https://doi.org/10.1063/1.5144819

[41] Sidikejiang, S., Henning, P., Horenburg, P., Bremers, H., Rossow, U., Menzel, D., & Hangleiter, A. (2022) *Low-temperature internal quantum efficiency of GaInN/GaN quantum wells under steady-state conditions*. Semiconductor Science and Technology, **37**(3). https://doi.org/10.1088/1361-6641/ac4b89

[42] Athanasiou, M., Smith, R. M., Pugh, J., Gong, Y., Cryan, M. J., & Wang, T. (2017). *Monolithically multi-color lasing from an InGaN microdisk on a Si substrate*.

[43] Laser Theory. (2022-03-20). https://chem.libretexts.org/@go/page/67372

[44] Reitzenstein, S., Forchel, A. (2012) *Highly efficient quantum dot micropillar lasers in Quantum Optics with Semiconductor Nanostructures*

[45] Lu, T.-C., Wu, T.-T., Chen, S.-W., Tu, P.-M., Li, Z.-Y., Chen, C.-K., Chen, C.-H., Kuo, H.-C., Wang, S.-C., Zan, H.-W., & Chang, C.-Y. (2011) *Characteristics of Current-Injected GaN-Based Vertical-Cavity Surface-Emitting Lasers*. IEEE Journal of Selected Topics in Quantum Electronics, **17**(6), 1594–1602. https://doi.org/10.1109/JSTQE.2011.2116771

5 OPTICAL INVESTIGATION OF OPTICALLY PUMPED VCSEL OBTAINED BY DIRECT EPITAXY

5.1 ABSTRACT

Optically pumped whispering gallery mode (WGM) lasing has been observed in many free-standing micro-disk structures. Dry etching is normally used during fabrication, causing severe side wall damages which degrades lasing performance of the microdisk structures, especially for electrically injected devices. In this paper, we combine selective overgrowth techniques with an epitaxial lattice-matched distributed Bragg reflectors (DBR) to overcome these issues and achieve high quality micro-disk cavities with 3.5 µm diameter topped with a highly reflective (>99%) dielectric DBR. It is observed that InGaN polaritons occur in the high-quality micro-cavities and WGM modes are measured though photoluminescence (PL) measurements. Moreover, finite difference time domain (FDTD) simulations show that the positions of the modes are in good agreement with the experiment. Furthermore, lasing behaviour is observed with a threshold at 410 µW and dominate mode at 488 nm.

5.2 INTRODUCTION

Recently there has been increased interest in developing GaN based micro light emitting diodes (LEDs) and lasers. The applications for such devices range from augmented reality (AR) micro displays [1], to high-speed communications with micro sensors [2]. The current method to create free standing micro disks is with using a top-down fabrication process. This has the advantage in creating high confinement in all directions due to the large refractive index difference between the surrounding air and InGaN [6].

The alternative method used to grow high quality micro disks introduced in the last chapter showed that the epitaxial overgrowth technique was able to recreate the high confinement using a Si mask along the sidewalls [7]. Thanks to recent developments a method to create high reflectance lattice matched GaN distributed Bragg reflectors (DBRs) was also used below the multi quantum well (MQW) [8]. To develop these micro disk arrays into vertically confined stimulated emitting lasers (VCSEL), further containment would be required above the MQW. In this chapter, we will demonstrate high quality InGaN-based micro-disk cavities with 3.5 μm diameter, topped with a highly reflective (>99%) dielectric DBR. Optically pumped whispering gallery modes (WGM) have been measured, and lasing behaviour is obtained with a threshold at 410 μW and a dominate mode at 488 nm.conclusion

In this chapter, we have developed further our InGaN/GaN MQW micro disk arrays into micro laser arrays. Enhancing the microcavity previously created by growing a highly reflective lattice-matched NP-GaN/GaN DBR underneath and a dielectric DBR on top of the MQW. This has allowed an optical pumped laser to be created at room temperature. Power dependent measurements have demonstrated a stimulated emission at 488 nm with a threshold of 410 μW. To further test these experimental results, they were compared to 3D Lumerical FTDT simulations that showed a good agreement with the experimental positions of the modes, also proving that these modes were indeed caused by WGM. While the performance can be further enhanced with the structure optimisation, the InGaN-based micro disk arrays are great candidates for creating high quality microcavities with lasing properties. Further work will be to recreate these results at smaller micro disk sizes below 3.5um.

5.3 EXPERIMENTS

Our InGaN-based micro-disk arrays are grown on a patterned GaN template by metal organic vapor phase epitaxy (MOVPE). First, the GaN template is grown on a c- plane sapphire substrate using a standard two-step growth method using MOVPE. It starts with a undoped GaN layer and 11 pairs of alternating highly silicon doped n-type GaN (n-GaN)/undoped-GaN (u-GaN) distributed Bragg reflectors (DBR), followed by a 600 nm n-GaN layer (doping level of $5x10^{19}$ cm^3). Then a SiO_2 dielectric layer is deposited on top of the template, roughly 500 nm thick, using a standard plasma enhanced chemical vapor deposition (PECVD) technique. Afterwards, the as-grown template is then patterned by photolithography and etched down to the n-GaN layer using inductively coupled plasma (ICP) to create micro hole arrays with a diameter of 3.6 μm and an interpitch of 2 μm. Finally, the patterned template is put into the MOVPE again for further growth of an InGaN/GaN light-emitting diode (LED) structure. It is composed of a starting n-type GaN layer, an InGaN pre layer with 5% indium content, and 5 periods of multi quantum wells (MQW) with 2.5 nm InGaN well and 13.5nm GaN barrier, topped with a 20 nm p-type $Al_{0.2}Ga_{0.8}N$ and a 200 nm p-type GaN. Due to the SiO_2 dielectric mask, the overgrowth only happens in the micro holes, forming an array of grown micro-LEDs, as shown in **figure 5.1a**. Through modifying the diameter and interpitch of photomasks, micro-LED arrays with different sizes, can be grown.

In order to form a lattice-matched DBR structure from the highly doped n-GaN/u-GaN layers, electrochemical-etching (EC) is performed on the micro-LED array sample. The EC process is conducted in 0.5M nitric acid at 8V bias for 10 mins, with the micro-LED sample as an anode and a Pt plate as cathode. **Figure 5.1b** is a typical scanning electron microscopy (SEM) image of an EC-etched micro-disk sample. It can be seen clearly that the highly doped n-GaN layers have become nanoporous GaN (NP-GaN) layers. There will be a large difference in the refractive indices between the NP-GaN layer and the u-GaN layer, which results in a high reflectivity of the lattice matched DBR structure. To finally form a VCSEL cavity, a dielectric lambda quarter DBR is deposited on top of the micro-LEDs composed of 6 pairs of SiO_2/SiN layers. In this work, 3D finite difference time domain (FDTD) simulations are used to help design the high-quality micro-cavity. The thicknesses of each layer for the dielectric DBR,

with 85 nm for SiO_2 and 61 nm for SiN, are estimated to be most effective by means of Lumerical FDTD simulations.

5.4 RESULTS AND DISCUSSION

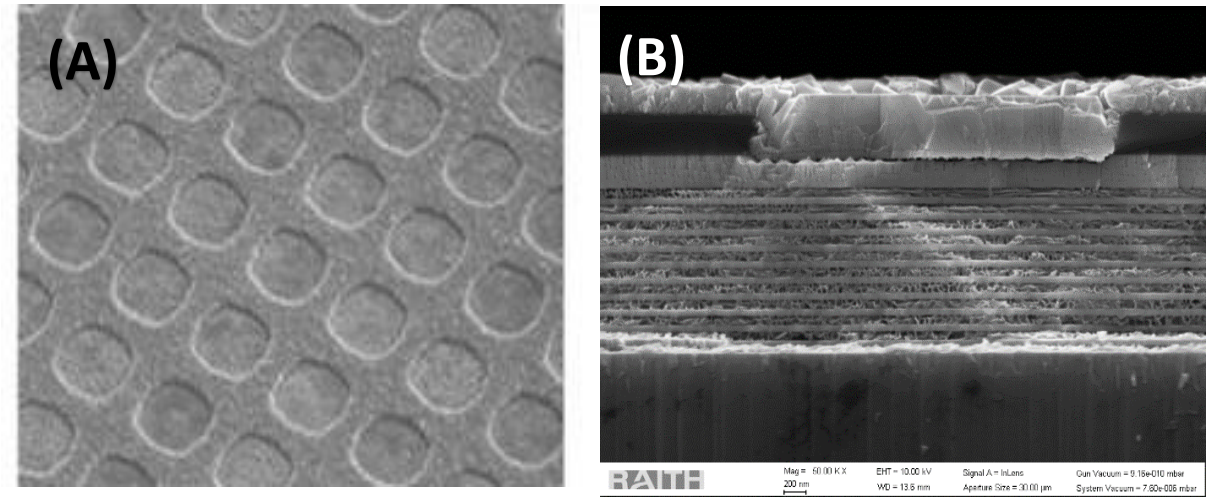

Figure 5.25 - Scanning electron microscopy images (A) Top-down SEM image of the array structure (B) cross section SEM of the nanoporous InGaN/GaN distributed Bragg reflectors

Figure 5.2 shows reflectance of the micro-cavity along with two respective DBRs. One is an EC-formed lattice-matched NP-GaN/u-GaN DBR, and the other one is a deposited dielectric DBR on sapphire. As shown in Figure 2, the reflective spectra of both the NP-GaN/u-GaN DBR and the dielectric DBR have large stop bands and high reflectance of >95% which can form optical modes in the green wavelength range. Though these is a small difference in the central wavelengths for the two stopbands, with the lattice matched DBR and the dielectric DBR having central wavelengths at 460 nm and 470 nm, respectively, the large stopbands have a sufficient overlap, allowing formation of optical modes. Further optimisation of these structures could lead to improved performance in the micro-cavity with a larger stop band overlap. The overall reflectance of the micro-cavity array is observed to

have 4 dips in the reflectivity, which agrees with several modes observed in both photoluminescence and FDTD spectra, which will be discussed later in this chapter.

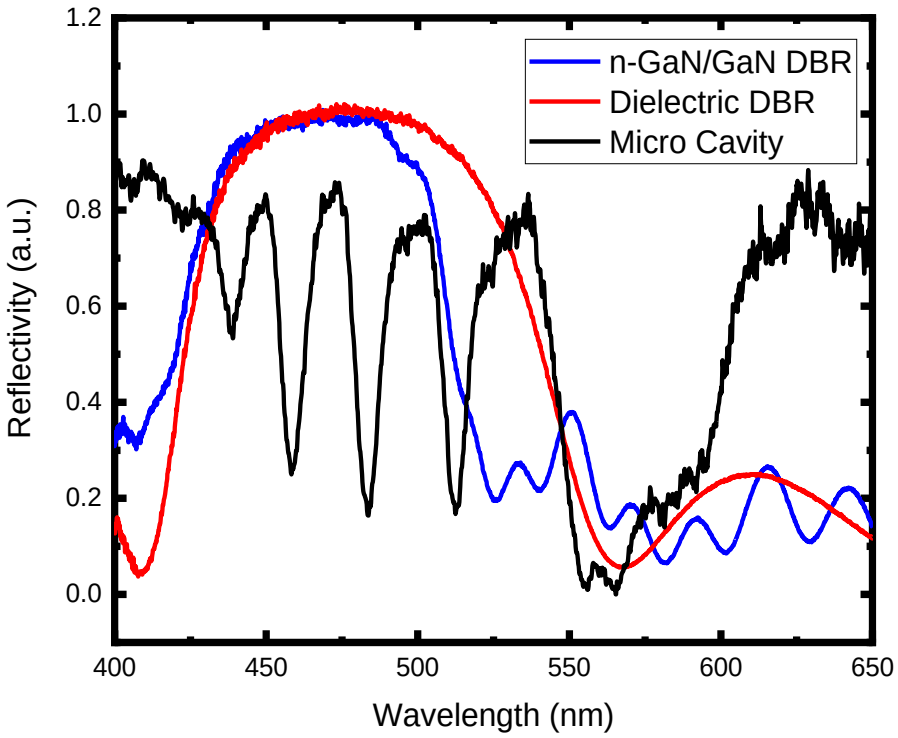

Figure 5.26 - Reflectivity spectra of the microcavity, a lattice matched NP-GaN/GaN, and a dielectric DBR. Showing both have high reflectivity DBRs > 95% both covering a range between 480–500 nm. The combined cavity creates a reflectance spectrum with dips representing apparent modes.

To achieve high quality cavities with lasing behaviour, micro-disks need to be formed [9] because, in such structures, strong coupling is expected to form between the photons and excitons, creating exciton polaritons [10]. However, it is difficult to observe exciton polaritons in InGaN MQWs due to the large inhomogeneity broadening [11]. Therefore, to enhance the lasing chances, the structure is designed to obtain a large stopband for a greater wavelength range of modes, allowing a greater chance of polaritons to be observed.

Angled reflectivity measurements have been carried out at room temperature to investigate polariton characteristics in the microcavities. The micro-cavities are illuminated with a broadband unpolarised high-density plasma light source and a calibrated reflectance as a reference. The reflected light is collected into an Andor 500i monochromator and analysed with a Newton couple charged device (CCD). **Figure 5.3a** shows reflectance as a

function of the varying angle for a microcavity between a top NP-GaN/GaN DBR and a dielectric DBR. An overall blue shift in wavelengths can be observed for all modes. However, at around 2.77 eV, the 420 nm mode becomes weaker before disappearing at around 60 degrees. **Figure 5.3b** plots the photon energies of the modes as a function of varying angle for the microcavity. It reveals a slight anti-crossing behaviour at 2.77 eV, where the upper and lower branches of the polariton begin to "repel" each other after closing in. The photon energy, at which the mode disappears, can be used as the energy of the exciton. In this case, it is observed to be 2.77 eV. The energy of the photon can be determined by fitting on the upper and lower branches using the detuning to calculate its value as various angles. Finally, the Rabi splitting can be calculated using **Equation 5.1**, which reflects the strength of the exciton-photon coupling,

Equation 5.1 $-E_{LP}E_{UP} = \frac{1}{2}[E_{exe} + E_{ph} \pm \sqrt{\Omega^2 + \left(E_{exe} + E_{ph}\right)^2}$

where Ω is Rabi splitting, $E_{LP}E_{UP}$ is energy of lower and upper branches, E_{exe} is energy of exciton during coupling, and E_{ph} is energy of photon where the anti-crossing begins [12]. In this work, the rabi splitting for the microcavities is 5 meV. Other works reported higher rabi splitting values the lowest stated to be around 30meV for GaN based micro cavities [13], but many of these studies are either in bulk GaN [14] or planar MQWs [15-16]. To further increase the rabi splitting would require the optimisation between the cavity resonance and InGaN exciton, whereas we are focusing on the WGMs [15].

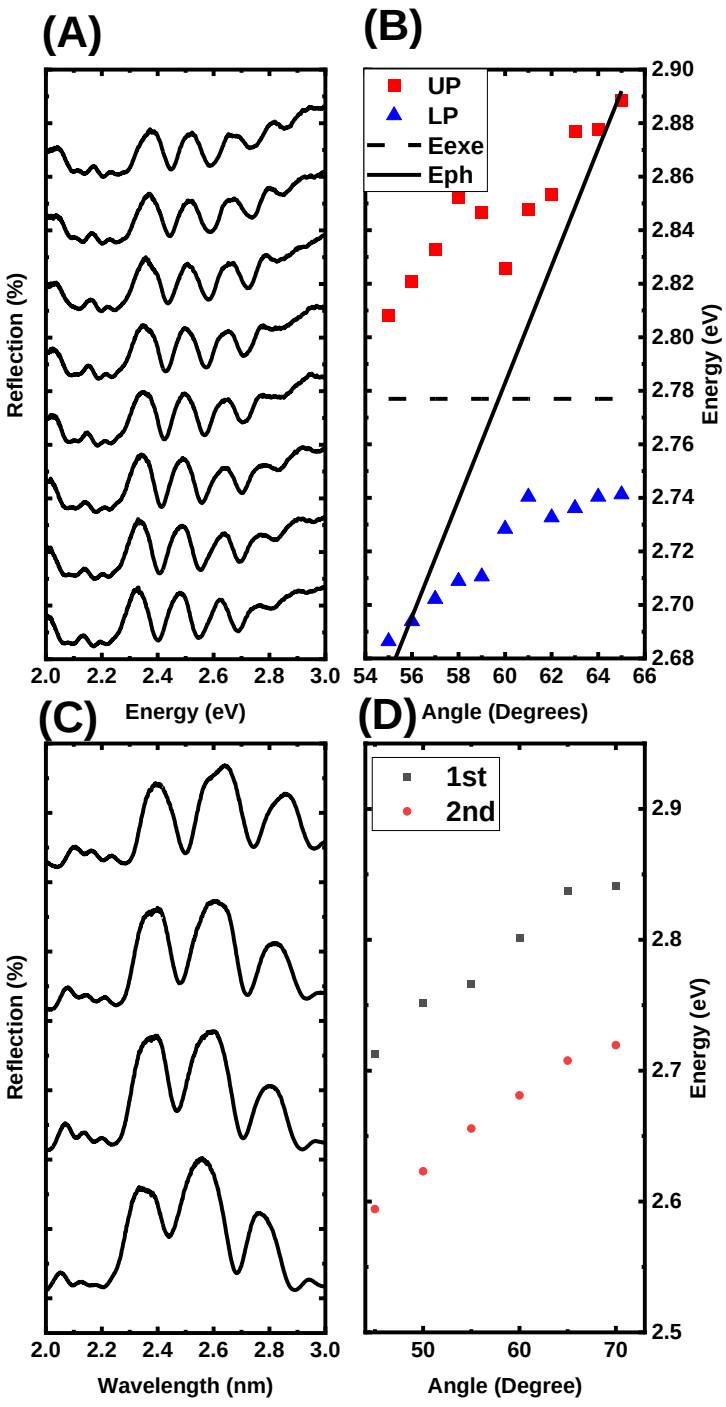

Figure 5.27 - (A) Angular reflectivity spectra of the microcavity between a NP-GaN/GaN DBR and a dielectric DBR (B) Photon energy vs angle of the microcavity between a nanoporous DBR and a dielectric DBR (C) Angular reflectivity spectrum of a micro cavity without a t top DBR **(D)** Photon energy vs angle of the microcavity without a top DBR.

Figure 5.3c presents the angular reflectivity of the microcavity without the top NP-GaN/GaN DBR, which has a larger separation compared to the microcavity with two DBRs, showing the increased cavity length when adding a top DBR. This is probably due to the reflectivity of DBR becoming >95% midway through the DBR structure. Plotting of the mode energies against the angle is shown in **Figure 5.3d.** It exhibits a linear change in wavelength for both the two modes with a constant separation, proving that polariton only forms in the enhanced cavity. Demonstration of the polariton behaviour combined with the rabi splitting value, indicates that the microcavity created along with a nanoporous lattice matched GaN DBR and a top dielectric DBR is capable of high-quality confinement required for lasing behaviour [16].

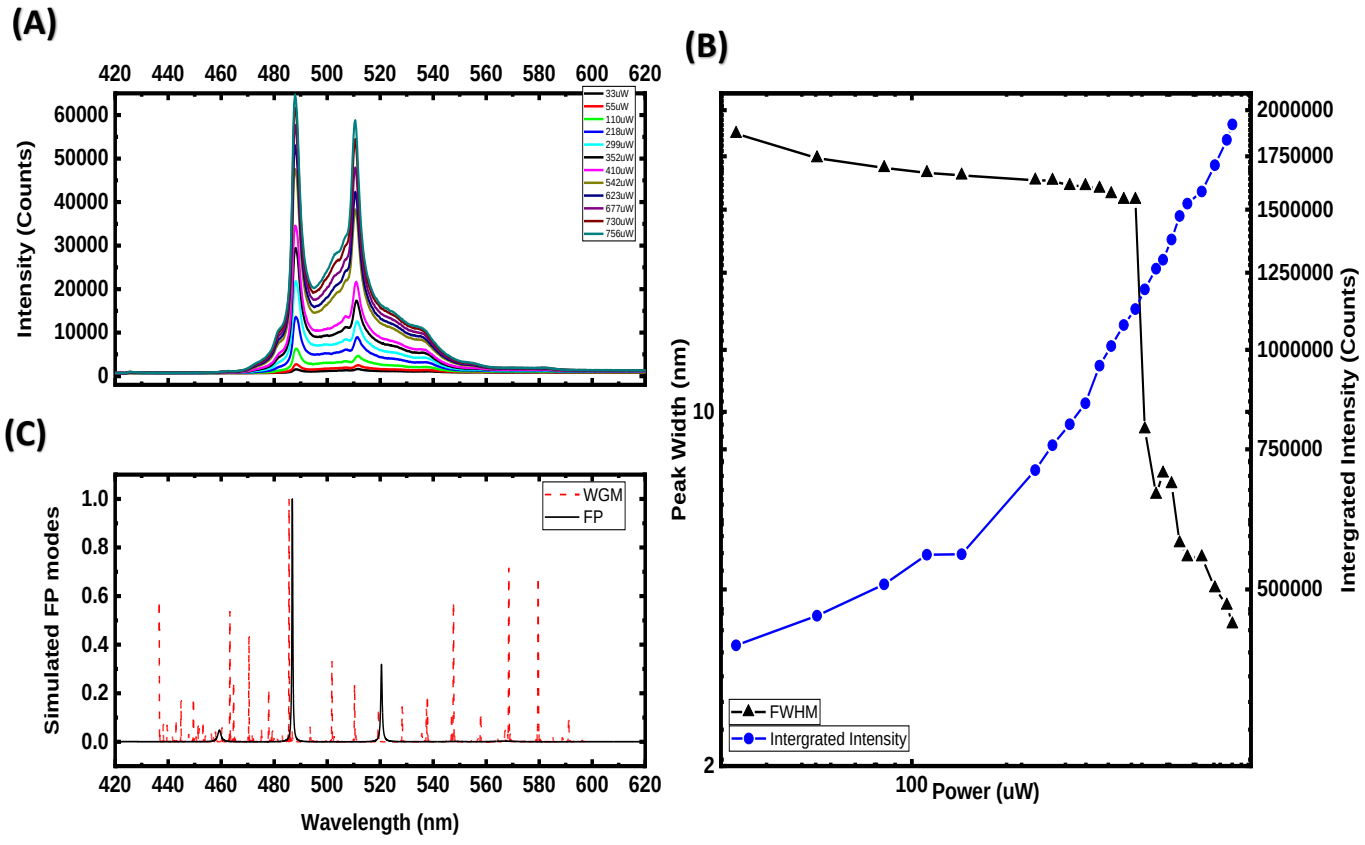

Figure 5.28 - (A) Power-dependent photoluminescence spectra excited with powers from 1-30mW of an InGaN/GaN microcavity. The main peaks at 480 nm shows a dramatic increase in intensity from 410 µW. (B) Integrated intensity and FWHM of the peak at 480 nm as a function of excitation power with a log-log scale. **(C)** FDTD simulation of the microcavity showing FP and WGM modes.

Furthermore, power-dependent Photoluminescence (PL) measurements are performed at room temperature to investigate optical characteristics of the MQW's in the microcavities with emphasis on its lasing properties. The lasing measurements were performed with a commercial confocal microscopy system equipped with a high-resolution x-y-z piezo-stage allowing the excitation and emission collection from a single micro disk device. The devices are non-resonantly excited using a 375nm continuous wave laser, and the emission is then collected into a monochromator and detected with a CCD. The laser spot size allows for spatial resolution for up to 200 nm, roughly 100 nm in diameter. The emission exhibits a series of spectral peaks which are associated with optical modes. **Figure 5.4a** displays power-dependent photoluminescence spectra with excitation powers from 30 to 800uW of the microcavity. It shows that the two main peaks are located at 488 nm and 511 nm with a roughly 20 nm separation. It does not agree with the theoretical spacing of vertical Fabre–Perot (FP), or circular whispering gallery modes (WGMs) for the microcavity between two DBRs, as estimated by **Equation 5.2**.

Equation 5.2 - $\Delta\lambda = \frac{\lambda^2}{nL}$ Where λ is peak wavelength, n is refractive index, L is cavity length (12).

However, upon closer examination there are a few other modes, like modes at 479 nm, 502 nm and 523 nm with a smaller separation. Combined with the main peaks, these could be ascribed to WGMs from the circular confinement in the microdisk. The overlap between the two types of modes can create interference, making it hard to separate. Optimisation in the structure by supressing one set of modes could further enhance the emission. Based on the reflectivity measurements, the shorter peak could also be a polariton mode. Previous papers show that at certain wavelengths both types of mode could form that can be separately activated by passing through different lasing thresholds [16]. This could explain in **Figure 5.4a** why the peak width appears to drop twice while decreasing with power.

As shown in Figure 4a, the emission intensity increases constantly with the increase of the power. When the power is above 410 μW, a strong and sharp emission peak at 488 nm appears and begins to go through a nonlinear change in the spectra. It demonstrates a dramatic intensity increase along with a reduction in peak width above a certain power threshold [17]. **Figure 5.4b** shows the integrated intensity and the full width half maximum

(FWHM) of the peak as a function of excitation power with a log-log scale. An 'S' shape curve is observed in the integrated intensity-power (L-L) plot [18], which is a typical indicator of lasing behaviour. The lasing threshold can be calculated to be 410 μW. This lasing threshold is a bit high compared to micro lasers in other reports, which can be attributed to the non-optimisation of the microstructure. It is noted that the FWHM shows a decreasing trend with increasing the power. Especially, the peak narrows dramatically from above 400 μW and the FWHM decreases to 4nm finally, which further confirms a stimulated emission.

The positions of modes within the microcavity have been calculated by standard FDTD simulations. For simulation, the electric field is injected by a plane wave source which is placed above the top DBR, with emission wavelength of 400nm-700nm. The geometrical data of these devices are from the in-situ growth characterisation. Monitors, placed inside the cavity, allow determination of the decay in the electric field, which was used to determine the wavelength of the resonant modes. The boundary conditions are set as periodic on X, Y and PML in the Z dimension to reduce the simulation requirements.

The effective indices of the nanoporous layers are approximated from the volume average theory (VAT) using **Equation 5.3**.

Equation 5.3 - $n_{por} = [\,(1-\varphi)n_{GaN}^2 + \varphi n_{air}^2]^{1/2}$

Where $n_{por}, n_{GaN}, n_{air}$ and Φ are the effective refractive index of the nanoporous layer, refractive index of GaN, refractive index of air and porosity, respectively [19]. The porosity is assumed to be 0.5 from SEM images, leading to n_{por}=1.9.

Figure 5.4c displays both the FP and WGM modes of the microcavity obtained by the FDTD simulation. It shows that the positions of the simulated modes are in line with those in the experimental spectra. Examining the mode separation of the simulation, the WGM has an average separation of 8.7 nm and FP has a separation of 34.8 nm. the mode separation of the experiment is closer to the WGM compared to the FP. In the simulation, there is an overlap between the two mode systems at 485 nm, which could lead to a competition, finally limiting the effectiveness of the microcavity. Supressing one mode system~~s~~ by reducing the size (either radially or vertically) should further improve the performance of the microcavity [20].

5.5 CONCLUSION

In this chapter, we have developed further our InGaN/GaN MQW micro disk arrays into micro laser arrays. We can enhance the microcavity previously created by growing a highly reflective lattice-matched NP-GaN/GaN DBR underneath, and a dielectric DBR on top of the MQW. This has allowed an optical pumped laser to be created at room temperature. Power dependent measurements have demonstrated a stimulated emission at 488 nm with a threshold of 410 μW. To further test these experimental results, they were compared to 3D Lumerical FTDT simulations that showed a good agreement with the experimental positions of the modes, also proving that these modes were indeed caused by WGM. While the performance can be further enhanced with the structure optimisation, the InGaN-based micro disk arrays are great candidates for creating high quality microcavities with lasing properties. Further work will be to recreate these results at smaller micro disk sizes below 3.5um.

5.6 REFERENCES

[1] Templier, F. (2016) *GaN-based emissive microdisplays: A very promising technology for compact, ultra-high brightness display systems*. J. Soc. Inf. Disp., **24** (11), 669−675.

[2] Wun, J. F., Lin, C.-W., Chen, W., Sheu, J. -K., Lin, C. -L., Li, Y.-L., Bowers, J. E., Shi, L.-W., Vinogradov, J., Kruglov, R., & Ziemann. O. (2012) *GaN-Based Miniaturized Cyan Light-Emitting Diodes on a Patterned Sapphire Substrate With Improved Fiber Coupling for Very High-Speed Plastic Optical Fiber Communication*. IEEE Photonics Journal, **4**(5), 1520–1529. https://doi.org/10.1109/JPHOT.2012.2210867

[3] Han, H.-V.; Lin, H.-Y.; Lin, C.-C.; Chong, W.-C.; Li, J.-R.; Chen, K.-J.; Yu, P.; Chen, Te. M.; Chen, H.-M.; Lau, K.-M.; Kuo, H.-C. (2015) *Resonant-Enhanced Full-Color Emission of Quantum-Dot-Based Micro LED Display Technology*. Opt. Express, **23**, 32504.

[4] Green, R. P., McKendry, J. J. D., Massoubre, D., Gu, E., Dawson, M. D., Kelly, A. E. (2013) *Modulation bandwidth studies of recombination processes in blue and green InGaN quantum well micro-light-emitting diodes*. Appl. Phys. Lett., **102** (9), 091103.

[5] Phillips, J.M., et al. (2007) Laser Photon. Rev. 1, 307

[6] Jiang, J., Xu, H., Sheikhi, M., Li, L., Yang, Z., Hoo, J., Guo, S., Zeng, Y., Guo, W., & Ye, J. (2019) *Omnidirectional whispering-gallery-mode lasing in GaN microdisk obtained by selective area growth on sapphire substrate*. *Optics Express*, **27**(11), 16195–16205. https://doi.org/10.1364/OE.27.016195

[7] Olivier, F., Daami, A., Licitra, C., Templier, F. (2017) *Influence of Size-Reduction on the Performances of GaN-Based Micro-LEDs for Display Application*. Appl. Phys. Lett., **111**, No. 022104.

[8] Bai, Cai, Y., Feng, P., Fletcher, P., Zhao, X., Zhu, C., & Wang, T. (2020). *A direct epitaxial approach to achieving ultrasmall and ultrabright InGaN micro light-emitting diodes (μLEDs)*.

[9] Zhu, G., Li, J., Zhang, N., et al. (2020) *Whispering-Gallery Mode Lasing in a Floating GaN Microdisk with a Vertical Slit* Sci Rep **10** 253

[10] Tawara, T., Gotoh, H., Akasaka, T., Kobayashi, N., & Saitoh, T (2004) *Observation of InGaN cavity polaritons at room temperature*. In Conference on Lasers and Electro-Optics/International Quantum Electronics Conference and Photonic Applications Systems Technologies Technical Digest (CD) Optical Society of America paper **IThB1**.

[11] Shi, X., et al. (2019) *Theoretical optimization of inhomogeneous broadening in InGaN/GaN MQWs to polariton splitting at low temperature* Superlattices and Microstructures Volume **128** Pages 151-156 ISSN 0749-6036

[12] Wu, J., *et al.* (2019) *Large Rabi splitting in InGaN quantum wells microcavity at room temperature* Mater. Res Express **6** 076204

[13] Faure, S., et al. (2008) *Comparison of strong coupling regimes in bulk GaAs, GaN, and ZnO semiconductor microcavities*, Physical review. B Condensed matter and materials physics **78**(23) p. 235323. doi:10.1103/PhysRevB.78.235323.

[14] Malpuech, G., et al. (2002) *Room-temperature polariton lasers based on GaN microcavities* Applied physics letters **81**(3) pp. 412–414. doi:10.1063/1.1494126.

[15] Wu, J. *et al.* (2019) *Large Rabi splitting in InGaN quantum wells microcavity at room temperature*. *Mater. Res. Express* **6** 076204

[16] Wu, J. Z. *et al*. (2019). Polariton lasing in InGaN quantum wells at room temperature. *Opto-Electron Adv* **2**, 190014 .

[17] Ghosh, P., Yu, D., Li, G., Huang, M., Liu, Y. *Size dependent polaritonic effects in GaN microrod studied through optical property investigation*. *Optik*, Volume **240**,2021,166829

[18] Athanasiou, M. et al. (2017) *Monolithically multi-color lasing from an InGaN microdisk on a Si substrate*. Scientific Reports, 7 (1). 10086. ISSN 2045-2322

[19] Zhang, X., Cheung, Y. F., Zhang, Y., & Choi, H. W. (2014) *Whispering-gallery mode lasing from optically free-standing InGaN microdisks*. *Opt. Lett*. **39**, 5614-5617

[20] Sellés, J. *et al.* (2016) *Deep-UV nitride-on-silicon microdisk lasers*. *Sci. Rep.* **6**, 21650

6 INFLUENCE OF IRREGULARITIES IN SHAPE ON OPTICAL PERFORMANCE

6.1 ABSTRACT

In this article we wish to investigate the effect of circularity of the micro disks structure. Not irregularity due to side wall roughness, but due to deformity in overall structure and shape. Though purposely made defects have been used selectively removes modes for lasing [20], these interrupt the Whispering Gallery Modes (WGMs) but not the overall circularity. Through use of 2D Finite Difference Time Domains (FDTD) simulations we can vary the degree of deformation suffered by devices. Using the calculated modes and spectra within the disks, we can find the tolerance point when the deformation is too much for WGM modes to form. Then we can compare with the experimental photoluminescence measurements to check they agree simulations. If smaller micro disks are extremely sensitive to their overall shape this could prove to be a hard limiting factor in creating such arrays.

6.2 INTRODUCTION

Recently progress has been made in the miniaturisation of GaN based optoelectrical devices for creating highly efficient LEDs in the UV to visible range [1]. The focus has been to create micro and nano sized LEDs, usually in disk form over large arrays [2,3]. As many studies have shown the ease at which Whispering Gallery Modes (WGM) can form in micro disks with properties such as high Quality (Q) factors and creation of low threshold lasers [4,5,6].

Our recent ways of creating micro disks through overgrowth methods have been done with the intention of overcoming the side wall issue which has been known to limit the size and uniformity of such arrays [16,17]. Even with improvements to said devices such as smoothing the side wall with techniques like passivation [11,12] or refining the structure with photoelectrochemical etching (PEC) to undercut the disk [13-15], towards recreating high quality disk arrays in nano scale has been slow. As micro disks continue becoming smaller, the circularity of micro disks becomes more difficult to maintain, regardless of side wall damage. Therefore, consistently creating micro disks arrays with bulk uniformity becomes a priority [18,19].

Following our previous work's attempts to recreate the lasing properties with micro disks of a smaller size have been met with difficulties. We were unable to form WGMs even though in theory the removal of the side wall limitation should have made the process easier [7,8]. SEM and confocal mapping showed irregularities in micro disk shape which will be discussed further into the chapter. We theorised that such irregularities could have a similar limiting effect to WGM formation through optical losses [9,10], and therefore used theoretical simulations to investigate.

6.3 METHODS

We used 2D Finite Difference Time Domains FDTD simulations to simulate the micro disks structures using a commercial grade software (Lumerical Solutions Inc.). A series of dipole sources with emission wavelength centred on 500nm with a gaussian profile were spread evenly near edge of the micro disk as this is where the WGM is the strongest. The

structures were simplified versions of our micro disk samples, with a InGaN (n = 2.4) layer sandwiched between two GaN (n = 2.44) [20] layers with radii varying from 1 µm – 10 µm and surrounded by SiO2 (n = 1.45) [21]. We added a straight edge deformity that varied in height, an example is shown in **Figure 6.1**. Using **Equation 6.1** we calculated the area of removed section which we converted into a percentage to easily compare different disk sizes.

Equation 6.1 $A = (r^2)acos(r - h/r) - (r - h)\sqrt{2rh - r^2}$ r - radius of micro disk, h - height of the straight edge deformation [21].

The mesh used has a minimum of ten mesh cells per wavelength and the simulation was run for 1000fs. Frequency domain monitors were used to record the emissions over the simulated region with end apodization as we are monitoring how photons are trapped within the structure. The spectra are collected by a grid of 25-time monitors placed both inside and the immediate outside of the structure to calculate accurately the time domain field signal. All simulations were simulated for room temperature.

We compared the varying electric field profiles with an increasing edge deformation to find the tolerance point, the point where the WGMs visibly fail to form. We extracted the emission spectra and found the integrated intensity to quantify the tolerance point with respect to the area remove from the deformity. We suspect the micro and nano disks to be incredibly sensitive to even slight deformations in the circularity of the disk.

To further confirm these simulations, we used Photoluminescence (PL) mapping across arrays with different sized disks. Using this overgrowth method designed to reduce sidewall roughness [18], allowed us to confirm the importance of overall disk shape. Our measurements use a commercial WITech confocal microscope with a 375nm continuous wave (CW)laser is used as an excitation source. The emission light is collected and processed through a Princeton instruments monochromator (SP2300i), and a Newton charged coupled device (CCD) that is air cooled. An objective lens of x100 is used to focus the laser beam, which allows a beam diameter of 220nm to measure micro and nano features. A high-resolution x-y-z piezo stage enables the creation of PL maps at a micro level. All measurements were done at room temperature.

Our arrays are grown on a patterned SiO2 mask GaN template by metal organic vapor phase epitaxy (MOVPE). All layers are grown on c- plane sapphire wafer using standard two

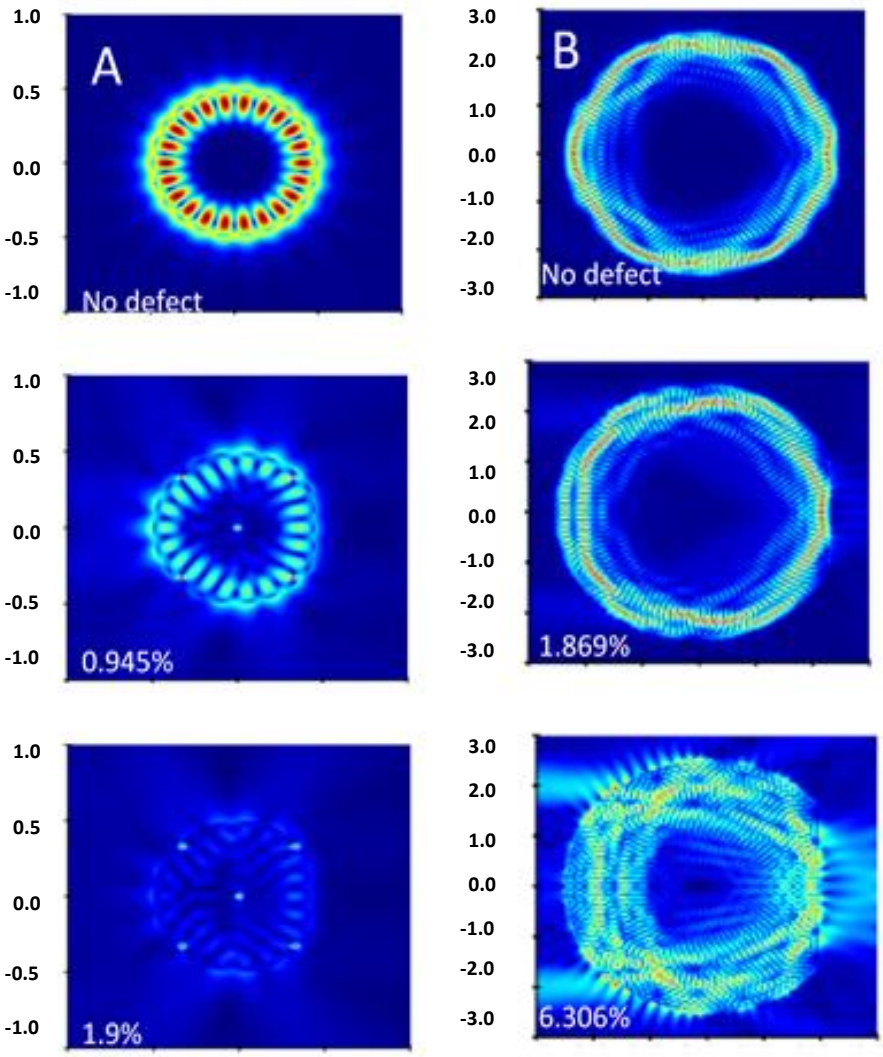

Figure 6.29 - Electric field distribution profile for 500nm modes along the horizontal. (A) 1 μm micro disk ranging from 0% - 1.9% (B) 5 μm micro disk ranging from 0% - 6.306%

step growth method using MOVPE. Starting with 11 layers of alternating highly n-doped GaN/undoped-GaN distributed Bragg reflectors (DBR), followed by a silicon doped n-GaN layer (doping level of $5x10^{19}$ cm^3) that is 600nm thick. Then a SiO2 dielectric layer is deposited on top, roughly 500nm thick, using a standard plasma enhanced chemical vapor deposition technique (PECVD). Afterwards using photolithography, we attached a Ni mask to the SiO2 layer, which is then etched down to the n-GaN layer to form a mask using inductively coupled plasma (ICP) to create the micro holes 3.6 μm diameter and an interpitch of 2 μm. Following the etching and using the mask created, an overgrowth method was performed using MOVPE to form a standard InGaN/GaN LED structure with 5 layers multi quantum wells (MQW) with 2.5nm InGaN well and 13.5nm GaN barrier with a starting n-type GaN layer and then an InGaN pre layer with 5% indium content. This is

topped with a 20nm p-type Al0.2Ga0.8N on which a 200nm p-type GaN is grown to finish the overgrowth. Due to the dielectric mask the overgrowth only happens in the micro holes creating a natural array of grown micro-LEDs, as shown in figure 4. While 10 µm diameter disks have been grown, successful attempts were made with different diameter micro-LEDs such as 5 µm, 3 µm and 2 µm.

6.4 SIZE VARIATION FDTD SIMULATIONS OF MICRO DISK STRUCTURES

Our electric field profiles start with a regular distribution of WGMs for both 1 µm and 5 µm samples. The mode spacing as calculated by **Equation 6.2**, confirm the simulation with 1 µm having 16.5nm spacing and 5 µm having 6.6nm at 500nm wavelength and a refractive index of 2.41 for InGaN, which we used as the main mode for our experiment**.**

Equation 6.2 $\Delta\lambda = \frac{\lambda^2}{nL}$ λ – peak wavelength, n – refractive index L – cavity length (22)

The 5 µm profile seem to exhibit second or higher order modes in the centre of the disk that causes interference patterns along the edge. We then introduce a straight edge defect slowly increasing till 10% of the total area is removed for different size disks. Though there are many types of defects that can affect the overall circularity and cavity effectiveness via losses, the straight edge defect allows an ease of control and definition to the simulation. As well as being present in many of the later SEM and mapping images.

As the edge defect area increases, we notice an overall reduction in intensity in the electrical field profile. Isolating the resonant peak at 500nm and creating electric field profiles, as shown in **Figure 6.2**, we can this reduction in intensity. We also see a break down in WGM shape as the path of the total internal refraction changes with small changes to the shape at 0.945%. The emission spectra also show a reduction in intensity through the spectra range. When the deformity reaches 1.9% of the total area, we see that the disk has no significant resonant peaks on the disk edge which means no WGMs form and there is

very little light being confined to the disk. When comparing against a 5 µm micro disk we can see the structure has greater stability with a similar defect at 1.869%the electric field profile is similar with some optical leakage where the defect is. The modes start to collapse in shape at 6.306% with a similar wavelength, though there is still light confined the large amount of optical leakage makes WGM very difficult to form. The intensity is overall weaker in the 5 µm disk due to the larger size requiring more source dipoles to fill the disk at a similar intensity as smaller systems, the trend is still visible in **Figure 6.3a**.

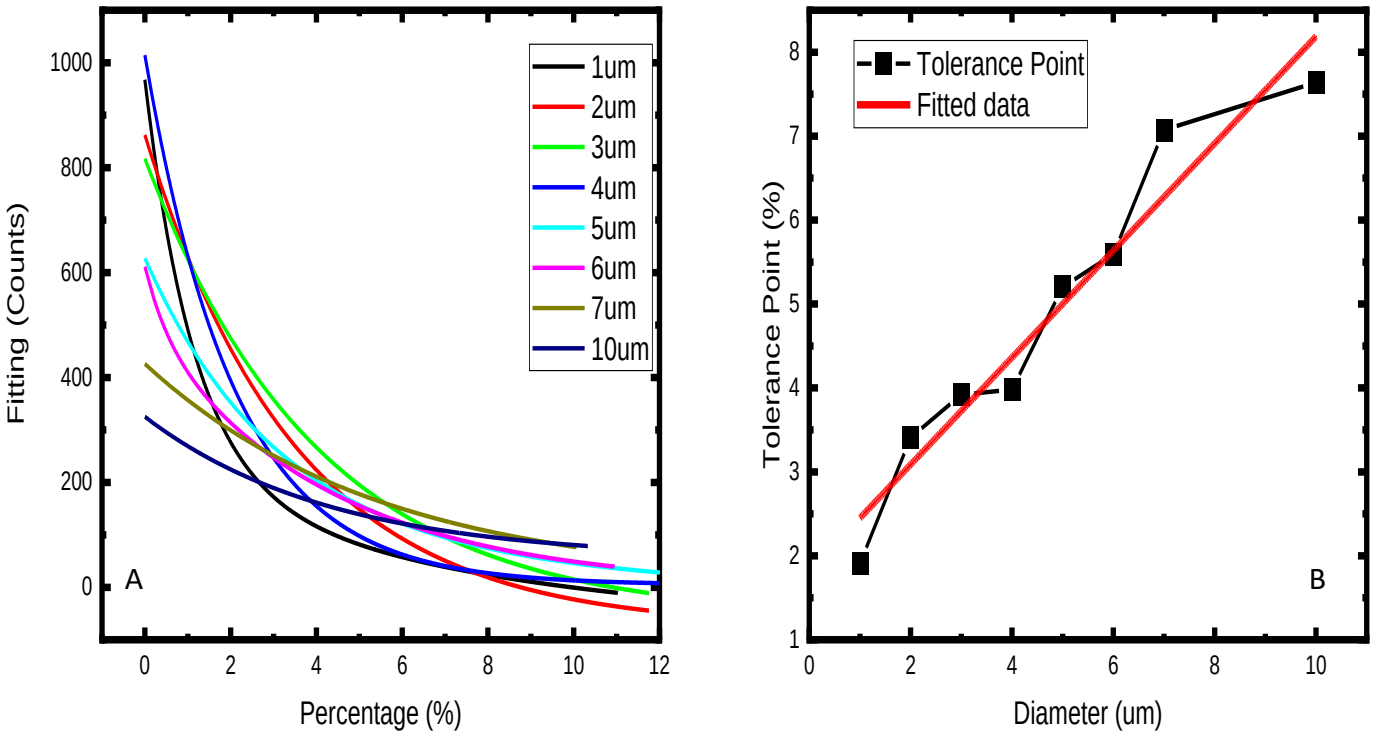

Figure 6.30 – (A) Integrated Intensity vs Percentage of area removed by defect (B) Tolerance points vs Diameter of micro disks

Creating simulated micro disks with different radii from 1 µm to 10 µm, we extracted the spectra calculated the integrated intensity. Plotting the integrated intensity against the area from deformity, as seen in **Figure 6.3a**, we can see how the overall intensity is affected by the change in shape. An overall decrease is expected due to the increase of optical

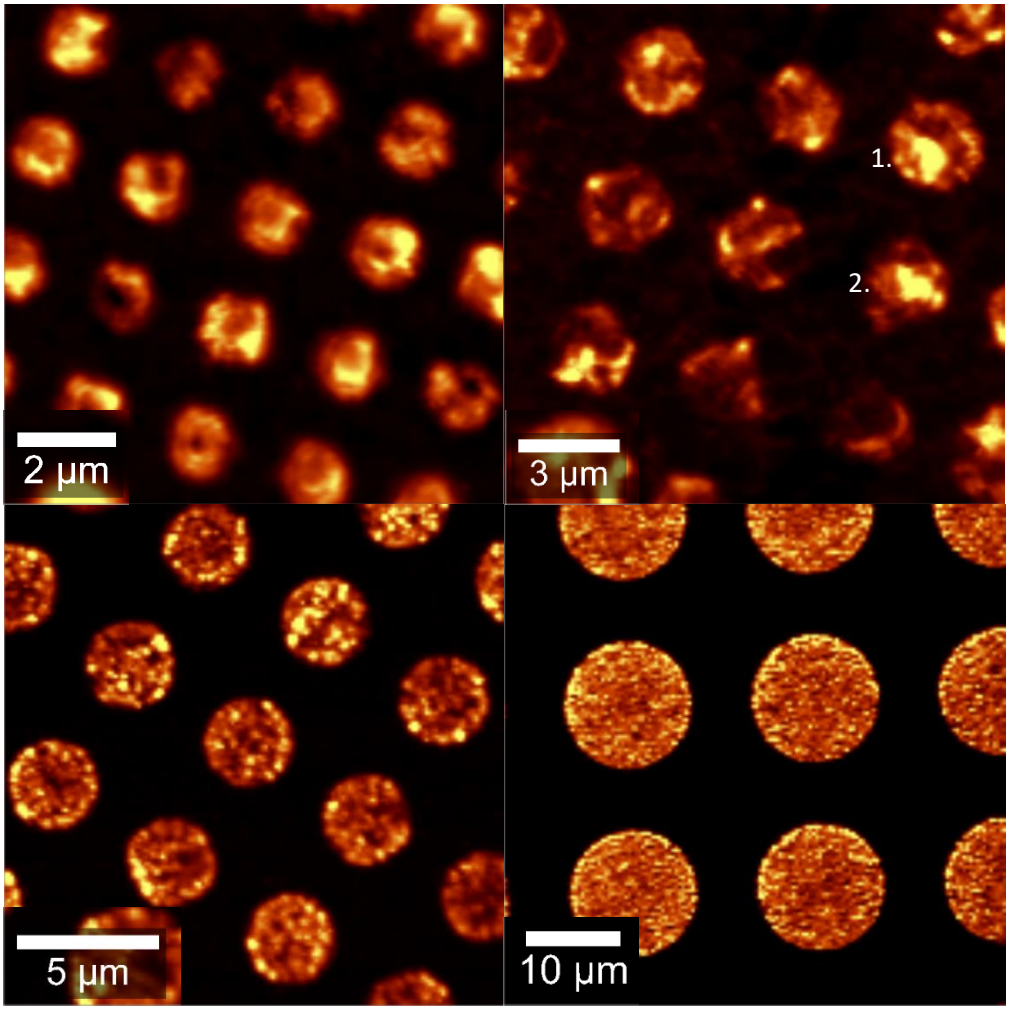

Figure 6.3 - Intensity Photoluminescence mapping of 2 µm*, 3* µm*, 5* µm *and 10* µm *micro disk arrays with a confocal microscope.*

leakage but all of them show a slowing down of this decrease till it becomes a constant intensity. This is obvious in our 1.9% simulations as there is a limit to how much light leave the disk till the disk is just a non-boundary. In our 5 µm simulations even after the modes have broken down there still seems to be a confinement of light, but the electric field profiles stay similar after this point confirming a similar equilibrium has been achieved. As we increase the radius of the disk the overall intensity goes down and the rate the disks achieve equilibrium decreases showing higher tolerance point. Through plotting these tolerance points, which we determine on the fitted graphs where the line evens out, we see how this trend evolves. In **Figure 6.3b**, we see a positive linear trend with larger micro disk sizes proving larger sizes are more stable. With 1 µm disks only allowing 2% irregularity before becoming unviable this is a significant obstacle in making miniaturised GaN based array devices.

6.5 PHOTOLUMINESCENCE MAPPING FOR OVERGROWN MICRO DISK

The mapping of 2 µm, 3 µm, 5 µm and 10 µm disks shows how integrated intensity changes, allowing us to check the uniformity across a 25 µm -by-25 µm area. As shown in **Figure 6.3**, the 2 µm and 3 µm disks show a greater variance in integrated intensity patterns. The intensity of each disk forms irregular shapes, unlike the circular disk they visibly seem to be. A small increase in size shows more regular shapes but there is still a random distribution of intensities within each disk. However, when compared to some of our simulations there are similarities confirming that our simulated defects are quite common,

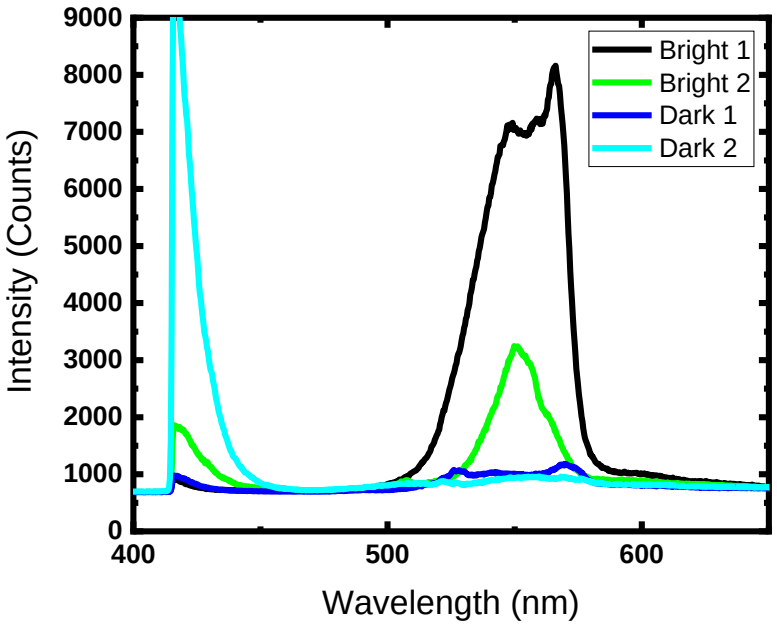

Figure 6.31 - Photoluminescence spectra of dark and bright points in 3.5 µm micro disk array

as seen in **Figure 6.5**. The simulation exhibited a criss-cross pattern as the mode patter is interrupted by reflections off the corners of the straight edge, with the PL mapping image showing a cross bright pattern with a one dark edge side opposite. Even with large amount of optical leakage the SiO2 mask gives enough confinement to allow a mode pattern to form, though no longer WGM.

Taking a closer look at the intensity mapping of the 3.5 µm array, we picked PL spectra from two different micro disks focusing on the bright and dark points on each disk, as shown in **Figure 6.3** labelled 1 and 2. From this we should be able to see if modes are still forming in such randomised patterns, this was attempted with the 2 µm array but no samples with modes have been able to form. On **Figure 6.4**, we can see that in disk 1 where we have an intensity pattern of a bright ring around the edge there is a bright signal centred at 550nm. The peak is split into several forming mode-like features, with a bright ring this suggest the presence of WGMs. In disk 2 there is a straight edge to the disk shape as no light is emitting from the edge, the bright point is more of a standard PL spectrum with the same central wavelength, showing a lack of modes forming while coming from the same growth conditions. The dark points are much weaker than the bright areas showing poor quality MQWs either from growth or mask defects, but they still have the same peak shape as the brighter spectra. This confirms with our previous measurements and simulations that modes can form in these disks but at smaller sizes a slight change in the circularity from defects can create a different spectrum.

These defects could form at any step during the fabrications process from mask alignment, irregularities in etching procedure and finally sidewall interference during overgrowth. The mapping for 5 µm disks is when some uniformity starts to appear with similar intensities and continuing pattern of a bright edge when WGM are formed as

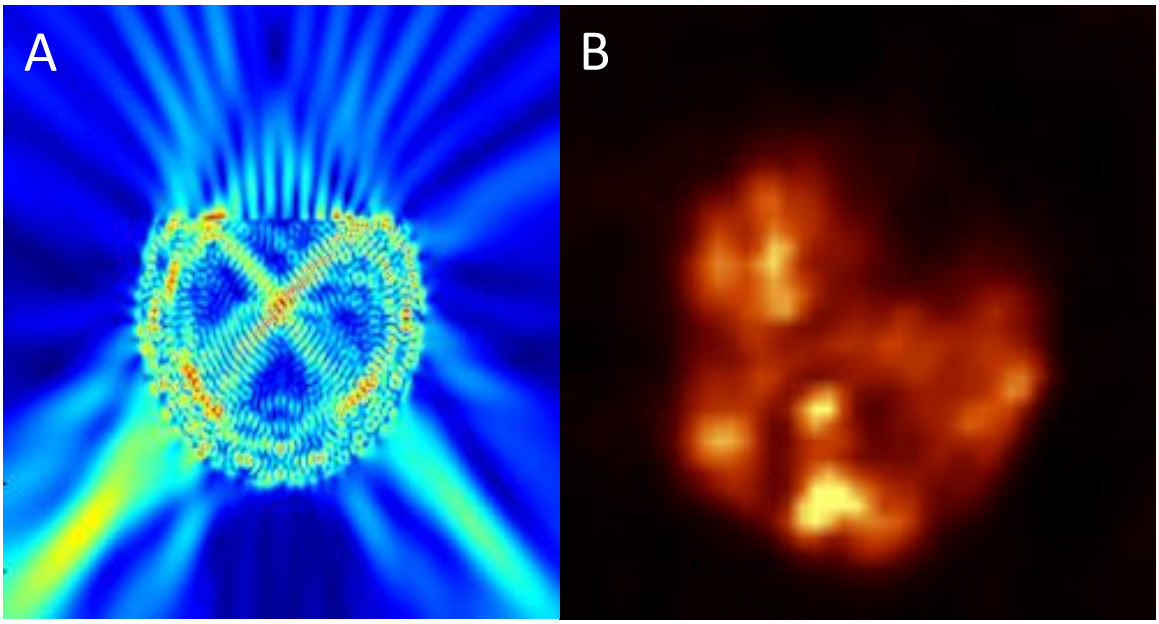

Figure 6.32 – (A) FDTD simulation of 3 µm micro disk with a straight edge defect (B) Photoluminescence mapping of a 3 µm micro disk

expected [20]. With increased size we can clearly see the circularity of the disks and there are irregular straight-line defects on many devices, though none appear to be significantly damaging as many have bright edges. This uniformity trend is furthered in the 10 µm disks where the overall pattern is the same in every disk, with randomness showing in the distribution of high/low points in the middle of the disk. The few times there was significant deviation was due to a large surface defect that stopped any growth of MQWs in the area rather than affecting the circularity. Therefore, the mapping shows a clear increase in uniformity with increasing micro disk size.

6.6 SEM INVESTIGATION INTO MICRO DISK DEFECTS

Using SEM, we measured 1.5 µm, 3.5 µm, 5 µm and 10 µm disk arrays to investigate the most common defects that can affect circularity in our micro disks. In **Figure 6.6** we can see the range of micro disks measured; each disk is surrounded SiO2 with has a rough quality. epitaxial growth is unlikely to happen on SiO2, but small deposits can form creating irregular crystal formations on the surface. They are unlikely to affect or interrupt the growth of the micro disks but can grow over the disk leading to interruptions in PL measurements.

Many of the disks show evidence of pits on the surface, but this is expected. Some defects are needed to be rule out as they are normal to MOCVD growth of GaN based devices. For instance, due to the large lattice mismatch between sapphire and GaN [7] we used a superlattice structure to improve the growth of the MQWs, this has led to a regular V pit defects developing on the surface of disk. V pits are when threading dislocations (TD) occur in many layered structures, when one layer is disrupted and penetrates to another epitaxial layer, this defect is enhanced by the many layers on top forming a V or cone shape in the cross section of the device. While obvious as long as the defect density is acceptable, they should not affect the quality of the modes or intensity, some papers even suggest that they can enhance MQW quality [24].Though it is interesting to not they it appears that smaller micro disks have decreased V put density as most of the 1.5 µm disks shown have none while 10 µm have a large number which can explain the large variance of intensities in the middle of the disk.

More relevant to our study are the disks that are measured in the SEM. With the 1.5 µm array we measured a disk with a straight edge. The edge-to-edge distance is measured to be 1.422 µm and a measured diameter of 1.482 µm, so about 4% of the area is removed. This is an example of a large defect in these disks, other disks have similar but smaller versions. These could have been due to a warping of the SiO2 mask used for growth as at

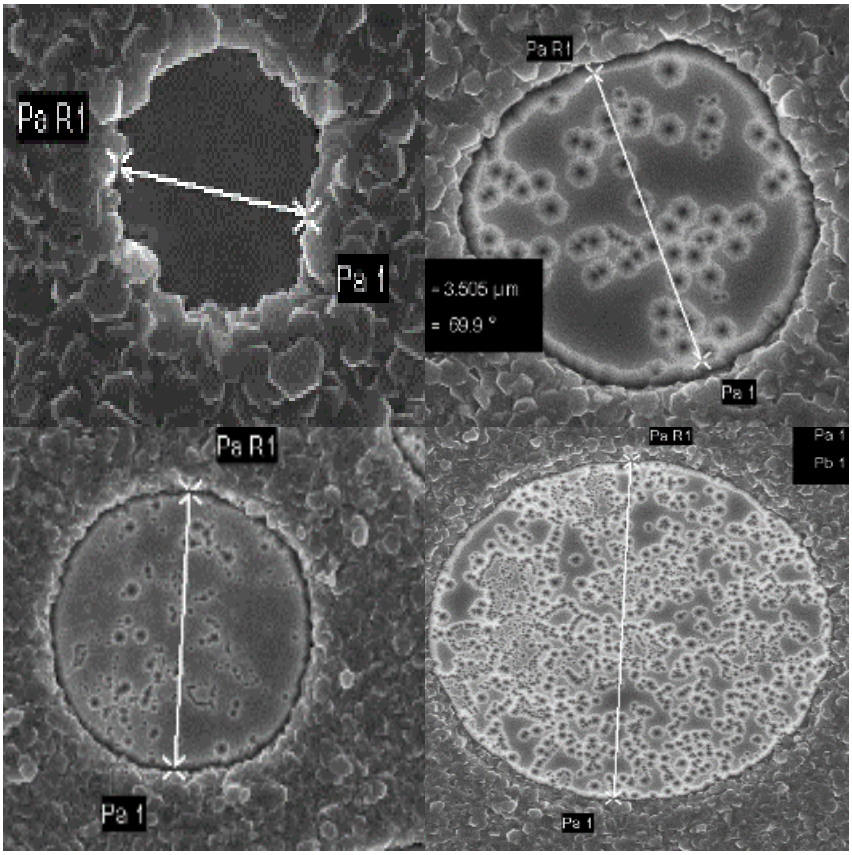

Figure 6.6 - SEM images of 2.5 µm, 3.5 µm, 5 µm and 10 µm micro disks with edge-to-edge measurements from the straight edge

smaller sizes these are more prone to deviations during the etching process. Other examples of straight edge defects are hexagonal micro disk shapes, which is a common growth problem as GaN has a wurtzite crystal structure [25].

The 3.5 µm array have similar deformities to the disk shape that is measured to have been on average 3.9%. This is the smallest disk with which we have been able to form modes with amplified stimulated emission. Looking at its tolerance point, which is around 3.9% this may be the limit of our current overgrowth method. With regards to 5 µm and 10 µm arrays they were calculated to have average straight-line defect of 3% and 1.59% respectively. The decrease of deformity area confirms that larger micro disk arrays have increased growth uniformity due to the limited damage the etching methods have to the disk shape.

6.7 CONCLUSION

This chapter goes through the process of designing and improving micro disk arrays and performing investigations into reducing the size of such disks. The overgrowth method was shown to be able to produce uniform micro disk with controllable size and interpatch. Starting with larger micro disks (>10um), IQE was used to check the quality of the disks. Samples were designed with large IQE (34%) at long wavelength (520nm), before experimenting with smaller micro disk sizes (<5um). To maintain the previous high IQE, improvements were introduced through the addition of lattice matched superlattice structures to improve relaxation of lattices in further grown layers. Further, the addition of nanoporous distributed Bragg reflectors, lattice matched to the MQW, allows for the improvement of the optical confinement in the LED structure. Reflectivity measurements showed these DBRs to have a reflectance > 95% with a stop band of 100nm. Power dependent measurements were performed which show the lasing capabilities of these micro disks. Calculated β- factors show that the smaller micro disks were capable of low lasing threshold. Future works will require optimisation of the micro cavity to further enhance these lasing properties, to finally create an integrated micro laser array device.

Contributions

T.W. conceived the idea and organized the project. P.F. performed the FDTD simulations and confocal microscopy PL measurements. G.M taught the FDTD simulations and added top DBR and etched the nano porous DBR. C.Z. grew the SiO2 mask, P.F. grew the overgrowth and micro disks. T.W. and P.F. prepared the manuscript.

6.8 REFERENCES

[1] Wasisto,H.S., Prades, J.D., Gülink, J., and Waag, A. (2019) *Beyond solid-state lighting: Miniaturization, hybrid integration, and applications of GaN nano- and micro-LEDs*, Applied Physics Reviews **6**, 041315

[2] Tchoe, Y., Chung, K., Lee, K. et al. (2019) *Free-standing and ultrathin inorganic light-emitting diode array*. NPG Asia Mater **11**, 37.

[3] Debnath, R., Ha, J.-Y., Wen, B., Paramanik, D., Motayed, A., King, M. R., and Davydov, A.V. (2014) *Top-down fabrication of large-area GaN micro- and nanopillars*, J. Vacuum Sci. Technol. B **32**, 021204.

[4] Zi, H., Fu, W. Y., Tabataba-Vakili, F., Kim-Chauveau, H., Frayssinet, E., De Mierry, P., Damilano, B., Duboz, J.- Y., Boucaud, Ph., Semond, F., and Choi, H. W. (2021) *Whispering-gallery mode InGaN microdisks on GaN substrates*, Opt. Express **29**, 21280-21289.

[5] Tamboli, A., Haberer, E., Sharma, R. et al. (2007) *Room-temperature continuous-wave lasing in GaN/InGaN microdisks*. Nature Photon 1, **61–64**. https://doi.org/10.1038/nphoton.2006.52

[6] Wang, D., Zhu, T., Oliver, R. A., and Hu, E. L. (2018) Ultra-*low-threshold InGaN/GaN quantum dot micro-ring lasers*, Opt. Lett. **43**, 799-802.

[7] Chung, K., Yoo, H., Hyun, J.K., Oh, H., Tchoe, Y., Lee, K., Baek, H., Kim, M. and Yi, G.-C. (2016) *Flexible GaN Light-Emitting Diodes Using GaN Microdisks Epitaxial Laterally Overgrown on Graphene Dots*. Adv. Mater., **28**: 7688-7694.

[8] Jiang, J., Xu, H., Sheikhi, M., Li, L., Yang, Z., Hoo, J., Guo, S., Zeng, Y., Guo, W., and Ye, J. (2019) *Omnidirectional whispering-gallery-mode lasing in GaN microdisk obtained by selective area growth on sapphire substrate*, Opt. Express **27**, 16195-16205.

[9] Wong, M. S., Hwang, D., Alhassan, A. I., Lee, C., Ley, R., Nakamura, S., and DenBaars, S. P. (2018) *High efficiency of III-nitride micro-light-emitting diodes by sidewall passivation using atomic layer deposition*, Opt. Express **26**, 21324-21331.

[10] Rousseau, I., Callsen, G., Jacopin, G., Carlin, J.-F., Butté, R., and Grandjean, N. (2018) *Optical absorption and oxygen passivation of surface states in III-nitride photonic devices*, J. Appl. Phys. **123**, 113103.

[11] Haberer, E. D. et al. (2004) *Free-standing, optically pumped, GaN/InGaN microdisk lasers fabricated by photoelectrochemical etching*. Appl. Phys. Lett. **85**, 5179–5181.

[12] Haberer, E. D., Sharma, R., Meier, C., Stonas, A.R., Nakamura, S., DenBaars, S. P., and Hu, E. L. (2004). *Free-standing, optically pumped, GaN/InGaN microdisk lasers fabricated by photoelectrochemical etching*, Appl. Phys. Lett. **85**, 5179–5181

[13] Zhang, Y., Zhang, X., Li, K.H., Cheung, Y.F., Feng, C. and Choi, H.W. (2015) *Advances in III-nitride semiconductor microdisk lasers*. Phys. Status Solidi A, **212**: 960-973.

[14] Bai, J., Cai, Y., Feng, P., Fletcher, P., Zhu, C., Tian, Y., and Wang, T. (2020). *Ultrasmall, ultracompact and ultrahigh efficient InGaN micro light emitting diodes (μLEDs) with narrow spectral line width*, *ACS Nano* **2020,** *14* (6), 6906-6911.

[15] Xie, E., et al. (2017) *Design, Fabrication, and Application of GaN-Based Micro-LED Arrays with Individual Addressing by N-Electrodes*, IEEE photonics journal, 9(6), pp. 1–11.

[16] Athanasiou, M., Smith, R.M., Pugh, J. *et al.* (2017). *Monolithically multi-color lasing from an InGaN microdisk on a Si substrate*. *Sci Rep* **7,** 10086

[17] Zhu, G., Li, J., Li, J., Jiyuan Guo, Dai, J., Xu, C., and Wang, Y. (2018) *Single-mode ultraviolet whispering gallery mode lasing from a floating GaN microdisk*, Opt. Lett. **43**, 647-650

[18] Tian, P., McKendry, J. J. D., Gong, Z., Guilhabert, B., Watson, I. M., Gu, E., Z. Chen, Zhang, G., and Dawson, M. D. (2012). *Size-dependent efficiency and efficiency droop of blue InGaN micro-light emitting diodes*, Appl. Phys. Lett. **101**, 231110

[19] Olivier, F., Tirano, S., Dupré, L., Aventurier, B., Largeron, C., Templier, F. (2017). *Influence of size-reduction on the performances of GaN-based micro-LEDs for display application*, Journal of Luminescence, Volume **191**, Part B,

[20] Zhu, G., Li, J., Zhang, N. *et al.* (2020). *Whispering-Gallery Mode Lasing in a Floating GaN Microdisk with a Vertical Slit*. *Sci Rep* **10,** 253

[21] Matsuoka, J., Kitamura, N., Fujinaga, S., Kitaoka, T., Yamashita, H. (1991). *Temperature dependence of refractive index of SiO2 glass, Journal of Non-Crystalline Solids*, Volume **135**, Issue 1, Pages 86-89,

[22] Harris, J., and Stöcker, Horst, (1998). *Handbook of mathematics and computational science*. New York; London: Springer.

[23] Kim, D. K., Park, Y. S., Kang, D., Kim, K.-K., Seong T.-H., Amano, H. (2019) *Combined effects of V pits and chip size on the electrical and optical properties of green InGaN-based light-emitting diodes*, Journal of Alloys and Compounds, Volume **796**, Pages 146-152, ISSN 0925-8388,

[24] Wang, W.-K. and Jiang, M.-C. (2016) *Growth behavior of hexagonal GaN on Si(100) and Si(111) substrates prepared by pulsed laser deposition*, Japanese Journal of Applied Physics, **55**(9), p. 95503.

[25] Hong, S.-K., *et al.* (2002) *Control of crystal polarity in a wurtzite crystal: ZnO films grown by plasma-assisted molecular-beam epitaxy on GaN*, Physical review. B, Condensed matter and materials physics, **65**(11), pp. 1–10.

7 SUMMARY OF WORK AND FUTURE WORK

7.1 SUMMARY OF RESULTS

7.1.1 Optical Investigation of micro-LED array as a function of dimension

Using a new overgrowth method of creating micro disk arrays initial optimisation was needed to allow high quality arrays to be grown. First planar multi quantum wells (MQW)s was grown and refined to have high internal quantum efficiency (IQE) at 500nm to be converted into a micro disk recipe. Initial wafers had varying micro disks from 400nm to 10nm. Size dependent IQE measurement were preformed to test the quality of micro disks. Results showed after 40 µm IQE began to increase showing smaller micro disk allowed enhanced qualities. Difficulties in growing 10 µm array due to lattice mismatch with sapphire was changed with the introduction of a super lattice structure below the MQWs. A sample with 40% IQE at 500nm comparable to an industry bought wafer was grown.

5 µm micro disks were grown to enhance light emitting diodes (LED) qualities and attempt to form whispering gallery modes (WGM). A study was conducted to increase surface quality to allow improved p-GaN growth against IQE, increasing the surface quality too high damaged the MQWs due to increase heat. A study was done to confirm the height of the micro disk against the SiO2 mask layer. Results showed little change in differing heights of MQWs as both SiO2 and air allowed high optical confinement.

To further increase LED quality and WGM formation a differential Bragg reflector (DBR) was added above the super lattice and below the MQW, used as a mirror to enhance intensity and increase confinement. A new nanoporous n-GaN/GaN DBR was created to reduce lattice mismatch, using selective electro chemical (EC) etching. PL measurements showed increased intensity in all samples allowing further decrease in sizes while maintaining quality. A sample with WGMs was grown and confirmed with micro-PL, later power dependent measurements were used to check for lasing properties.

Further success was found when electro luminescence measurements were done to a fabricated LED array, though no modes were shown. Therefore, optimisation was needed of cavity quality and fabrication method.

7.1.2 Optical investigation of optically pumped VCSEL obtained by a direct epitaxy method

Using the previous high quality micro disk arrays, we added a Si based dielectric DBR on top to form a lasing cavity centred on 500nm. In order to confirm the quality of lasing cavity angular reflectivity studies were done to confirm the presence of polaritons. Reflectivity showed the dielectric DBR had a high reflection >99% and overlapped with the nano porous DBR allowing an overall cavity reflectivity spectrum to form. The angular reflectivity showed the presence of weak polaritons and the rabi splitting was calculated to be 5meV.

Power dependent PL was used to confirm WGMs and amplified stimulated emission. Initial spectrum shows modes at 488nm and 510nm. Integrated intensity against power shows a nonlinear increase in intensity along with full width half maximum narrowing with increased power, indicators of lasing. FDTD simulations were done to confirm the type of modes along with the wavelength for these structures. They confirmed WGMs and that a peak at around 485nm was likely to form.

Results agree that these disk array can form WGM, and the cavity has a high enough quality for lasing to happen. But low q factor and high lasing threshold prevent effective use. Either higher refinement of cavity is needed to lower the threshold or growing small disks arrays.

7.1.3 Influence of irregularities in shape on optical performance

Smaller micro disks were grown to increase the chances of a high-quality laser to be created. PL mapping shows increased in randomness in intensity patterns within the micro disks. Measurements were performed on a variety of array sizes to check uniformity. 2.5 µm, 3.5 µm, 5 µm and 10 µm disk arrays were measured and found that larger sizes had a more uniform intensity distribution. Due to the reduced effect of side wall roughness using overgrowth method, the shape of the disks studied to see how they affect the WGMs. PL spectra allowed us to see where modes still were present in different disks. SEM was used to confirm the most common reasons the shape would be affected.

FDTD simulation were used to simulate disk with straight edge defects to varying degree of deformity across many sizes. Simulation showed an increase in sensitivity in smaller sizes where even small changes to the circularity will prevent the formation of modes. Plotting the integrated intensity against the size of defect allowed us to find the tolerance point where the micro disk no longer can form modes. This showed a linear relationship to the diameter of the micro disks.

Further study is needed to confirm where these defects are most likely to form and the limit of growing smaller micro disks with our current methods

7.2 FUTURE WORK

The micro disks arrays that were created from chapter 3 has resulted in highly efficient LED InGaN arrays that can be electrically excited, the results of which have been published. [1] While current samples have been shown to have both WGM and lasing properties under optical excitation, there is increase interest in integrating micro lasers with electrical devices. [2] Chapter 4 proved that the micro disks are capable of confinement the high lasing threshold limits the electrical capabilities, as devices are more likely to be overwhelmed at high voltages. Further optimisation of the arrays is needed to allow improve the cavity quality and reduce the lasing threshold; greater reduction of micro disk size is one of the most likely methods of improvements. Other ways could also include the optimisation of the fabrication method, designing the MQW structure to align the dips in the reflectivity spectra with WGM can increase the chances of amplifying those modes. [3] Increasing the inter pitch between micro disks can allow fewer disks per array devices, allowing higher currents to be reached during excitation.

Reducing the micro disk size toward the nano could have limitations as outlined in chapter 5, so more FDTD simulations are needed to continue the investigation. If the linear trend of tolerance points continues through the nano range, then there could be a hard limit to nano disk arrays, or if the trend is nonlinear below 1 µm then circularity could become a non-factor with new challenges replacing it. Following such theoretical investigation, a further one is needed to systematically check the overgrowth method for where these defects are most likely to come from and new techniques need to be developed to overcome them.

Most of these samples have been designed to have peak wavelengths and modes around 500nm, using the incorporation of indium in GaN MQWs. Though to create microstructures with longer wavelengths a higher percentage of indium is needed but it is interrupted by the green/yellow gap effect. To counter it we can grow micro disks in a semi-polar or non-polar configuration allowing for a reduced repulsive interaction and therefore an increase in indium incorporation. Growing such structures in different growth orientation is a difficult challenge, many papers describe the issues of growing simples bulk LEDs structures [4] increasing the issues with a micro disk array structure as well is a significant project. Though

if done could lead the creation of yellow/ red micro-LEDs and lasers, which if taken even further can be used to create multi wavelength wafers with different arrays with wavelengths across the visible range, being a great improvement for the visual and communication industries. [5]

7.3 REFERENCES

[1] Bai, J., Cai, Y., Feng, P., Fletcher, P., Zhu, C., Tian, Y., and Wang, T. *Ultrasmall, ultracompact and ultrahigh efficient InGaN micro light emitting diodes (μLEDs) with narrow spectral line width*, *ACS Nano* **2020,** *14* (6), 6906-6911. (2020).

[2] Mei, Y., Xie, M., Xu, H., Long, H., Ying, L., & Zhang, B. (2021). Electrically injected GaN-based microdisk towards an efficient whispering gallery mode laser. *Optics Express*, *29*(4), 5598–5606. https://doi.org/10.1364/OE.416873

[3] Shaw, A., McCormack, T., Bradley, A., Lunney, J., & Donegan, J. (2002) Modelling of Extraction Efficiency of GaN-Based Resonant Cavity Light Emitting Diodes Emitting at 510 nm. *Physica Status Solidi. A, Applied Research*, *192*(1), 103–109. https://doi.org/10.1002/1521-396X(200207)192:1<103::AID-PSSA103>3.0.CO;2-F

[4] Jiu, L., Gong, Y., & Wang, T. (2018). Overgrowth and strain investigation of (11-20) non-polar GaN on patterned templates on sapphire. *Scientific Reports*, *8*(1), 9898–8. https://doi.org/10.1038/s41598-018-28328-7

[5] Athanasiou, M., Smith, R.M., Pugh, J., Gong, Y., Cryan M. J., &Wang**,** T. *Monolithically multi-color lasing from an InGaN microdisk on a Si substrate*, Scientific Reports **7**, Article number: 10086 (2017), doi:10.1038/s41598-017-10712-4